CORROSION RESISTANCE OF AUSTENITIC STAINLESS STEEL IN ACETIC ACID SOLUTION CONTAINING BROMIDE IONS

A thesis submitted to The University of Manchester for the degree

of Doctor of Philosophy (PhD)

In the Faculty of Engineering and Physical Science

2011

Saud Ghunaim Al-Subai

SCHOOL OF MATERIALS

Corrosion and Protection Centre

Table of Contents

Abstract

In this research, the corrosion performance of two austenitic stainless steels, namely 316L and 254SMO, in concentrated acetic acid solutions containing bromide ions has been investigated. In this research, the influence of two different electrochemical surface treatments (electropolishing and nitric acid passivation) on the corrosion behaviour of 316L stainless steel immersed in 15.3M HAc with 18.7mM bromide ions at 90^0C was examined. Also, attempts were made to study the performance of three organic inhibitors in the same conditions.

Corrosion rates are assessed both by weight loss, and linear polarisation resistance. Interfacial corrosion chemistry is further characterised by open circuit potential and potentiodynamic polarization measurements. Substrate morphology is elucidated with optical microscopy, including 3D surface profiling, and scanning electron microscopy. Also, X-ray photoelectron spectroscopy is employed to gain further insight into the quite different corrosion performances of 316L and 254SMO in 15.3M acetic acid with 18.7mM Br ions.

It was found that 316L and 254SMO steels have good corrosion resistance and low corrosion rates in 11.9M-HAc-Br-. Increasing acid concentration to 15.3 M led to a dramatic increase in corrosion rate of 316L with clear evidence of uniform and pitting corrosion proceeding simultaneously. Notably, the step increase in OCP for 316L steel and 254SMO during immersion in 15.3M-HAc-Br- solution indicates sudden changes in corrosion activity of the steels. The step seen for the 254SMO in 15.3M-HAc-Br- is indicative of passivation which is also supported by the XPS results, as a stable passive film was observed on the surface of alloy over the immersion time. However, the step increase in the OCP observed for 316L in 15.3M-HAc-Br- is not associated with a significant decrease in corrosion rate. An

alternative explanation is that the step coincides with an increase in the importance of pitting due to the evolving surface structure.

From the attempts which were made to improve the corrosion resistance of the 316L stainless steel in 15.3M-HAc-Br$^-$, both electropolishing and nitric acid passivation treatments were not sufficient to give any noticeable protection from the aggressive solution. Also, no corrosion inhibition was achieved when the three organic inhibitors, BTA, TU and 2MBI were utilised.

Declaration

No portion of the work referred to in the thesis has been submitted in support of an application for another degree or qualification of this or any other university or other institute of learning.

Saud G. Al Subai

Copyright statement

i. The author of this thesis (including any appendices and/or schedules to this thesis) owns any copyright in it (the "copyright") and he has given The University of Manchester the right to use such copyright for any administrative, promotional, educational and/or teaching purposes.

ii. Copies of this thesis, either in full or in extracts, may be made only in accordance with the regulations of the John Rylands University Library of Manchester. Details of these regulations may be obtained from the Librarian. This page must form part of any such copies made.

iii. The ownership of any patents, designs, trade marks and any and all other intellectual property rights except for the Copyright (the "Intellectual Property Rights") and any reproductions of copyright works, for example graphs and tables ("Reproductions"), which may be described in this thesis, may not be owned by the author and may be owned by third parties. Such Intellectual Property Rights and Reproductions cannot and must not be made available for use without the prior written permission of the owner(s) of the relevant Intellectual Property Rights and/or Reproductions.

iv. Further information on the conditions under which disclosure, publication and exploitation of this thesis, the Copyright and any Intellectual Property Rights and/or Reproductions described in it may take place is available from the Head of School of Materials.

ACKNOWLEDGMENTS

1 INTRODUCTION

Terephthalic acid (TA) is an organic compound that used in a variety of industrial applications and chemical processes such as manufacturing of polyester films which used to produce audio films, moulded resins used to make polyethylene terephthalate (PET) bottles and polyester textile fibers [1, 2]. This acid is commercially produced by purifying crude terephthalic acid which is produced by catalytic, liquid phase air oxidation of para-xylene (PX). In this production processes acetic acid is used as a solvent coupled with heavy metal based on cobalt and manganese compounds and with presence of bromide as assistant catalysts as shown in Equation 1-1 [3-5]. Subsequently, acetic acid containing bromide ions is considered as the main corrosive electrolyte in the TA production process that may introduce serious corrosion problems into the process equipment. Type 316L stainless steel is the alloy most commonly used in equipment processing acetic acid, even glacial acid at temperatures above the atmospheric boiling point can be handled if the impurities are held within proper levels [6]. However, their corrosion resistance will be affected by the presence of halide ions and/or uncontrolled incursion of impurities into the process that caused by a temporary system upset[4, 5, 7].

Motivated by the aggressive environment encountered in the industrial synthesis of the TA and the limited literature available on the corrosion

behaviour of stainless steel materials under these conditions, the corrosion behaviour of 316L stainless steel in concentrated acetic acid solution (11.9M - 15.3M) at 90⁰C containing 18.7mM bromide ions has been studied. In addition, to study the effect of alloy composition on corrosion resistance, 254SMO austenitic stainless steel was also examined in the same environments. The 254SMO stainless steel was developed by using alloying elements, especially molybdenum (6.0 wt %), to stabilize the passive film in high corrosive media and thus reduce susceptibility to pitting and crevice corrosion [1, 2]. In this research, an attempt was also done to evaluate the possible impact of the addition of three organic corrosion inhibitors, namely Benzotriazole (BTA), Thiourea (TU) and 2-mercaptobenzimidazole (2MBI), on the corrosion behaviour of the 316L stainless steel in the 15.3M acetic acid at 90ᵒC.

A number of techniques have been employed in this study. Corrosion rates are assessed both by linear polarisation resistance (LPR) and weight loss methods. The electrochemical behaviour of the two alloys is further characterised by open circuit potential (OCP) and potentiodynamic polarisation measurements (PDP). Substrate characterisation techniques, including optical microscopy and scanning electron microscopy (SEM) are used to evaluate the surface of the alloys. Also, X-ray photoelectron spectroscopy (XPS) is employed to gain further insight into the quite different corrosion performances of 316L and 254SMO in test solutions,

especially in 15.3M HAc. Finally, white light inteferometry is used in the current study to estimate the amount of material removed from the pits formed on the surface of 316L steel that undergoes uniform corrosion and pitting during immersion in 15.3MHAc.

This thesis consists of number of chapters. Chapter two provides background information about corrosion in general and specifically corrosion types and corrosion behaviour of stainless steel alloys. Chapter three outlines the various experimental techniques and instrumentation employed in the current study. Chapter four focuses on assessing the corrosion resistance of the alloys, 316L and 254SMO, under the prevailing experimental conditions, using mainly weight loss and electrochemical measurement techniques. Chapter five elucidates the composition and structure of the surface films that are gained by XPS. Chapter six details work concerning the surface treatments that may improve the corrosion resistant of the 316L alloy and the results of employing the organic corrosion inhibitors. Finally, general conclusions and possible future work are given in chapter seven.

$$CH_3-C_6H_4-CH_3 + 3O_2 \xrightarrow{\text{Co(Ac)}_2 +\text{Mn(Ac)}_2 +\text{C}_2\text{H}_2\text{Br}_4} HOOC-C_6H_4-COOH + 2H_2O \qquad \text{1-1}$$

Para-xylene $\qquad\qquad\qquad\qquad\qquad$ TA
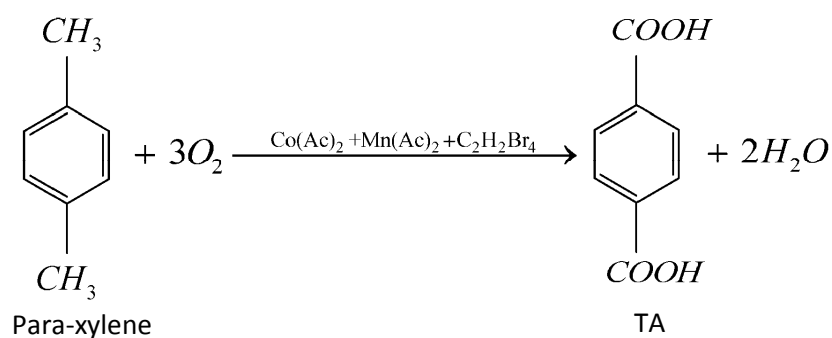
References

1. H. Macarie, A. Noyola and J. Guyot, *Anaerobic Treatment of a Petrochemical Wastewater from a Terephthalic Acid Plant,* . Water Science and Technology, 1992. **25**(7): p. 223-235.

2. Lettinga, R. Kleerebezem and G., *High Rate Anaerobic Treatment of Purified Terephthalic Acid Wastewater.* Water Science and Technology, 2000. **42**(5-6): p. 259-268.

3. G.R. Pophali, R. Khan, R.S. Dhodapkar, T. Nandy, S. Devotta, *Anaerobic-Aerobic Treatment of Purified Terephthalic Acid (Pta) Effluent; a Techno-Economic Alternative to Two-Stage Aerobic Process.* Journal of Environmental Management, 2007. **85**(4): p. 1024-1033.

4. Y. Gong, J. Cao, X.-H. Meng, Z.-G. Yang, *Pitting Corrosion on 316l Pipes in Terephthalic Acid (Ta) Dryer.* Materials and Corrosion, 2009. **60**(11): p. 899-908.

5. Al-Refaie, Oluwatoyin Ashiru and Abdullah, *Pitting Corrosion Problems of Stainless Steels in a Pta Plant*, in *NACE International*. 2007: Nashville, Tennessee.

6. Scribner, L.A., *Corrosion by Organic Acids,*, in *CORROSION*. 2001: NACE International Houston, Tx. paper No. 01343.

7. G.Q. Liu, Z.Y. Zhu, W. Ke, E.H. Han, and C.L. Zeng, *Corrosion Behavior of Stainless Steels and Nickel-Based Alloys in Acetic Acid Solutions Containing Bromide Ions.* Corrosion, 2001. **57**(8).

CHAPTER TWO

CORROSION FUNDAMENTAL AND STAINLESS STEEL CORROSION

2   Corrosion Fundamentals and Stainless Steel Corrosion

2.1 Introduction

This chapter is divided into four main sections. The goal of the first section is to provide a fundamental understanding of the processes involved in corrosion phenomena. The second section of this chapter briefly introduces the concepts behind passivity of engineering materials to corrosion. Then, stainless steel alloys especially the austenitic group and their corrosion will be discussed in section three. In this section, pitting corrosion and factors influencing the pitting corrosion are detailed. Corrosion behaviours of stainless steel particularly the 316 grade in acetic acid environments will be covered in the fourth section. The final section will outline some of earlier studies and research efforts of interest to characterize the composition of the passive film formed on the surface of stainless steel.

2.2 Basic Aspects of Corrosion

2.2.1 Definition

Corrosion is a process created by the reaction (chemical or electrochemical) between a material, often a metal or alloy, and its environment that results in destruction or deterioration of that material [4]. Corrosion has been classified in many different ways. One method classifies corrosion into low and high temperature corrosion. Wet corrosion and dry corrosion is the preferred classification method. The wet corrosion involves liquid solutions, such as corrosion of steel by water whereas dry corrosion is most often associated

with high temperatures and occurs in absence of a liquid phase, by mechanisms such as carburization, metal dusting [5]. Some principles and basic aspects of corrosion processes will be discussed in the following sub-sections.

2.2.2 Principles of Electrochemical Corrosion

Corrosion in aqueous environments occurs by an electrochemical mechanism. The phenomenon involves electrons and ions and can be separated into two partial reactions, anodic (oxidation) and cathodic (reduction) [6]. At anodic sites an oxidation reaction occurs which is the loss of electrons. For this reaction to take place a simultaneous reduction process – a net gain of electrons – will occur at cathodic sites [7, 8]. The anodic reaction of the metal is of the form:

$$M \rightarrow M^{n+} + ne^{-} \qquad\qquad `` (2\text{-}1)$$

Depending on the corroded metals, examples of some anodic reaction are:

Zn	$\rightarrow Zn^{2+} + 2e^{-}$	Zinc corrosion	(2-2)
Fe	$\rightarrow Fe^{2+} + 2e^{-}$	Iron corrosion	(2-3)
Al	$\rightarrow Al^{3+} + 3e^{-}$	Aluminium corrosion	(2-4)
Fe^{2+}	$\rightarrow Fe^{3+} + e^{-}$	Ferrous ion oxidation	(2-5)
H_2	$\rightarrow 2H^{+} + 2e^{-}$	Hydrogen oxidation	(2-6)
$2H_2O$	$\rightarrow O_2 + 4H^{+} + 4e^{-}$	Oxygen evolution	(2-7)
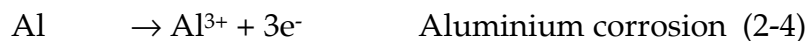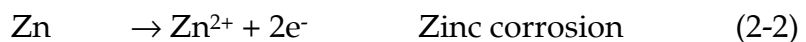
On the other hand, cathodic reaction of the metal is of the form:

$$X^{x+} + xe^- \rightarrow X \qquad\qquad (2\text{-}8)$$

The reduction of dissolved oxygen and release of hydrogen gas by the reduction of hydrogen ions are the most common reactions during aqueous corrosion of metals [7]. However, there are other cathodic reactions encountered during the corrosion process, examples of these are:

$O_2 + 2H_2O + 4e^- \quad \rightarrow 4OH^-$ Oxygen reduction (neutral solution) $\qquad$ (2-9)

$2H^+ + 2e^- \qquad\qquad \rightarrow H_2 \qquad$ Hydrogen evolution (in acid solution) $\quad$ (2-10)

$Cu^{2+} + 2e^- \qquad\qquad \rightarrow Cu \qquad$ Copper plating (metal deposition) $\qquad$ (2-11)

$Fe^{3+} + e^- \qquad\qquad \rightarrow Fe^{2+} \quad$ Ferric ion reduction $\qquad\qquad\qquad$ (2-12)
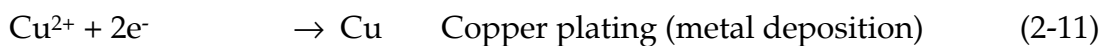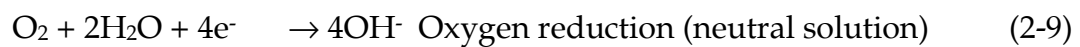
The two reactions, anodic and cathodic, are complementary events and must proceed at the same rate. Anodic and cathodic sites can form on the surface of the metal for many reasons: composition or grain size differences, discontinuities on the surface, impurities or inclusions in the metal, local differences in the environment (e.g., temperature, oxygen, or salt concentration), localized stresses. The basic corrosion process is shown in Figure 2-1.

For electrochemical corrosion to take place, there are four fundamental requirements [9]: An anode, A cathode, A conducting environment for ionic movement (electrolyte), and An electrical connection between the anode and

cathode for the flow of (electron) current. If any of these elements is missing or disabled, electrochemical corrosion cannot occur.
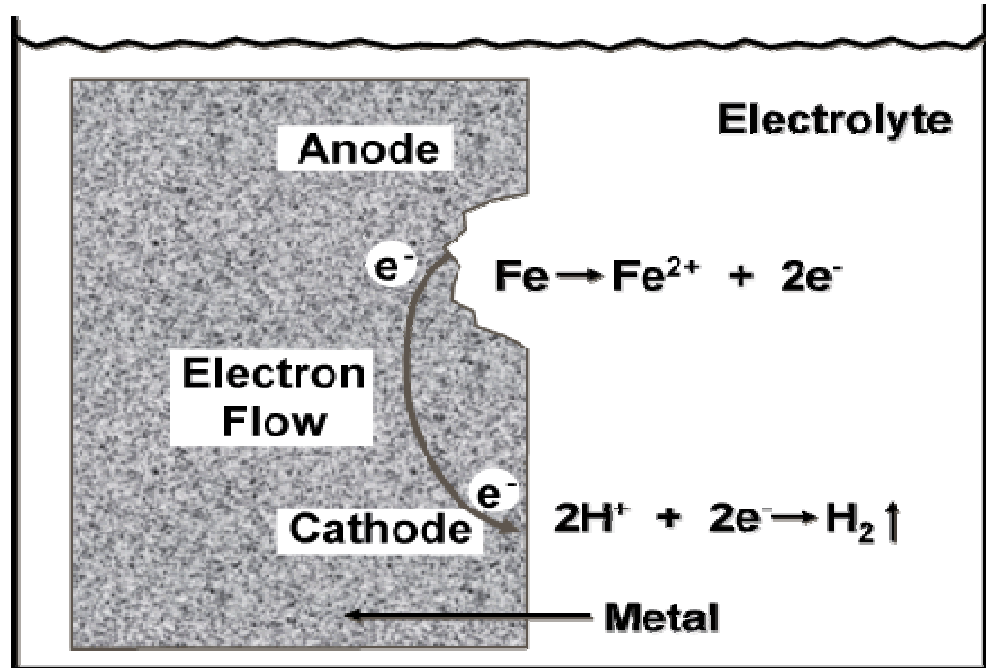
Figure 2-1 Example of basic corrosion process [1].

2.2.3 Corrosion Thermodynamics and Kinetics

When considering a metal in a specific environment a number of questions need to be addressed, including: will the metal corrode in this environment, and if yes how fast will it corrode? These questions can be answered by studying the thermodynamics and kinetics of corrosion.

2.2.3.1 Thermodynamics of Electrochemical Corrosion

Thermodynamics gives an understanding of the energy changes involved in the electrochemical reactions of corrosion. These energy changes provide the driving force and control the direction for a chemical reaction. Therefore,

thermodynamics shows how conditions may be adjusted to make the corrosion impossible, when corrosion is possible, thermodynamics cannot predict the rate; corrosion may range from fast to very slow [3].

A metal will exhibit a potential with respect to its environment. This potential is dependent on the ionic strength and composition of the electrolyte, the temperature, the metal or the alloy itself, and other subsidiary factors. The potential of a galvanic cell is the sum of the potentials of the anodic and cathodic half cells in the environment surrounding it. From thermodynamic considerations, the potential of an electrochemical reaction can be related to the change in Gibbs free energy , ΔG= G (products) – G (reactants), as shown in the below equation [5]:

$$\Delta G= -nFE \qquad\qquad\qquad (2\text{-}13)$$

where n is the number of electrons participating in the reaction, F is Faraday's constant (96,500 Coulomb/mole), and E is the electrode potential. The potential of the galvanic cell will depend on the concentrations of the reactants and products of the respective partial reactions, and on the pH of the aqueous solutions in contact with the metal.

Corrosion will not occur unless the spontaneous direction of the reaction (that is, $\Delta G < 0$) indicates metal oxidation. A negative free energy change

(ΔG) indicates that the stability of the products is greater than that of the reactants.

The change in electrode potential as a function of concentration is given by the Nernst equation [3, 5]:

$$E = E° + 2.3(RT / n F) \log (ox)^x / (red)^r \qquad \text{(2-14)}$$

Where $E°$ is the standard electrode potential, (ox) is the activity of an oxidized species, (red) is the activity of the reduced species, and x and r are stoichiometric coefficients involved in the respective half cell reactions.

The application of thermodynamics to corrosion phenomena has been generalized by use of potential-pH plots (Pourbaix diagrams). Such diagrams are constructed from calculations based on the Nernst equation, above, and solubility data for various metal compounds. From these diagrams, it is possible to differentiate regions of potential as a function of pH in which metal is either immune (no corrosion) or will be passivated by a thin film [10, 11]. Example of such diagrams is shown in Figure 2-2 which represents iron in an aqueous solution. The diagram gives regions of existence: iron is inert and stable (region A), actively dissolve (region B) or the oxide layer can form (region C).
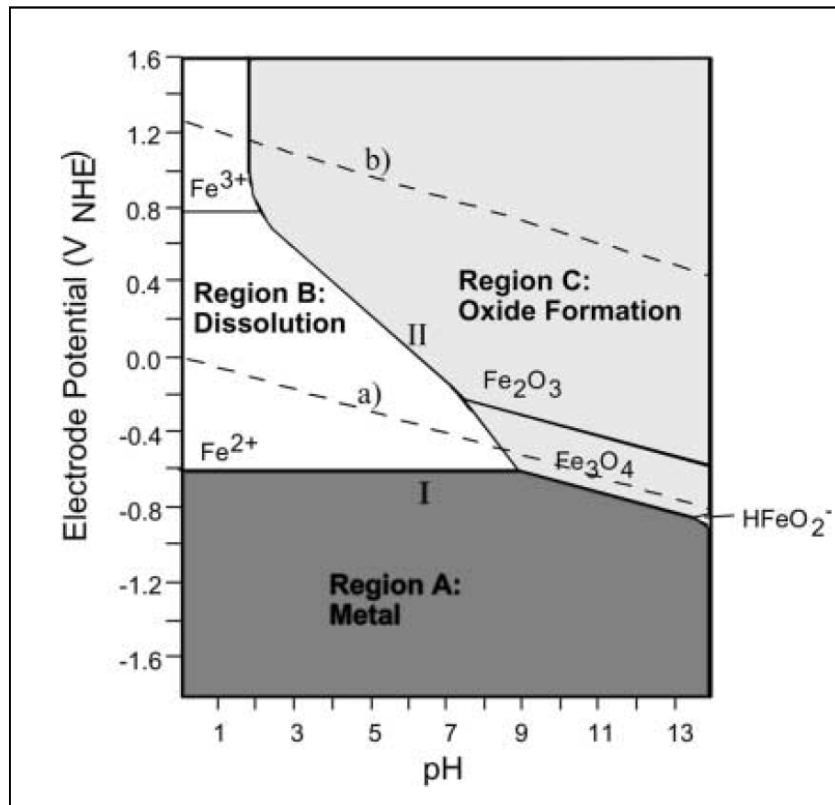
Figure 2-2 Simplified E/pH diagram (Pourbaix diagram) for Iron-water system at 25°C. the potentials are given vs. normal hydrogen electrode (NHE) [2].

2.2.3.2 Kinetics of Electrochemical Corrosion

Corroding systems are not in equilibrium, the oxidation and reduction reactions in the corroding metal each occur at a potential displaced from its equilibrium value [12]. Thus, kinetic studies of the processes are necessary.

A system is out of equilibrium when the potential is displaced from the equilibrium potential by the application of an external voltage or by the spontaneous production of a voltage away from equilibrium. This deviation in potential is defined as polarization (η) [5].

$$\eta = \mid E - E_{eq} \mid \qquad\qquad (2\text{-}15)$$

where E_{eq} is the equilibrium potential.

There are mainly three types of polarisation in any electrochemical cell: (1) Activation polarization, (2) Concentration polarization, and/or (3) Resistance polarization [13, 14].

2.2.3.3 Activation Polarization

A system is referred to be as activation controlled when the rate of the electrochemical process is controlled by the charge transfer across the metal solution interface. For anodic and cathodic polarization on activation controlled system, the activation polarization for the anodic reaction (η_a (A)) can be expressed as:

$$\eta_a\ (A) = \beta_A \log i_A\ /\ i_o \qquad\qquad (2\text{-}16)$$

Where,

i_A = Anodic current density (A/cm^2)

i_o = Exchange current density (A/cm^2)

β_A = Tafel slope for the anodic reaction

An identical expression can be written for the cathodic reaction.

2.2.3.4 Concentration Polarization

When the transport of ions or molecules to or away from the metal surface determines the rate of the electrochemical process, the system is said to be under concentration polarization (η_c), or transport control. For example, when the cathodic process in corroded system depends on the reduction of dissolved oxygen, the diffusion of oxygen to the metal surface will often limit the rate of corrosion.

The concentration polarization can be expressed as:

$$\eta_c = 2.3RT/nF * \log (1- i/i_{lim}) \qquad (2\text{-}17)$$

Where, i_{lim} = Limiting current density

2.2.3.5 Resistance Polarization

Resistance polarization (η_r) is a consequence of the ohmic resistance in the system. It is the sum of the resistance in the electrolyte ($R_{sol.}$) and the resistance of any apparent scale on the surface (R_{scale}):

$$\eta_r = i \sum R \qquad (2\text{-}18)$$

Where, $$\sum R = R_{sol.} + R_{scale} \qquad (2\text{-}19)$$

High-resistivity solutions and insulating films deposited at either the cathode or anode restrict or completely block contact between the metal and the solution and will promote a high-resistance polarization.

The total polarization (η_{total}) across an electrochemical cell is the sum of the above individual polarizations:

$$\eta_{total} = \eta_a + \eta_c + \eta_r \qquad (2\text{-}20)$$

2.2.3.6 Rate of Corrosion and Faraday's law

The rate of electron flow to or from a reacting interface is a measurement of the reaction rate [3]. The electron flow is conveniently measured as the magnitude of a current; therefore, the current can be used to determine the reaction rate of the process through Faraday's law. If we consider the anodic metal oxidation reaction in equation 2-1 ($M \rightarrow M^{n+} + ne^{-}$):

$$Q = nFm/M \qquad (2\text{-}21)$$

Where,

Q = the electrical charge (coulomb)

F = Faraday's constant (96500 coulombs/mole)

n = Number of electrons transferred

m = Mass of metal oxidised (g)

M = Atomic weight of metal (g/mole)

Also, this can be expressed in terms of the rate of the reaction:

$$I = nFK/M \qquad (2\text{-}22)$$

Where,

I = Corrosion current (A)

K = Rate of corrosion (g/s)

2.2.4 Mixed Potential Theory

Kinetic information of corroded surface is usually presented in a graphical forms called Evans or polarization diagrams that represent the relation between the electrode potential and current density [15]. These diagrams are developed based on the principles of mixed potential theory.

The theory of mixed potential was developed by Wagner and Traud in 1938 [16]. The theory proposes that the electron released during oxidation process (anodic) is consumed by a corresponding reduction process (cathodic). Therefore the total rate of the oxidation reaction will equal the total rate of the reduction [17]. The cause of the entire process is based on two factors. The oxidation and reduction reactions each have a unique half-cell electrode potential and exchange current density (i_o). The second factor is that, the half-cell potentials cannot coexist separately in the same conductive environment. There must be a polarization in potential to a common intermediate value referred to as the mixed potential.

Figure 2-3 illustrates the two half-cell reactions occurring when zinc is placed

in an acid solution. The two half-cell potentials are plotted with respect to

the corresponding current density of the half-cell reactions (i_o). The corrosion

potential (E_{corr}) and the corrosion current density (i_{corr}) values are located

where hydrogen reduction line and zinc oxidation line converge.
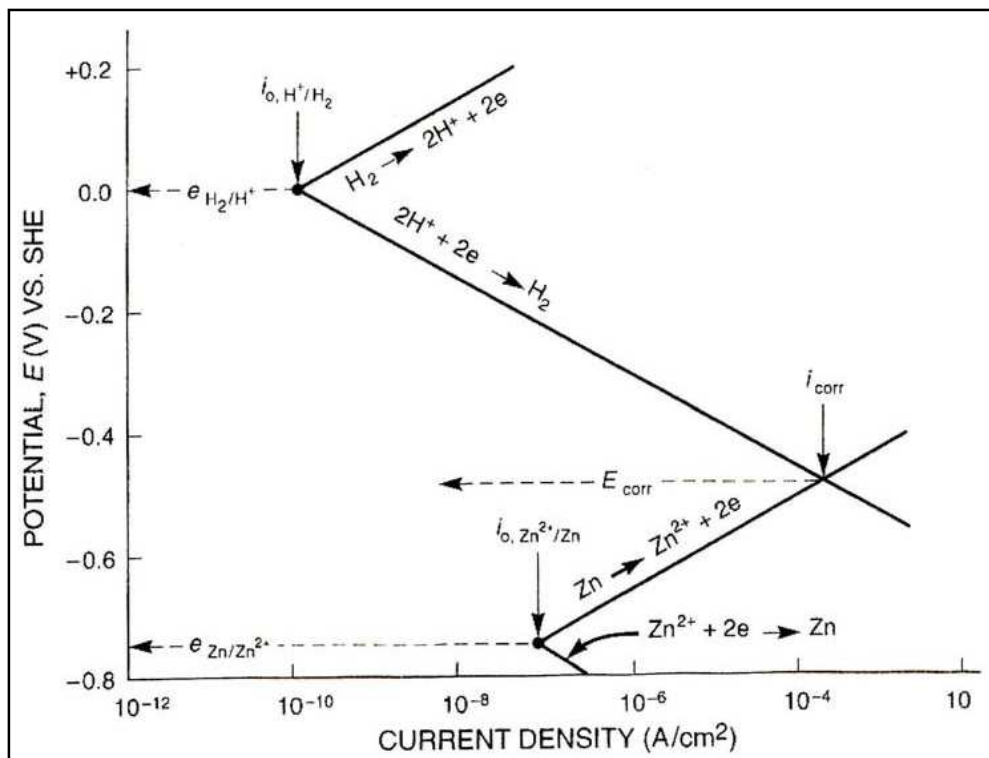
Figure 2-3 Schematic Evans diagram for zinc in acid solution shows the corrosion potential (E_{corr}) and corrosion current density (i_{corr}) [3].

2.3 Passivity to Corrosion

2.3.1 Introduction

All metals and alloys (commonly, gold is exception) have a thin protective corrosion product film present on their surface due to the reaction with the environment [18]. Some of these films are passive and on some metals and alloys have certain characteristics that enable them to provide more corrosion resistant metal surfaces. These protective surface films are responsible for the phenomenon of passivity [4, 19] which is the reason a metal does not corrode when it would be expected to.

2.3.2 Definition of passivity

Two generally accepted definitions of the passivity were reported [18, 20]:

1. A metal is passive if, on increasing its potential to more positive values, the rate of dissolution decreases (low corrosion rate , noble potentials)

2. A metal is passive if it substantially resists corrosion in an environment where there is a large thermodynamic tendency to react (low corrosion rate, active potential).

Also, an additional definition has been provided by NACE/ASTM [21], the passive is the state of a metal surface characterized by low corrosion rates in potential region that is strongly oxidizing for the metal.

2.3.3 Active-passive Behaviour

During anodic polarization, metals and alloys with a passivated surface will typically display a polarisation curve of the shape shown in Figure 2-4 [18]. At relatively low potential within the active region, when the potential value is plotted against log current density the behaviour is linear for normal metals. With the beginning of the formation of a passive layer the measured current begins to decrease. The turning point on the curve marking the beginning of this decrease is known as the active-passive transition and the corresponding value of the applied potential is the primary passivation potential (E_{PP}). Also, in Figure 2-4, the current density decreases rapidly to a very low value called the passive current density (i_p) due to the formation of quite a passive layer.

With the presence of a stable uniform non-conducting layer (passive oxide) on the surface of the metal the system enters a region where further increase in potential causes no noticeable increase in current density, this is the passive region. This current density remains relatively independent of potential because it is controlled by the rate of dissolution of the passive film.

In environments without aggressive species such as Cl$^-$, with further increase in potential to more positive value, most of the metal passive oxides can be further oxidized to a more soluble state. Therefore, the effectiveness of the passivation layer is reduced and/or removed so corrosion can re-occur. This

region where the current density begins to increase again is called the transpassive region [22, 23]. For example, the protective layer of stainless steel containing chromium as Cr (III), when the potential is raised to the transpassive region, Cr (III) is oxidized to Cr (VI). However, for metals such as aluminum and tantalum, that can form electronically insulating passive oxide films the passive region extends to very positive potentials and neither transpassive metal dissolution nor oxygen evolution will occur [24].

Hoar [25] stated that four conditions, are usually, but not always, required for the passivity breakdown that initiates localized attack:

1) **Critical potential:** a certain critical potential must be exceeded.

2) **Damaging species:** such as chloride or higher atomic weight halides, are needed in the environment to initiate breakdown and propagate localized corrosion processes like pitting.

3) **Induction time:** an induction time exists, which starts with the initiation of the breakdown process (introduction of breakdown conditions) and ends when the localized corrosion density begins to rise.

4) **Local sites:** the presence of highly localized sites such as inclusions and second-phase precipitates.

Whatever the causes of the breakdown of the passive film, the result will be a fresh metal surface exposed to the environment leading to localized attack

such as pitting, crevice, inter-granular corrosion or stress corrosion cracking [19, 26]. Further details will be discussed in the later section on pitting corrosion.
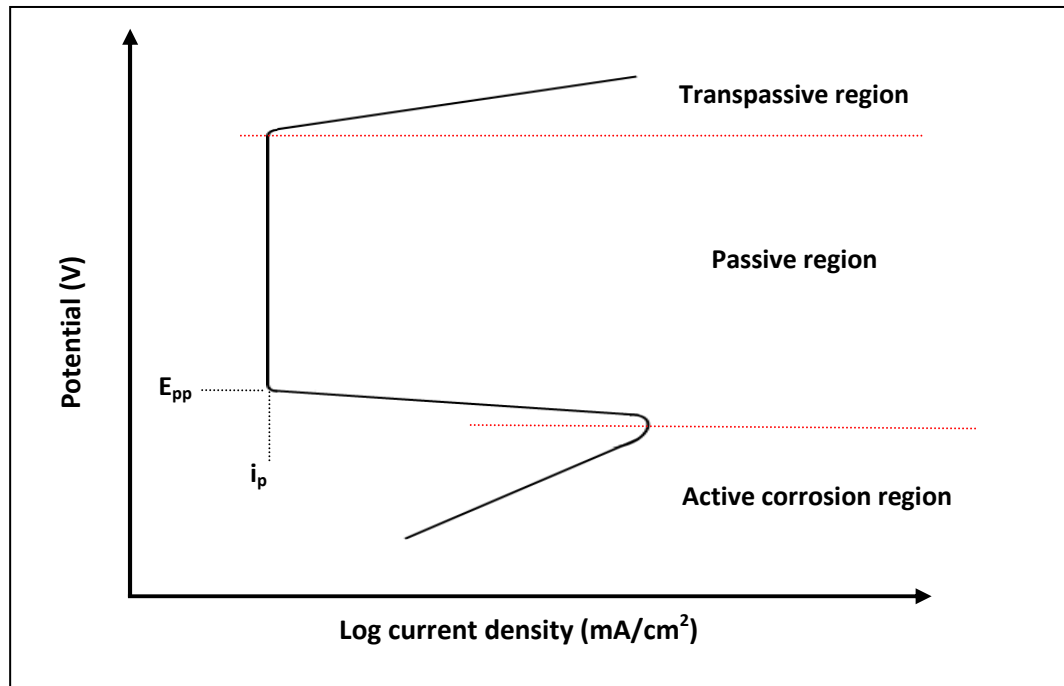
Figure 2-4 Schematic diagram showing current density vs. potential curve (anodic polarization curve) for metal with active, passive and transpassive potential range.

2.4 Corrosion of Stainless Steel

2.4.1 Introduction

Harry Brearley of the Brown-Firth research laboratory in Sheffield, England is credited as inventing stainless steel in 1913, [27]. Stainless steel alloys are commonly used as construction materials for key rust-resistant components in most of the major industries: chemical, construction, petroleum, power, process, etc.

Stainless steel is a general term for a large group of corrosion resistant alloy steels. These stainless steels are iron-based alloys containing at least 11wt% chromium [16]. This amount of chromium gives the stainless steel the ability to form a protective or passive film that resists corrosion. This protective film is self-forming and self-healing and is what makes stainless steel resistant to corrosion[28].

The stability of the passive film is enhanced by increasing the chromium content [29]. At about 10.5% chromium, a weak film is formed and will provide mild atmospheric protection. By increasing the chromium to 17-20%, which is typical concentration in the type 300 series of austenitic stainless steels, the stability of the passive film is much increased and therefore more corrosion resistant is gained. However, stainless steels cannot be considered to be 100% corrosion resistant. The passive state can be broken down under certain conditions and corrosion can result [30].

As stated above, stainless steel has a good corrosion resistance, but is not resistant to corrosion in all environments and might suffer from certain types of corrosion in some media. Corrosion of stainless steels can be categorised as one of: crevice corrosion, general corrosion, inter-granular corrosion, pitting corrosion, stress corrosion cracking and/or galvanic corrosion [48]. General and pitting corrosion are the most likely types of corrosion and most

relevant to our present study, so further information about these two types of corrosion will be provided in this thesis.

The general corrosion is a uniform attack and is the most commonly encountered type of corrosion. It is characterized by a chemical or electrochemical reaction which proceeds uniformly over the entire surface of the exposed material. This general corrosion happens where none of the alloying elements in the material could form a protective layer and normally this is the case during the active and transpassive dissolution of materials [49]. Thus, the metal becomes thinner and eventually fails.

The general corrosion of stainless steels normally occurs in acids and hot caustic solutions, and corrosion resistance of the stainless steel usually increases with increasing levels of chromium, nickel and molybdenum. Moreover, other alloying elements are added to the stainless steel alloys to modify their structure and enhance properties such as formability, strength and cryogenic toughness. Further information about the effects of alloying elements will be covered in the next section.

2.4.2 Effects of Alloying Elements

The properties of metals can be modified by adding alloying elements. In this way the properties of stainless steel can be adapted so it can be usefully

used in specific environments. Below is brief information about the benefits of each ingredient added to stainless steel [31]:

Chromium: is the main element that improves the corrosion resistance of the alloy by forming the passive film on the surface. Chromium provides resistance to oxidizing environments and also provides resistance to pitting and crevice attack. Other elements in the alloy can influence the effectiveness of chromium in forming or maintaining the surface film.

Nickel: is added to stabilize the austenitic structure of the stainless steel and enhance the mechanical properties and fabrication characteristics. Nickel also promotes re-passivation if the film is damaged.

Molybdenum: next to chromium, molybdenum provides the largest increase in corrosion resistance in stainless steel. Molybdenum, in combination with chromium, is very effective in stabilizing the passive film in the presence of chlorides. It is effective in preventing crevice or pitting corrosion.

Manganese: also stabilizes the austenite. In association with nickel it performs many of the functions attributed to nickel but by substituting manganese for nickel, and then combining it with nitrogen, strength is also increased.

 Nitrogen: is used to stabilize the austenitic structure of stainless steel. It enhances the resistance of stainless steel to pitting and crevice corrosion especially in presence of molybdenum [32].

Carbon: it increases the strength of steel and is considered as a very strong austenitizer. In low carbon grades stainless steels, carbon is kept in 0.005% to

0.03% level to maintain desired properties and mechanical characteristics. Carbon can combine with chromium forming chromium carbide precipitation usually at grain boundaries. This may have a negative effect on corrosion resistance by removing some of the chromium from solid solution in the alloy and, as a result, reducing the amount of chromium available to ensure corrosion resistance [31].

Titanium and Niobium: are used to reduce the sensitization of stainless steel to reduce the possibility of inter-granular corrosion when the stainless steel in welded or heat treated. Titanium and niobium interact with carbon to form carbides, leaving the chromium in solution so a passive film can form.

Copper and Aluminum: along with titanium, can be added to stainless steel to precipitate its hardening. These elements form a hard intermetallic microstructure during the soaking process at an elevated temperature.

Silicon: is added to some alloys for high temperature oxidation resistance.

Figure 2-5 summarized how these elements can influence the corrosion behaviour of stainless steel [33].
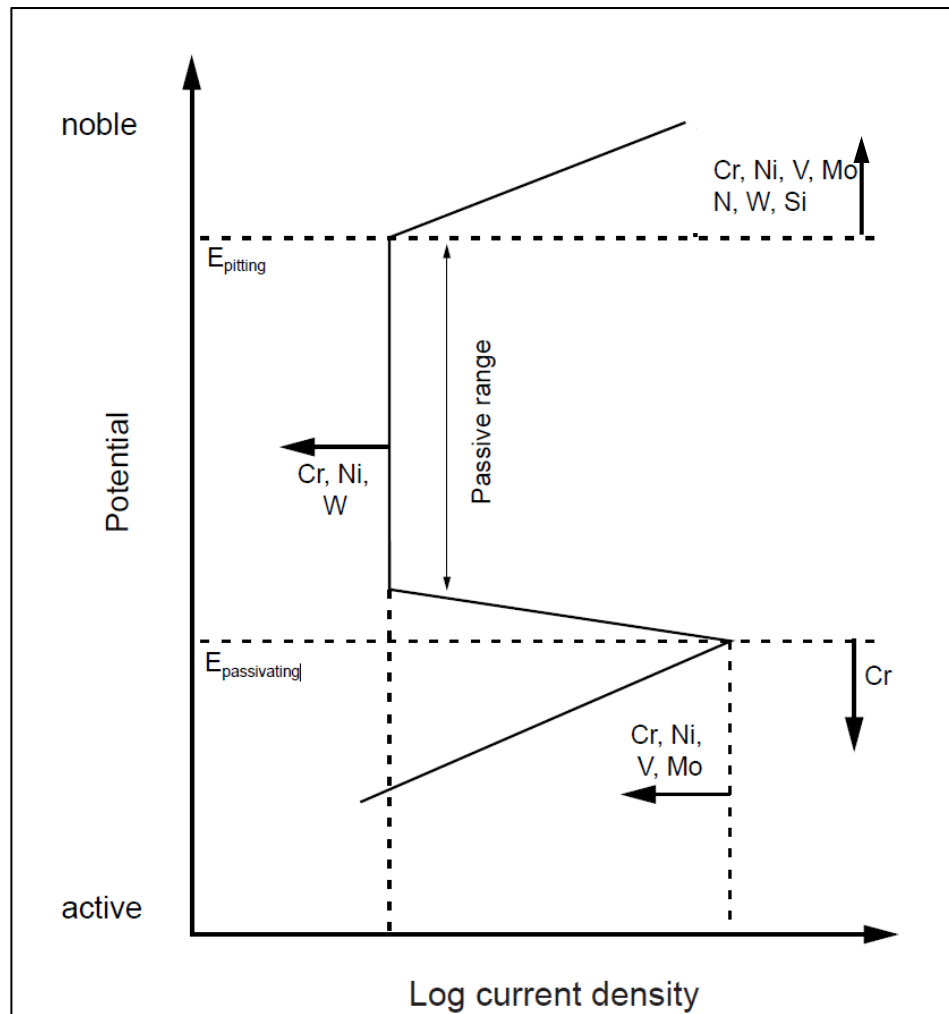
Figure 2-5 Schematic summary of the effects of alloying elements on the anodic polarization curve of stainless steel [33].

2.4.3 Stainless Steel Classifications

Stainless steels can be classified into five main groups according to their metallurgical structure [19, 33, 34]:

- Austenitic

- Ferritic

- Martensitic

- Duplex (austenite/ferrite) and

- Precipitation-hardening alloy

Schaeffler diagram as shown in Figure 2-6 is useful way to determine the likely structure of a stainless steel. This diagram is based on the presence of ferrite or austenite in the stainless steel in terms of nickel and chromium equivalents [35].

The chromium equivalent ($Cr_{eq.}$) has been determined using the most common ferrite forming elements [35]:

$$Cr_{eq.} = (Cr) + 2(Si) + 1.5(Mo) + 5(V) + 5.5(Al) + 1.75(Nb) + 1.5(Ti) + 0.75(W)$$

(2-23)

While the nickel equivalent (Nieq.) has likewise been determined with the familiar austenite forming elements:

$$Ni_{eq.} = (Ni) + (Co) + 0.5(Mn) + 0.3(Cu) + 25(N) + 30(C)$$ (2-24)

In this research, the two stainless steel alloys, 316L and 254SMO, which are considered as austenitic type, were used. Thus, this group, austenitic, of the stainless steels will be further described.
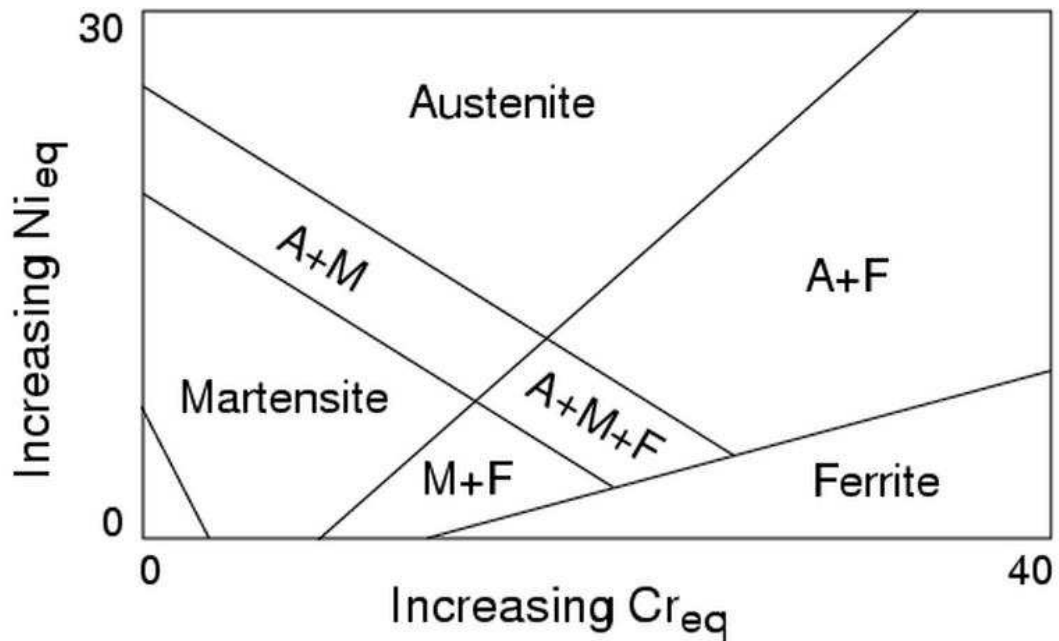
Figure 2-6 Schaeffler diagram, effect of alloying elements on the basic structure of Cr- Ni stainless steels [35].

2.4.4 Austenitic Stainless Steels

Austenitic stainless steels are the most widely used group of stainless steels. They are alloys containing iron (Fe) with 16-30% chromium (Cr), 8-25% nickel (Ni) and less than 0.15% carbon (C). These alloys have face-centred cubic (fcc) structures and they are nonmagnetic materials [36]. These stainless steels cannot be hardened by heat treatment [31].

Austenitic stainless steels appear to have significantly greater potential for aqueous corrosion resistance than their ferritic counterparts. This is because the three most commonly used austenite stabilizers, nickel, manganese and nitrogen all contribute to the passivity [37].

The alloys of this group of stainless steel have an excellent resistance to general corrosion. However in specific environments, they are highly susceptible to localized corrosion such as pitting, crevice corrosion and stress corrosion cracking.

The 300 series of austenitic stainless steels is widely used and accounts for about 50% of all stainless steel production[38]. Type 304 stainless steel is the basic (18Cr, 8Ni) austenitic stainless steel and grade 316 is the second most popular grade in the stainless steel family.

The 316 stainless steel has excellent corrosion resistance in a wide range of media. It offers much better resistance to pitting and crevice corrosion in environments having halide ions than the 304 stainless steel and this is due to the addition of $\approx$ 2.5wt% of molybdenum to the 316 alloy. The 316L stainless steel is mostly chosen to give better resistance to sensitisation in welding [39] where the letter "L" after the stainless steel type indicates low carbon (<0.03 wt %).

Other grades of austenitic stainless steel have different preferred applications. For example, in severe conditions, when the 316 stainless steel cannot resist the corrosivity of the environment, super austenitic stainless steels can be used. The super austenitic alloys have the same structure as the general austenitic alloys, though the superior strength and corrosion

resistance of these alloys are further improved by increasing the level of specific elements such as chromium, nickel, molybdenum, nitrogen and copper.

An example of these super austenitic alloys is 254SMO (elemental compositions is shown in Chapter 4) which contains higher quantities of chromium, nickel, molybdenum and nitrogen than common stainless steels, such as 316 [40]. The effect of these elements promotes a higher corrosion resistance of the alloy, especially in media containing halide ions [40-43]. Studies performed by De Micheli et al. [44, 45] showed that the corrosion resistance of 254SMO alloy in hydrochloric and phosphoric acid media with and without chloride ions is better than 316L stainless steel and almost the same as nickel-molybdenum-chromium alloy (Hastelloy-C276).

Also, Qvarfort [46] determined the critical pitting temperature of 254SMO to be about 89°C in 5 molar sodium chloride (NaCl) solution. Also, in 4%NaCl, the alloy critical pitting temperature and critical protection temperature been reported by Abd El Meguid et al. [47] to be 89 and 64°C respectively and these values decreased with increase of chloride concentration.

2.4.5 Pitting Corrosion

2.4.5.1 Introduction

Pitting corrosion is the most common form of localized corrosion that occurs in passive metals such as stainless steel alloys. Similar to other localized corrosion processes, pitting is also a multiple step process and is generally aggravated when the materials is exposed to halide solutions or to slightly acidic solutions that contain halide ions such as chloride and bromide [49]. The passive material can be perforated by pitting corrosion while most of its surface remains unaffected by corrosion. These pits can provide sites for crack initiation.

2.4.5.2 Mechanism and Stages of Pitting Corrosion

The mechanism of pitting corrosion had been widely studied in the literature. Almost all pits initiate at some chemical or physical heterogeneity at the surface such as an inclusion, second phase particles, mechanical damage, solute-segregated grain boundary or dislocation [50-52]. As the passive film or any another protective surface layer breaks down locally, pitting corrosion normally takes place. An anode forms where the film has broken, while the unbroken surface film acts as a cathode. In this case the localized attack will be accelerated and pits will develop at the anodic spot. The environment within the pit may become very aggressive which will further accelerate corrosion. A typical schematic for pitting corrosion process is presented by Figure 2-7 [53].

With pitting corrosion, shapes of pits vary widely and depend on the alloy and the environmental conditions, see Figure 2-8. They can be narrow and deep, wide and shallow, elliptical, collections of vertical or horizontal attack sites, subsurface or undercutting [29]. The pitting corrosion process can be divided into two main stages [54, 55]:

1. Pit initiation stage (passive film breakdown) and

2. Pit propagation stage.

Based on various experimental studies of the pitting process a number of theories have been developed to explain the first step of the pitting corrosion process (initiation stage). The most commonly used pit initiation theories are divided according to one of three main mechanisms: (1) film penetration, (2) adsorption mechanism or (3) film breaking mechanism [52, 56, 57]. Principally, pits in engineering alloys are most often associated with inclusions or second phase particles; however, the theories mentioned in this section were suggested based on pure metal systems. These mechanisms are schematically represented in Figure 2-9 [52, 56].

In the penetration mechanism, the aggressive anions migrate from the electrolyte into the passive film under the influence of the high electric field in the passive film. Thus, the film is contaminated by this anion. As a result of changes of the properties of the film, high current could start to circulate through the contaminated area and pitting would start [58]. Pit initiation by

film-breaking mechanisms considers that the thin passive film is in a continual state of breakdown and repair. Mechanical stresses at weak sites or flaws resulting from electrostriction and surface tension effects may cause local breakdown events, which rapidly heal in nonaggressive environments. However, according to this model, breakdown will only lead to pitting under conditions where pit growth is possible. However, in adsorption mechanism of pit initiation, aggressive anion adsorption at the outer side of the film and this will result in formation of cationic vacancies. The excess of vacancies at the metal/film interfaces will lead to the formation of voids exposing the bare metal surface to the electrolyte and pitting will initiate[59].

The second stage of the pitting process is the continued propagation of the resulting defect, in which an extreme local electrolyte composition and an extreme local rate of dissolution are coupled. Acidification and aggressive anions concentration within the pit are important factors to sustain the pit growth; the pH of the local pit environments is decreased due to the hydrolysis of the dissolving metal cation. Whereas, anions such as chloride are concentrated into the pit from the external solution by electromigration due to the potential gradient that develops as result of the ohmic potential drop along the current path between the inside of the pit and the cathodic sites on the outside surface. In the presence of halide inions, the solubility of the metal cations, which are produced by dissolution, in the pit is higher which is further enhancing pit growth. In the propagation stage, a pit may

propagate and grow for a short period before repassivating and die (this type of pit is called a metastable pit), or it may continue to propagate indefinitely (called stable pitting) [54, 60]. Metastable and stable pits, when monitored by electrochemical polarization measurement are demonstrated in Figure 2-10 [61].
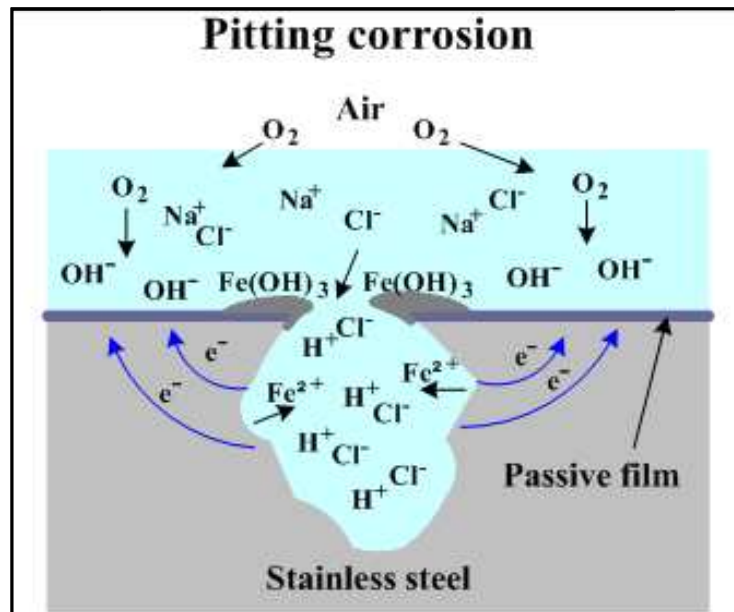
Figure 2-7 Schematic diagram illustrates the pitting corrosion [53].
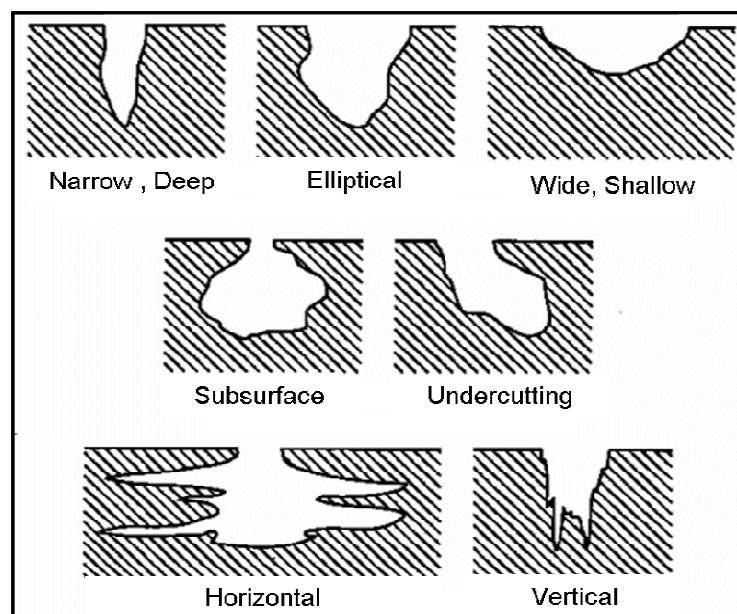
Figure 2-8 Schematic representation of different pitting corrosion shapes [29].
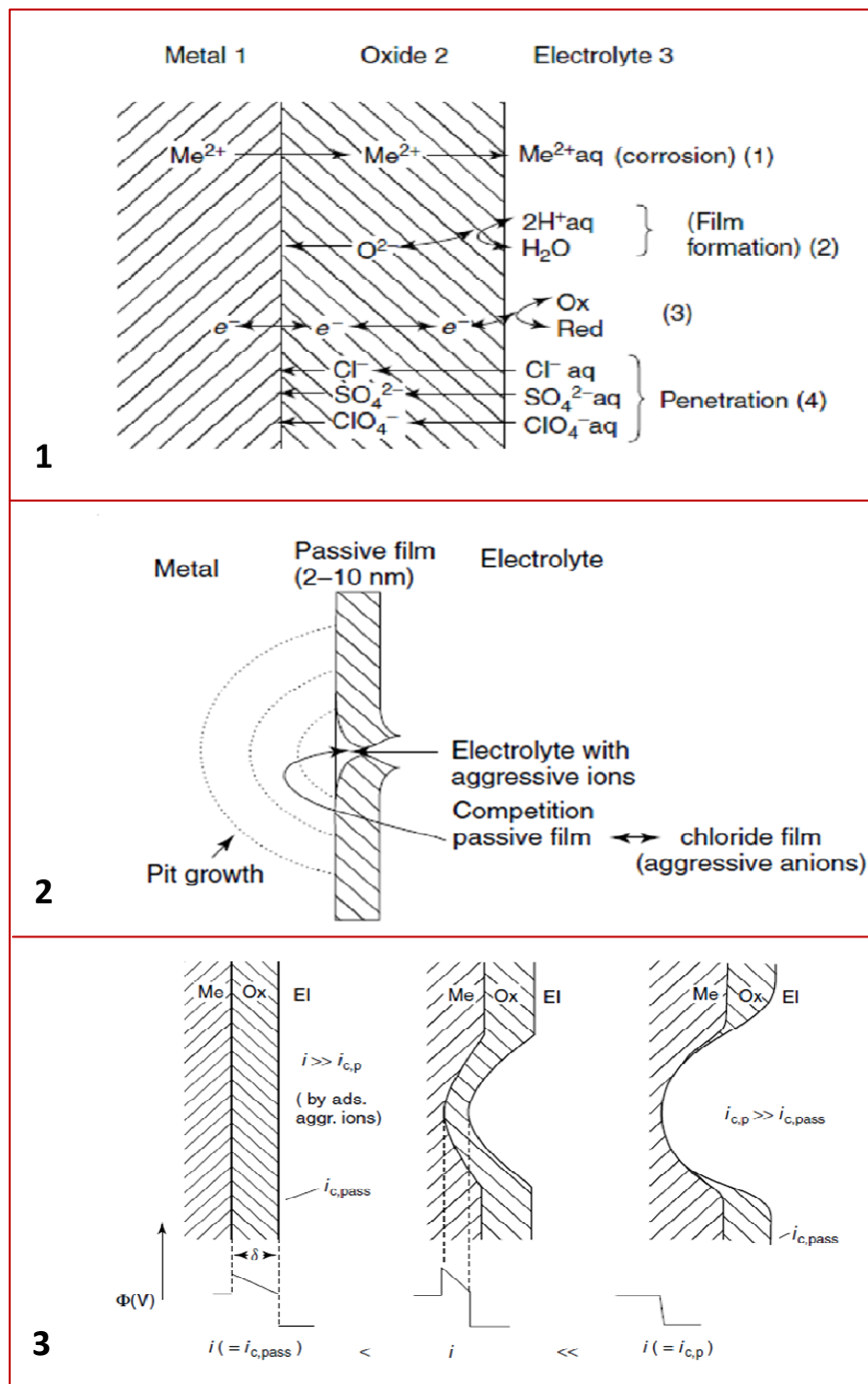
Figure 2-9 Schematic diagram demonstrating the three mechanisms leading to the breakdown of passivity and pit nucleation:(1) penetration mechanism, (2) film-breaking mechanism and (3) adsorption mechanism [52].
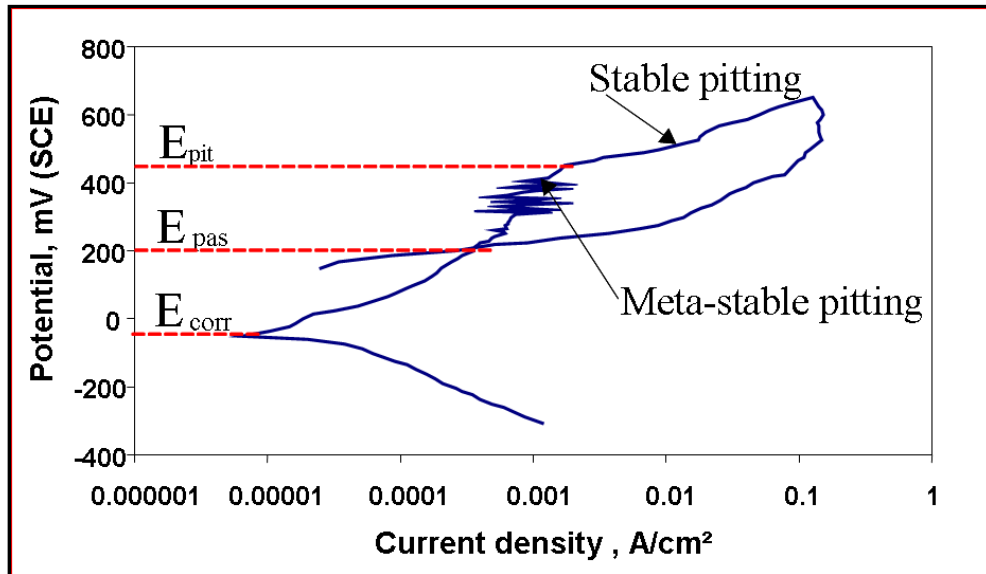
Figure 2-10 Polarisation curve of 316 stainless steel tested in 0.1M NaCl solution showing the metastable and stable pits in the process of pitting corrosion [61].

2.4.5.3 Factors influencing pitting corrosion:

Influences of the main environmental variables on pitting corrosion of 300 series stainless steels have been discussed by Uhlig et al. [62]. It was concluded that pitting potential (the lowest potential where the pitting corrosion can start but below this value, no pitting corrosion will initiate) is increased with decreasing chloride concentration, decreasing temperature and increasing pH or concentration of non-chloride anions such as sulphate.

As well, investigations carried out on the effect of the chloride ion (Cl⁻) concentration, pH, dissolved oxygen and temperature on the pitting behaviour of 316L stainless steel in aqueous solutions [63] found that the

number and depth of pits increase with increasing Cl⁻ concentration. Also it was established that low pH, high Cl⁻ content and stagnancy are the conditions most suitable for initiation and propagation of pitting in 316L stainless steel.

Chloride ions are considered as the most common cause of pitting with stainless steel [64, 65]. Abd Elaal [66] studied the aggressiveness of pitting caused by halide ions in terms of pitting potentials and found at a constant aggressive anion concentration, the aggressiveness to be in the order of chloride > bromide > iodide for stainless steels under different experimental conditions and alloy compositions.

One of the most critical factors in pitting corrosion is the temperature. Some materials will not undergo pitting corrosion at a temperature below a certain value called the critical pitting temperature (CPT) [46, 67]. The effect of temperature on pitting corrosion of a specific material can be determined either by changing the temperature at a range of constant applied potentials (potentiostatic test) or varying the potential for a range of constant temperature experiments [68-70] At low temperatures, a very high breakdown potential is observed and this potential corresponds to transpassive dissolution not to pitting corrosion [71]. However, above the critical pitting temperature, the pitting corrosion occurs at a potential that is far less than the transpassive breakdown potential [72, 73].

Generally, the pitting potential becomes less noble, decreasing with increasing temperature and aggressive ion concentration such Cl⁻ or Br⁻ [71, 72, 74-77], as seen in Figure 2-11, where the pitting potential of 304 stainless steel alloy decreases as the temperature increases [78]. Such behaviour occurs because with increase in temperature, the number of locally limited defects in the film will increase and there will also be an increased tendency for the oxide film to incorporate the aggressive ions [79, 80].

Similar to pitting potential, the CPT can be used as a means for ranking susceptibility of the material to pitting corrosion and the alloy with higher CPT is considered more resistant to pitting corrosion [81, 82].

Another important parameter to be considered when determining susceptibility of stainless steel to localized, pitting, attack especially in chloride environments is the solution (electrolyte) velocity. Generally, slightly slow velocity of the solution tends to make conditions more uniform on surface of the metal and this will tend to make corrosion uniform and prevent the local attack [83]. Austenitic stainless steels, such as 304 and 316, will suffer less pitting corrosion when the velocity of the solution is increased. An approximate velocity of greater than 1.5 m/s is recommended to avoid pitting corrosion, this is called the critical velocity and it is supposed that, a velocity above 1.5 m/s discourages accumulation of non

protecting corrosion product in the system and thus the occurrence of localised corrosion such as pitting or crevice corrosion will reduced[84-86]. It should be emphasis, the high velocities that may cause a mechanical damage to the protective films and accelerates attack by erosion corrosion and cavitation erosion is excluded in this discussion.
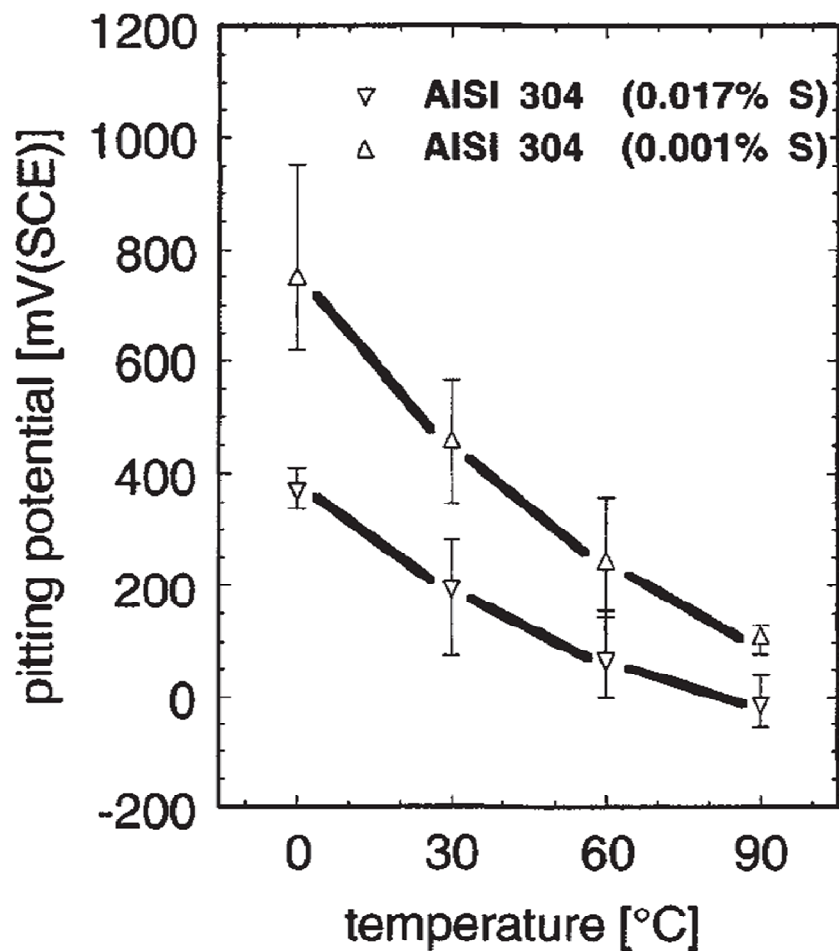
Figure 2-11 Effect of temperature on the pitting potential of 304 stainless steel (with different sulphur content) in 0.1M NaCl [78].

2.4.5.4 Effects of MnS Inclusion

In order to prevent the formation of iron sulphide (FeS) along grain boundaries which is a problem that occurs in the steel production process, manganese (Mn) is added to steels to segregate sulphur as manganese sulphide (MnS). This MnS is thermo-dynamically much more stable than FeS and has a much higher melting temperature [55]. However, the control of the density and size of the inclusions has a critical effect on pitting corrosion initiation in most commercial engineering alloys, especially stainless steel [87, 88].

The role of MnS inclusions in promoting passivity breakdown and localized corrosion of stainless steels has been well known and documented for some time [89, 90]. Pitting was observed to occur at or adjacent to MnS inclusions and explanations have focused on dissolution products of the sulphides. It has been suggested that sulphides oxidize to form sulphate and acid [89], elemental sulphur or thiosulfate [90] and that these inclusions may also chemically dissolve to form hydrogen sulphide, H_2S [88, 89].

Figure 2-12 shows schematic diagram originally presented by Ryan et al. [91]. It provides an illustration of a possible pitting corrosion process of stainless steel in the presence of inclusions. This diagram is divided to two possible cases, (a) dissolution of the inclusion (MnS) or (b) chromium (Cr) depletion. For case **a**, at the first step (1), high rate electrochemical

dissolution of MnS inclusions has taken place as described by Williams et al. [92]. This dissolution will give rise to sulphur capped occluded zone at step (2) within which sulphide and chloride rich acidic solution could develop through further dissolution of the inclusion. In such solution, the stainless steel is unstable [88] and thus, the parent metal dissolves and the pit develops by undercutting the metal surface as shown in step (3).

However, for case **b,** in the same diagram**,** it is shown that chromium (Cr) depletion of the parent metal around the inclusion, as shown in (4), that can be related to the thermodynamics of interaction between sulphide and metal during the steel manufacturing process as supported by Williams et al. [93]. They found pits initiated by dissolution of the chromium depleted area around the MnS inclusions. This dissolution can create an acidic environment by hydrolysis of the dissolving metal cations, within which the inclusion is unstable resulting in high rate electrochemical dissolution of the inclusion, and the subsequent breakdown of the steel beyond the chromium depleted zone. Webb et al. [94] had shown that narrow trenches were formed at the edge of sulphide inclusions prompted by the pitting corrosion. Hence the high rate of the inclusion dissolution, which triggers the final breakdown, is started.
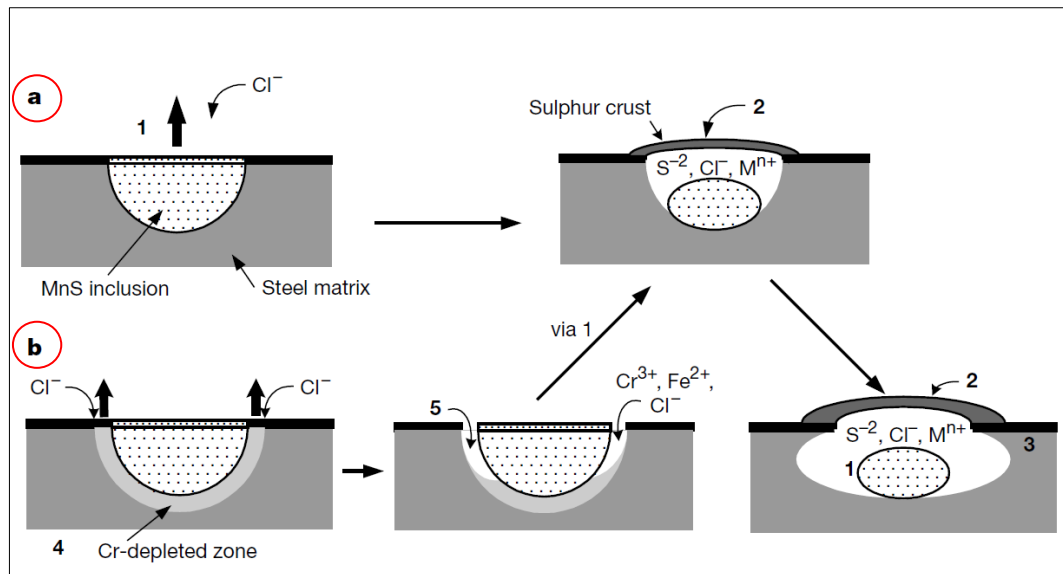
Figure 2-12 Schematic diagram that illustrates the start of pitting corrosion process of stainless steel in presence of inclusions [91].

2.4.5.5 Pitting Resistance Equivalent Number (PREN):

To quantify the effect of alloying elements on the pitting resistance of the stainless steels alloys, Pitting Resistance Equivalent Number (PREN) can be used and this number can give a good indication of the pitting resistance of stainless steels based on their compositions. However, the PREN cannot be used to predict whether a particular grade of materials will be suitable for a given application where pitting corrosion may be a hazard. The most commonly used formula to calculate the PRE value is [95-98].

$$PRE = \%Cr + 3.3 \times \%Mo + 16 \times \%N \qquad (2\text{-}25)$$

Other formulas give greater weight to nitrogen, with factor of 27 or 30. But because nitrogen level is relatively modest in most of stainless steels alloys this factor does not have a dramatic effect on ranking. From the formula, it is clear that grades with high chromium, molybdenum and nitrogen content are more resistant to pitting corrosion.

2.5 Corrosion by Acetic Acid

2.5.1 Introduction

Acetic acid (CH_3COOH) is one of the most important intermediates and the most frequently used carboxylic acid. When pure, acetic acid is a clear, colourless liquid with the smell of vinegar. At ambient temperature, 25°C, the pure acetic acid boils at 118°C and its freezing point is only slightly below room temperature at 16.7°C [99].

Acetic acid is classified as a weak acid, because it does not completely dissociate into its component ions when dissolved in aqueous solution [100]. Acid dissociation constant (Ka) is a quantitative measure of the strength of the acid in solution. It is equal to the concentration of the products divided by the concentration of reactants. For the acetic acid it can be written as:

$$CH_3COOH \ (aq) \longrightarrow CH_3COOH^- (aq) + H^+ (aq)$$
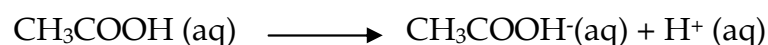
$$Ka = [CH_3COO^-] * [H^+] / [CH_3COOH] \qquad (2\text{-}26)$$

The acid dissociation constant (Ka) value for acetic acid is 1.8×10^{-5} (mol/L) at 25°C.

2.5.2 Corrosivity

In general terms, carboxylic acid aggressiveness increases with decreasing number of carbon atoms in the alkyl chain [101, 102]:

$$C_4H_9COOH < C_3H_7COOH < C_2H_5COOH < CH_3COOH < HCOOH$$

Usually, acetic acid is not considered to be a highly aggressive medium, however it can severely attack most materials at higher temperatures, near its boiling point, upon aeration and if it contains impurities, for example oxidizing agents, chlorides, formic acid or acetic anhydride [33].

In acetic acid systems, steel is attacked quite rapidly at all concentrations and temperatures and is normally unacceptable for use in acetic acid environment. Also, field experience with the 400 series stainless steel group indicates high rates of corrosion and pitting attack [103]. However, the 304 stainless steel alloy can be used to handle glacial acetic acid to a temperature of about 80°C and it has been satisfactory for lower concentrations up to the boiling point of the acid.

The 316 stainless steel alloy is most commonly used in equipment processing acetic acid. However, the behaviour of this alloy is greatly affected by impurities in the acid. Contamination with chloride ions can cause pitting, rapid stress corrosion cracking and accelerated corrosion of 316 stainless steel [104]. Similar to chloride, also presence of other halides such as bromide (Br) in the acetic acid environment may lead to corrosion problems for stainless steel alloys [105].

A number of field failure investigations and laboratory studies carried out on 316 stainless steel type in acetic acid environments have been reported in the open literature. Some of those studies were dealing with corrosion problems in terephthalic acid production plant where acetic acid solution is used as solvent.

Sekine *et al.* [106, 107] worked extensively on the corrosion behaviour of stainless steels in different concentrations of acetic acid. They concluded that the corrosion rate depends markedly on concentration, temperature, solution conductivity, water and oxygen content. It was found that 316 stainless steel had sufficient corrosion resistance at room temperature in each acid concentration. At boiling acetic acid, a maximum corrosion rate of 0.09 mm/year was measured for the 316 stainless steel and that was in 90 vol. % acid concentration. Also, they concluded that chromium and molybdenum mainly contribute to corrosion resistance in aqueous solution, while nitrogen

contributes only slightly. With the presence of aggressive ions such as chloride and bromide in the acetic acid environments Ashiru et al. reported severe pitting corrosion problems occurred in terephthalic acid production plant[108]. The materials of construction were 316L stainless steel and 2205 duplex stainless steel. It was concluded that the pitting corrosion was caused by process upset and the presence of aggressive chloride contaminant in the acetic acid media. Also, Li et al. [109] reported relatively serious intergranular corrosion and pitting in 316L stainless steel packing of a solvent recovery tower in a terephthalic acid plant. Inter-granular corrosion attack was due to the lack (depletion) of chromium in the grain boundaries while the pitting problem was caused by the damage to the local passivation film due to the presence of bromide ions in the acetic acid solution.

Turnbull et al. [110] investigated corrosion and electrochemical behaviour of 316L stainless steel in conditions typical of the process environments in terephthalic acid plant (aerated 70% and 90% acetic acid containing 1500 ppm Br ions at 90°C). A step increase in potential was noticed after about 30 hours of exposure in 70% acetic acid, indicative of formation of a protective film and passivation. No passivation was observed in the aerated 90% acetic acid base solution or when chloride was present in the 70% acetic acid base solution. Moreover, pitting corrosion and uniform corrosion behaviour of austenitic stainless steel (316L type) and duplex stainless steel (SAF 2205 type) in bromide containing acetic acid at various temperatures and bromide

concentrations were investigated by Bin et al. [111]. With increasing temperature and bromide concentration, the corrosion rate of 316L and SAF 2205 increased, and the pitting corrosion became more severe. The corrosion rate of 316L rapidly decreased with increasing exposure time, while the corrosion rate of SAF 2205 slowly increased. Also, it was noticed that the corrosion rate of 316L and SAF 2205 stainless steels slightly reduced after 72 hours. As well, the author concluded that, Cl^- was more aggressive than Br^- in 80% acetic acid solution at 80°C.

Furthermore, results of a study conducted on different stainless steels and nickel-based alloys in 50% acetic acid solutions containing 0.29M bromide ions showed that materials suffered serious general corrosion, and some alloys with very low molybdenum content rapidly suffered pitting attack [112]. However, the alloys with higher molybdenum content showed excellent pitting resistance. It was concluded that chromium and molybdenum could form a passive film that can protect the materials from the aggressive ions. Additionally, stainless steel corrosion behaviour in acetic acid environments containing halides other than chloride and bromide was considered in some of the literature. The corrosion behaviour of 316 stainless steel has been investigated in dilute acetic acid solutions (0.1M) containing fluoride ions (F^-) at 25°C [113]. The results showed that low concentrations of F^- ion (less or equal to 0.001M NaF) have no significant influence on the passivity of the 316 stainless steel. However, the passivity was reduced by

high concentrations of F$^-$ ions (0.1M NaF). During the anodic polarisation, the iron (Fe) component was selectively dissolved from the stainless steel into the solution and oxide films containing fluoride ions, F$^-$, formed on the surface.

2.6 Passive Films of Stainless Steels

Excellent corrosion resistance of the stainless steels alloys is due to the protective passive film with thickness of few nanometres that forms on the surface of the alloy [114, 115]. This film acts as a barrier separating the alloys surface from the corrosive environments however, the film changes with the surrounding environment thus, it can grow or dissolve, and may absorb/adsorb anions [116].

One of the important factors controlling the properties (composition, protectiveness, thickness) of the passive film is the composition of the alloy. Various studies attempting to characterise: (1) the film structure, layers (2) composition (3) chemical states of the elements (4) distribution of the species in the film and (5) thickness of the passive films formed on different types of stainless steel have already been reported. A general agreement in the previously studies is that chromium and molybdenum have a more significant influence on the stainless steel passive film formation than the other alloying elements.

The passive surface films described in this part of the thesis were evaluated by means of the X-ray photoelectron spectroscopy (XPS) and/or Auger electron spectroscopy (AES). Some observations and findings of these studies will be briefly described below.

Basically, the passive film formed on the stainless steel consists of chromium oxide and/or hydroxide[117-120]. Also, there is significant evidence suggesting a dual structure consisting of an inner oxide and an outer hydroxide layer[121-123].

The passive films formed on pure chromium and Fe-Cr alloy in sulphuric acid (0.5M H_2SO_4) were described by a bilayer structure model[117, 118]. The authors postulated that the passive films consisted of a mixed chromium Cr (III) and Fe (III) oxide inner layer enriched with Cr_2O_3 and a chromium hydroxide, Cr (OH)₃, outer layer. Similar findings were observed by Keller and Strehblow [119] for electrochemically formed passive layers on Fe-Cr stainless steel alloy in 0.5M H_2SO_4 solution. However, in the transpassive potential range a change in the layer composition was observed, the outer part of the transpassive layer is formed predominantly by Fe (III) species whereas the inner part still contains a strong enrichment of Cr_2O_3. In a study by Marcus et al. [120] for similar alloys in the same environment (0.5M H_2SO_4) the analyses clearly showed chromium enrichment in the passive films formed on the surface of these alloys.

It is well known that molybdenum in stainless steels has a strong beneficial influence on the corrosion resistance especially for pitting corrosion [116, 124]. Though, Mo did not always show beneficially effects in lessening the pitting corrosion in Br containing solutions. Previous study by H. Isaacs et al. [65] comparing the effects of Mo on the pitting in the chloride and bromide solutions suggested that, Mo is dramatically increase the pitting resistance in solution containing chloride but to a much smaller extent in solution containing bromide.

Studies have attempted to determine the role of molybdenum in improving the properties of the surface passive film that leads to higher corrosion resistance of stainless steels in different media[123-127]. A number of these studies have verified the presence of molybdenum (VI), particularly in the outer regions of the passive film [124, 126], and molybdenum (IV) has been identified in the inner parts of the film in some of these studies[123].

It was noticed that the main difference in the corrosion behaviours of the Fe-Cr and the Fe-Cr-Mo alloys examined in 0.5M H_2SO_4 was the decrease in dissolution rate in the active region of the alloy with molybdenum and that was confirmed by the electrochemical behaviour [120]. Furthermore, it has been concluded that additions of 2.5 wt% molybdenum to Fe-19Cr-9Ni alloy in 0.1M hydrochloric acid, resulted in the formation of a passive film with

interfacial barrier film composed mainly of Cr_2O_3 [123]. Molybdenum was present as molybdenum (IV) and molybdenum (VI). It was proposed that MoO_4^{2-} anions were formed in the solid state along with CrO_4^{2-}, which together are responsible for producing a bipolar film consisting of a cation selective outer layer containing CrO_4^{2-} and MoO_4^{2-} and an intrinsically anion selective inner layer.

From the study conducted by Olsson et al. [128], an example of the concentration gradients of molybdenum in a passive film on a stainless steel is given in Figure 2-13. The figure illustrates the angular dependency of different oxidation states of molybdenum in the passive film after immersion the 254SMO alloy (with 6.0wt% Mo) in a ferric chloride solution. An increment in the molybdenum (VI) concentration on the outer surface of the passive layer while molybdenum (IV) remained underneath was confirmed by angles surface analysis. There are two possible hexavalent states: MoO_3, which is soluble in acidic electrolytes and MoO_4^{2-} which shows a higher stability.
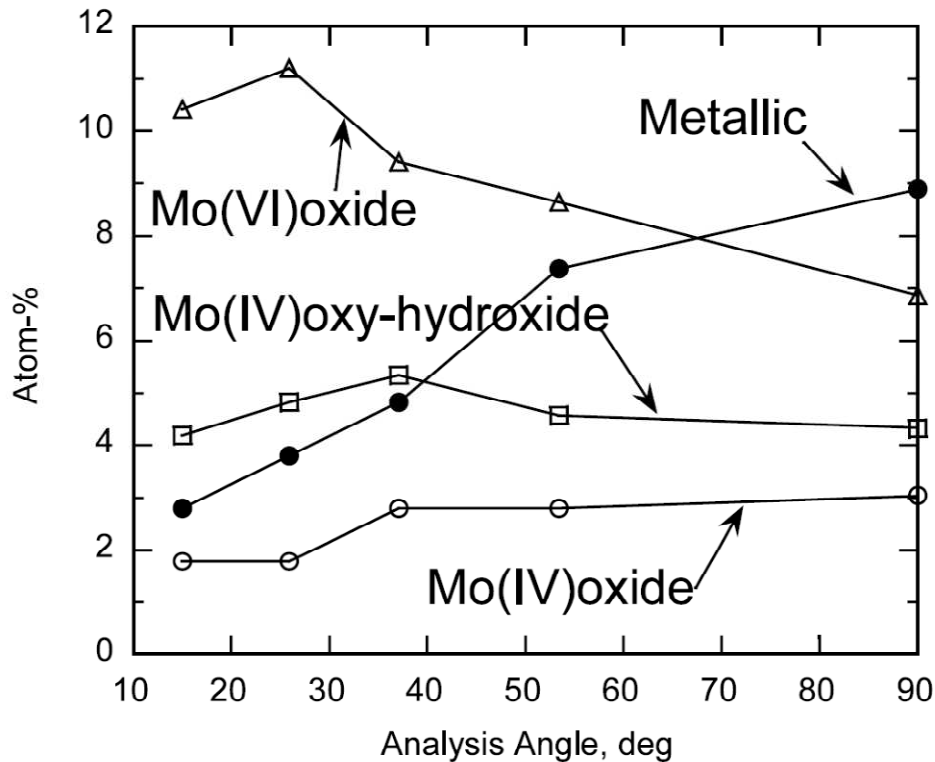
Figure 2-13 Concentration gradients in a passive film for molybdenum, recorded for a 6Mo superaustenitic stainless steel after immersion in ferric chloride using XPS. For angles close to grazing, there is a strong contribution of Mo (VI), whereas metallic Mo dominates for angles close to perpendicular. The IV-valued oxide and oxy-hydroxide states show less angular dependence [128].

Also, the beneficial effects of molybdenum on the passivation of ferritic stainless steels in 1M HCl were studied by Hashimoto [125] who suggested that molybdenum eliminated the active sites, which hindered stable passive film formation, through the formation of molybdenum oxy-hydroxide or molybdate (Cr or Fe molybdate) on these active sites and this may have led to the formation of a homogeneous passive film. In addition, the presence of molybdenum (VI) in the outer region of the passive layer was demonstrated when austenitic stainless steels with more than 2 wt% molybdenum were tested in 30% sulphuric acid solutions [127]. It was concluded that

molybdenum appears to improve the corrosion resistance of the stainless steels by modification of passive film composition and modification of active dissolution by formation of insoluble oxides.

The pH of the environment where the passive film is structured also has an important influence on the properties of this film. The dissolution rate of the film is lowered with increasing pH which leads to a thicker passive film and a larger fraction of iron in the film, as iron oxides are more stable in basic solutions. Such effects on the passive layer of Fe-Cr alloys have been studied by Strehblow et al. [129, 130]. The films were found to be thicker in basic solutions. In addition, there was a marked increase of the amount of Fe (III) oxide. The cationic fraction of Cr, Fe, Mo and Ni in the passive film formed on the surface of 254SMO tested in 3.5% NaCl solution with two different pH values (pH 5 and 0.8) was evaluated by Liu et al. [131] as demonstrated in Figure 2-14. The results indicate that the primary component of the outermost layer of the films in strong acid solutions (pH 0.8) was Cr (OH)$_3$ and the inner layer was Cr$_2$O$_3$ while in the weak acid (pH 5) iron oxide was the main constituents of the passive film. Molybdenum oxides exist in the passive film in the form of a bi-layer with outer molybdenum (VI) rich layer and inner molybdenum (IV) rich layer. Further, in the weak acid (pH 5) solution, a small quantity of nickel oxidized species also exists in the passive film.
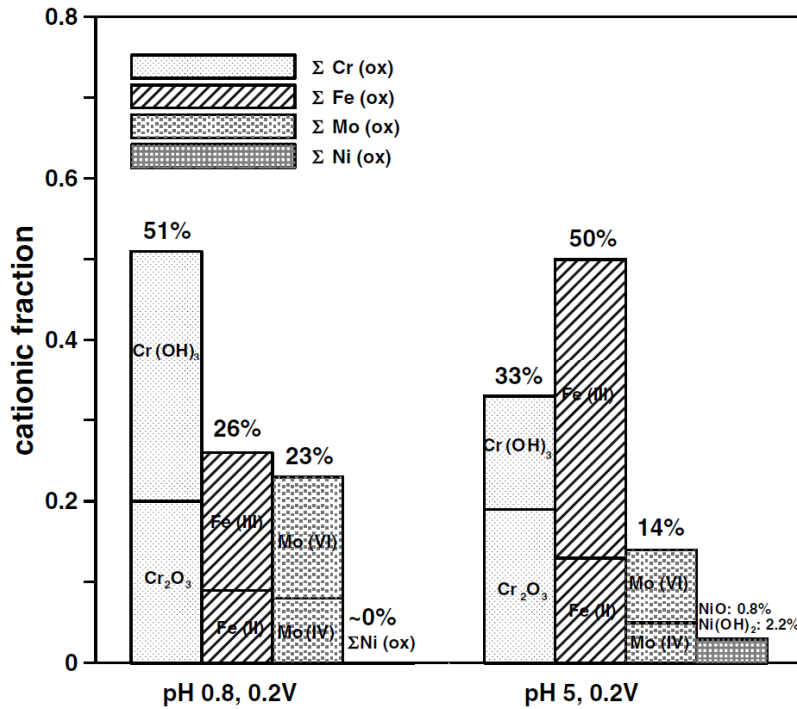
Figure 2-14 XPS cationic fraction (Cx) in the passive film of 254SMO stainless steel after passivation at 0.2V (SCE) in the 3.5%NaCl solaution with pH 0.8 amd 5 [131].

Temperature of the environment also can alter composition and thickness of the passive film. The effect of temperature on the passive film formed on Fe-Cr-Mo alloys was studied by Mischler et al. They observed slightly thicker films at 65°C when compared to room temperature [132]. As well, the temperature effect on film thickness for a 6.0wt% Mo stainless steel has been quantified by Wegrelius and Olefjord using XPS [133]. They compared film formation at 22 and 65°C in an acidic chloride solution. The film was found to be only 2 A° thicker for the higher temperature. On contrast, Jin et al. found no differences in composition and thickness between passive films formed at room temperature and at 90°C in a 0.5 M sodium chloride solution [134].

There are relatively few investigations concerning the passive surface film of stainless steel in acetic acid environments. Sekine et al. [106, 135] worked on the corrosion behaviour of stainless steels in acetic and formic acids. They concluded that chromium and molybdenum mainly contributed to corrosion resistance in aqueous acetic acid solution. Turnbull [110] reported an increase in the corrosion potential to more noble values after an exposure time of 30 hours for 316L stainless steel in 70% acetic acid solution containing bromide ions at 90°C. It was concluded that this was due to the formation of a protective film and passivation due to local enrichment of Mo.

Liu et al. [124] tested different stainless steels and nickel-based alloys in 50% acetic acid solutions containing 0.29M bromide ions. Alloys with higher molybdenum content showed excellent pitting resistance due to a protective film of Cr oxide (Cr_2O_3) and molybdenum dioxide (MoO_2) being formed which protected the materials from the attack of aggressive ions. Cheng [136] studied the passive film formed on 2205 stainless steel in 60% acetic acid solution containing chloride ions at 85°C. It was found that about 50% of the top surface of the passive film was Cr cations when the potential is in the passive region, while if potential is higher than the transpassive potential, the molybdenum content accounted about 45% of the metal cations in the near-surface region.

2.7 References

1.   *New Mexico Water and Infrastructure Data System, Corrosion Pages*. [cited 2010; Available from: http://octane.nmt.edu/waterquality/corrosion/corrosion.htm.

2.   Schmuki, Patrik, *From Bacon to Barriers: A Review on the Passivity of Metal and Alloys.* Journal of solid state electrochemistry, 2002. **6**(3): p. 145-164.

3.   Jones, Denny A., *Principles and Prevention of Corrosion*. 2nd ed. 1996: Prentice Hall, NJ

4.   Uhlig, R. Winston Revie and Herbert H., *Corrosion and Corrosion Control-an Introduction to Corrosion Seince and Engineering*. 4th ed. 2008 New jersey, USA: John wiley & sons,Inc.

5.   Fontana, M. G., *Corrosion Engineering*. 3rd ed. 1987: McGraw-Hill.Inc., singaporw.

6.   R. Sandoval-Jabalera, E. Arias-del Campo, J.G. Chacón-Nava, J.M. Malo-Tamayo, J.L. Mora-Mendoza, and A. Martínez-Villafañe, , *Corrosion Behavior of Engineering Alloys in Synthetic Wastewater.* Journal of Materials Engineering and Performance, 2006. **15**(1): p. 53-58.

7.   Scully, J.C., *The Fundamentals of Corrosion*. 2nd ed. 1975.

8.   Buchanan, E. E. Stansbury and R., *Fundamentals of Electrochemical Corrosion*. 2000: ASM International.

9.   Tullmin, N. Rothwell and M., *The Corrosion Monitoring Handbook*. 1st ed. 2000: COXMOOR Publishing Company.

10.   Puigdomenech, B. Beverskog and I., *Revised Pourbaix Diagrams for Chromium at 25–300 °C* Corrosion Science, 1997. **39**(1): p. 43-57.

11.   Pourbaix, Marcel, *Some Applications of Potential-Ph Diagrams to the Study of Localized Corrosion* Journal of electrochemical society 1976. **123**(2): p. 25C-36C.

12.   Roberge, Pierre R., *Corrosion Engineering, Principles and Practice*. 2008: The McGraw-Hill Inc.

13.   Baumeister, E. A. Avallone and T., *Marks Standard Handbook for Mechanical Engineers*. 10th ed. 1996: McGraw-Hill companies Inc. chapter 6, p96.

14.   Uhig H.H., R.Revie *Corrosion and Corrosion Control-an Introduction to Corrosion Seince and Engineering*. 4th ed. 2008 New jersey, USA: John wiley & sons,Inc.

15.   *Mixed Potential Theory*, in *Electrochemistry and Corrosion Science*, Nestor Perez, Editor. 2004, Springer, US.

16.   Sedriks, A. John, *Corrosion of Stainless Steels*. 1979: John Wiley & Sons, Inc. , New York.

17.   Traud, C. Wagner and W., Zeitschrift fur Electrochemie, 1938. **44**(391).

18.   Kruger, J., *Passivity*, in *Uhlig'S Corrosion Handbook*, R. Winston Revrie, Editor. 2011, John Wiley & sons, Inc. p. 151.

19.   Qiu, J. H., *Passivity and Its Breakdown on Stainless Steels and Alloys.* Surface and Interface Analysis, 2002. **33**(10-11): p. 830-833.

20.   Robert Kelly, John Scully, David Shoesmith and Rudolph Buchheit, *Electrochemical Techniques in Corrosion Science and Engineering*. 2003, New York Marcel Dekker, Inc.

21.   NACE/ASTM G193-10b, Standard Terminology and Acronyms Relating to Corrosion, 2010.

22.   Jan Olsson and Rolf Qvarfort, Avesta Polarit AB, *Transpassive Corrosion of High Alloy Stainless Steels and Nickel Base Alloys*, in *Corrosion*. 2002, NACE International Denver, Co, paper No. 02133.

23.   M. Graham, J. Bardwell, G. Sproule, D. Mitchell and B. MacDougall, *The Growth and Stability of Passive Films* Corrosion Science, 1993. **35**(1-4): p. 13-18.

24.   Landolt, Gerald Frankel and Dieter, *Fundamentals of Corrosion*, in *Encyclopedia of Electrochemistry*. 2007.

25.   Hoar, T. P., *The Production and Breakdown of the Passivity of Metals.* Corrosion Science, 1967. **7**(6): p. 341-355.

26.   Kruger, J., *Passivity*, in *Uhlig'S Corrosion Handbook*, R. Winston Revrie, Editor. 2000, John Wiley & sons.

27.   *Stainless Steel ,from Wikipedia, the Free Encyclopedia*.   [cited 2011; Available from: http://en.wikipedia.org/wiki/Stainless_steel.

28.   Schweitzer, Philip A., *Corrosion Engineering Handbook ,Fundamentals of Metallic Corrosion , Atmospheric and Media Corrosion of Metals*. 2nd ed. 2007: Taylor and Francis Group LLC.

29.   H. S. Khatak , Baldev Raj, *Corrosion of Austenitic Stainless Steels, Mechanism, Mitigation and Monitoring*. 2002: alpha science international.

30.   Leif Karlsson, *Stainless Steels Past, Present and Future, .* 2004 ESAB AB, Gothenburg, Svetsamn p. 47-52.

31.   Cunat, Pierre-Jean, *Alloying Elements in Stainless Steel and Other Chromium-Containing Alloys*. 2004, International Chromium Development Association : http://www.euro-inox.org/pdf/map/AlloyingElements_EN.pdf.

32.   Martian, James W., *Chapter 51-Stainless Steel*, in *Corrosion Testing and Standards Manual*. 2005, ASTM International.

33.   R.Roberge, Pierre, *Handbook of Corrosion Engineering*. 2000: McGraw-Hill.

34.   *Stainless Steel by Metallurgical Consultants*. 2007 [cited 2011]; Available from: http://www.materialsengineer.com/E-Stainless-Steel.htm.

35.   Sourmail, T. *Stainless Steels*.   [cited 2011 February]; Available from: http://www.thomas-sourmail.org/stainless/index.html.

36.   McGuire, M. F., *Austenitic Stainless Steels.* Encyclopedia of Materials: Science and Technology, 2008: p. 406-410.

37.   Clive R. Clayton, Ingemar Olefjord   *Passivity of Austenitic Stainless Steels*, in *Corrosion Mechanisms in Theory and Practice*, Philippe Marcus, Editor. 2002, Mareel Dekker, Inc. New York. p. 217-241.

38.   Singhal, V. Shankar Rao and L. K., *Corrosion Behavior and Passive Film Chemistry of 216l Stainless Steel in Sulphuric Acid.* Journal of Materials Science 2009. **44**(9): p. 2327-2333.

39.   *The Australian Stainless Steel Development Association (Assda), What Is Stainless Steel*.   2010 [cited 2011; Available from: http://www.assda.asn.au/what-is-stainless-steel.

40.   Shahrabi, R.C. Newman and T., *The Effect of Alloyed Nitrogen or Dissolved Nitrate Ions on the Anodic Behaviour of Austenitic Stainless Steel in Hydrochloric Acid.* corrosion Science, 1987. **27**(8): p. 827.

41.   Lorenzo De Micheli, Silvia Maria Leite Agostinho, Giordano Trabanelli, Fabrizio Zucchi, *Susceptibility to Stress Corrosion Cracking of 254smo Ss.* Materials Research, 2002. **5**(1): p. 63-69.

42.   J. Koltz, J. B. Wu, P .E. Manning, A. I. Asphahani,, Corrosion Rev., 1986. **6**(4): p. 279.

43. Latif, E.A. Abd El Meguid and A.A. Abd El, *Electrochemical and Sem Study on Type 254 Smo Stainless Steel in Chloride Solutions.* Corrosion Science, 2004. **46**(10): p. 2431-2444.

44. L. De Micheli, C. A. Barbosa, A. H. Andrade, S. M. Agostinho, *Electrochemical Behaviour of 254smo Stainless Steel in Comparison with 316l Stainless Steel and Hastelloy C276 in Hcl Media.* British Corrrosion Journal, 2000. **35**(4): p. 297-300.

45. L. De Micheli, A. H. Andrade, C. A. Barbosa, S. M. Agostinho, *Electrochemical Studies of 254smo Stainless Steel in Comparison with 316l Stainless Steel and Hastelloy C276 in Phosphoric Acid Media in Absence and Presence of Chloride Ions.* Brithish Corrosion Journal, 1999. **34**(1): p. 67-70.

46. Qvarfort, R., *Critical Pitting Temperature Measurements of Stainless Steels with an Improved Electrochemical Method,.* Corrosion science, 1989. **29**(8): p. 987-993.

47. E A Abd El Meguid , A Abd El Latif, *Critical Pitting Temperature for Type 254 Smo Stainless Steel in Chloride Solutions.* Corrosion Science, 2007. **49**(2): p. 263-275.

48. Kadry, Seifedine, *Corrosion Analysis of Stainless Steel.* European Journal of Scientific Research, 2008. **22**(4): p. 508-516.

49. Kritzer, Peter, *Corrosion in High-Temperature and Supercritical Water and Aqueous Solutions: A Review.* The Journal of Supercritical Fluids, 2004. **29**(1-2): p. 1-29.

50. M. P. Ryan, N. J. Laycock, R. C. Newman and H. S. Isaacs, , *The Pitting Behavior of Iron-Chromium Thin Film Alloys in Hydrochloric Acid.* Journal of Electrochemical Society, 1998. **145**(5): p. 1566-1571.

51. D. E. Williams, R. C. Newman, q. Song and R. G. Kelly, *Passivity Breakdown and Pitting Corrosion of Binary Alloys.* Nature 1991. **350**: p. 216 - 219.

52. Frankel, G. S., *Pitting Corrosion of Metals, a Review of the Critical Factors.* Journal of Electrochemical Society, 1998 **145**(6).

53. Kopeliovich, Dmitri. *Pitting Corrosion.* 2009 [cited 2011]; Available from: http://www.substech.com/dokuwiki/doku.php?id=pitting_corrosion.

54. D.E. Williams, J. Stewart and P.H. Balkwill, *The Nucleation, Growth and Stability of Micropits in Stainless Steel.* Corrosion Science, 1994. **36** (7): p. 1213-1235.

55. D. E. Williams , Matt R. Kilburn, John Cliff, Geoffrey and I.N. Waterhouse, *Composition Changes around Sulphide Inclusions in Stainless Steels, and Implications for the Initiation of Pitting Corrosion.* Corrosion Science, 2010. **52**(11): p. 3702-3716.

56. Strehblow, H. H., *Breakdown of Passivity and Localized Corrosion: Theoretical Concepts and Fundamental Experimental Results.* Materials and Corrosion, 1984. **35**(10): p. 437-448.

57. Szklarska-Smialowska, Z. , *Pitting and Crevice Corrosion.* 2005: NACE International.

58. T. Hoar, D. Mears and G. Rothwell, *The Relationships between Anodic Passivity, Brightening and Pitting.* Corrosion Science, 1965. **5**(4): p. 279-289

59. Galvele, M. Alvares and J., *Pitting Corrosion*, in *ShreiŕS Corrosion*, Mike Graham Bob Cottis, Rob Lindsay, Stuart Lyon, Tony Richardson, David Scantlebury and Howard Stott, Editor. 2010, Elsevier. p. 772.

60. P. C. Pistorius , G.T. Burstein, *Metastable Pitting Corrosion of Stainless Steel and the Transition to Stability.* Philosophical Transactions the Royal Society A: Mathematical, Physical, and Engineering Sciences, 1992. **341**(1662): p. 531-559.

61. Koroleva, Elena, *Lecture Note of Localized Corrosion for Msc Course in Corrosion Control and Engineering* 2010, The University of Manchester.

62. Uhlig, H. P. Leckie and H. H., *Environmental Factors Affecting the Critical Potential for Pitting in 18–8 Stainless Steel.* Journal of the Electrochemical Society, 1966. **113**(12): p. 1262-1267.

63. A. U. Malik, P. C. Mayankutty, Nadeem A. Siddiqi, Ismaeel N. Andijani, and Shahreer Ahmed, *The Influence of Ph and Chloride Concentration on the Corrosion Behaviour of Aisi 316l Steel in Aqueous Solutions.* Corrosion science, 1992. **33**(11): p. 1809-1827.

64. Seung Uk Lee, Jae Chen Ahn, Dong Hyun Kim, Seung Chan Hong, Kyung Sub Lee, *Influence of Chloride and Bromide Anions on Localized Corrosion of 15%Cr Ferritic Stainless Steel.* Materials Science and Engineering: A, 2006. **434**(1-2): p. 155-159.

65. M. Kaneko, and H. S. Isaacs, *Pitting of Stainless Steel in Bromide, Chloride and Bromide/Chloride Solutions.* Corrosion Science, 2000. **42**(1): p. 67-78

66. Abdelaal, E. E., *Breakdown of Passive Film on Nickel in Borate Solutions Containing Halide Anions* Corrosion Science, 2003. **45**(4): p. 759-775.

67. P. E. Arnvig , A. D. Bisgard. . *Determining the Potential Independent Critical Pitting Temperature (Cpt) by a Potentiostatic Method Using the Avesta Cell.* in *Corrosion 96.* 1996. NACE,Houston,TX. Paper No. 437.

68. Lihua Zhang, Yiming Jiang, Bo Deng, Daoming Sun, Juan Gao and Jin Li, *Effect of Temperature Change Rate on the Critical Pitting Temperature for Duplex Stainless Steel,.* Journal of Applied Electrochemistry 2009. **39**(10): p. 1703-708.

69. K. Vu Quang, P.L. Guevel and N. Jallerat *Fast Method for Determination of Critical Pitting Temperature.* Corrosion Science, 1988. **28**(4): p. 423-424.

70. N. J. Laycock, M. H. Moayed and R. C. Newman, *Metastable Pitting and the Critical Pitting Temperature.* Journal of Electrochemical Society, 1998. **145**(8): p. 2622-2628.

71. N. J. Laycock , R.C. Newman *Temperature Dependence of Pitting Potentials for Austenitic Stainless Steels above Their Critical Pitting Temperature.* Corrosion Science, 1998. **40**(5): p. 887-902.

72. E. Blasco-Tamarit, D.M. García-García, J. García Antón, *Imposed Potential Measurements to Evaluate the Pitting Corrosion Resistance and the Galvanic Behaviour of a Highly Alloyed Austenitic Stainless Steel and Its Weldment in a Libr Solution at Temperatures up to 150°c.* Corrosion Science 2011. **53**: p. 784-795.

73. M.H. Moayed, N.J. Laycock, R.C. Newman, *Dependence of the Critical Pitting Temperature on Surface Roughness.* Corrosion Science, 2003. **45**(6): p. 1203-1216.

74. Szklarska-Smialowska, Z., *Review of Literature on Pitting Corrosion Published since 1960.* Corrosion, 1971. **27**(6): p. 223.

75. A. Gebert, F. Schneider and K. Mummert, *Influence of Oxide Structure on the Elevated Temperature Pitting Behaviour of Fe-Cr-Ni Alloys.* Nuclear Engineering and Design., 1997. **174** p. 327-334.

76.   E. Blasco-Tamarit, A. Igual-Muñoz, J. García-Antón and D. García-García, *Effect of Temperature on the Corrosion Resistance and Pitting Behaviour of Alloy 31 in Libr Solutions.* Corrosion Science, 2008. **50**(7): p. 1848-1857

77.   J. O. Park, S. Matsch, and H. Böhni, *Effects of Temperature and Chloride Concentration on Pit Initiation and Early Pit Growth of Stainless Steel,.* Journal of Electrochem. Societey, 2002. **149**(2): p. 34-39.

78.   BOHNI, H., *Localized Corrosion of Passive Metals*, in *Uhlig's Corrosion Handbook* R. Winston Revie, Editor. 2000, John Wiley & Sons. p. 176.

79.   P.E. Manning and D.J. Duquette, *The Effect of Temperature (25-289 °C) on Pit Initiation in Single Phase and Duplex 304l Stainless Steels in 100 Ppm Cl− Solution.* Corrosion science, 1980. **20**(4): p. 597-609

80.   R.M. Carranza , M. G. Alvarez, *The Effect of Temperature on the Passive Film Properties and Pitting Behaviour of a Fe-Cr-Ni Alloy.* Corrosion science, 1996. **38**(6): p. 909-925.

81.   Tozer, R. J. Brigham and E. W., *Pitting Resistance of 18% Cr Ferritic Stainless Steels Containing Molybdenum.* Journal of Electrochem society, 1974. **121**(9): p. 1192-1193.

82.   Galvele, M.G. Alvarez and J. R., *Pitting Corrosion*, in *Sharer's Corrosion*, Mike Graham Bob Cottis, Rob Lindsay, Stuart Lyon, Tony Richardson, David Scantlebury and Howard Stott Editor. 2010, Elsevier Ltd. p. 797.

83.   Copson, H. R., *Effects of Velocity on Corrosion by Water.* Industrial and engineering chemistry, 1952. **44**(8).

84.   Ezuber, H. M., *Metallurgical and Environmental Factors Affecting the Pitting Behavior of Uns S 32205 Duplex Stainless Steel in Chloride Solutions.* Materials and Corrosion, 2010. **61**(9999).

85.   Wood, J. Wharton and R., *Influence of Flow Conditions on the Corrosion of Aisi 304l Stainless Steel* Wear, 2004. **256**(5): p. 525-536.

86.   J.A. Wharton, and R.J. Wood, *Flow Corrosion Behavior of Austenitic Stainless Steels Uns S30403 and Uns S31603.* Corrosion, 2005. **61**(8).

87.   J. Stewart , D.E. Williams, *The Initiation of Pitting Corrosion on Austenitic Stainless Steels - on the Role and Importance of Sulfide Inclusions,.* Corrosion Science 1992. **33**(3): p. 457-474

88.   C.S. Brossia , R.G. Kelly, *Influence of Alloy Sulfur Content and Bulk Electrolyte Composition on Crevice Corrosion Initiation of Austenitic Stainless Steel.* Corrosion, NACE International., 1998. **54**(2).

89.   Eklund, G. S., *Initiation of Pitting at Sulfide Inclusions in Stainless Steel.* Journal of the Electrochemical Society, 1974. **121**(4): p. 467- 473.

90.   Wranglen, G., *Pitting and Sulphide Inclusions in Steel.* Corrosion science, 1974. **14**(5): p. 331-349.

91.   Mary P. Ryan, David E. Williams, Richard J. Chater, Bernie M. Hutton and David S. McPhail, *Why Stainless Steel Corrodes.* NATURE 2002. **415**: p. 770-774.

92.   David Williams, T. Mohiuddin and Y. Zhu, *Elucidation of a Triggermechanism for Pitting Corrosion of Stainless Steels Using Sub-Micron Resolution Secm and Photoelectrochemical Microscopy.* Journal of Electrochemical Society, 1998. **145**(8): p. 2664 - 2672.

93.   Zhu, David Williams and Y., *Explanation for Initiation of Pitting Corrosion of Stainless Steels at Sulfide Inclusions.* Journal of the Electrochemical Society, 2000. **147**(5): p. 1763-1766.

94. E. Webb, T. Suter and R. Alkire, *Microelectrochemical Measurements of the Dissolution of Single Mns Inclusions, and the Prediction of the Critical Conditions for Pit Initiation on Stainless Steel.* Journal of Electrochemical Society, 2001. **148**(5): p. B186-B195.

95. J. *S. Kim, W. H. A. Peelen, K. Hemmes and R. C. Makkus, Effect of Alloying Elements on the Contact Resistance and the Passivation Behaviour of Stainless Steels. Corrosion Science, 2002. 44(4): p. 635-655*

96. *V. Vignal , H. Zhang , O. Delrue , O. Heintz , I. Popa , J. Peultier, Influence of Long-Term Ageing in Solution Containing Chloride Ions on the Passivity and the Corrosion Resistance of Duplex Stainless Steels. Corrosion Scien*ce, 2001. **53**(3): p. 894-903.

97. *Technical Information: Calculation of Pitting Resistance Equivalents Number, Internet Website Of* British Stainless Steel Association [cited 2011]; Available from: http://www.bssa.org.uk/technical_information.php.

98. Radenkovic, Z. Cvijovic and G., *Microstructure and Pitting Corrosion Resistance of Annealed Duplex Stainless Steel.* Corrosion Science, 2006. **48**(12): p. 3887-3906.

99. *Material Safety Data Sheet (Msds) for Acetic Acid Provided by Hands-on Science (H-Sci) ,Oxford - U.K.* January 6, 2006 [cited 2011 February]; Available from: http://msds.chem.ox.ac.uk/AC/acetic_acid.html.

100. Ricardo M. Carranza, C. Mabel Giordano, Martín A. Rodríguez and Raúl B. Rebak, *Corrosion Behavior of Alloy 22 in Chloride Solutions Containing Organic Acid*, in *Corrosion*. 2006, NACE International , Paper No. 06627.

101. E. Otero, A. Pardo, M. V. Utrilla, F. J. P&rez and C. Merino *Corrosion Behaviour of Aisi 304l and 316l Stainless Steels Prepared by Powder Metallurgy in the Presence of Organic Acids.* corrosions science, 1997. **39**(3): p. 453-463.

102. A.J. Invernizzi, E. Sivieri , S.P. Trasatti, *Corrosion Behaviour of Duplex Stainless Steels Inorganic Acid Aqueous Solutions.* Materials Science and Engineering A 2008. **485**(1-2): p. 234–242.

103. Garverick, Linda, *Corrosion in the Petrochemical Industry.* 1994: ASM international.

104. Schütze, G. Kreysa and M., ed. *Dechema Corrosion Handbook.* 2nd ed. 2008, DECHEMA.

105. Koch, G.H., *Localised Corrosion in Halides Other Than Chlorides, Mti Publication,Materials Technology Institute of the Chemical Process Industries.* Vol. 41. 1995: by NACE Int. Houston, TX

106. I. Sekine, A. Masucko, K. Senoo, *Corrosion Behavior of Aisi 316 Stainless Steel in Formic and Acetic Acid Solutions.* Corrosion 1987. **43** p. 553-560.

107. I. Sekine, T. Kawase, M. Kobayashi, M. Yuasa, *The Effects of Chromium and Molybdenum on the Corrosion Behaviour of Ferritic Stainless Steels in Boiling Acetic Acid Solutions.* Corrosion Science, 1991. **32**(8): p. 815-825.

108. Oluwatoyin Ashiru , Abdullah Al Refaie, *Pitting Corrosion Problems of Stainless Steel in Pta Plant*, in *Corrosion* 2007, NACE international. Paper No. 07196: Nashville, Tennessee.

109. Shu-ying, Li, *Research on Corrosion Mechanism of Stainless Steel Stuffing in T-403 Tower in Acetic Acid Solution.* Journal of Dalian University of Technology, 2005. **45**(3): p. 335-339

110. Alan Turnbull a, Mary Ryan b, Anthony Willetts a, Shengqi Zhou a, *Corrosion and Electrochemical Behaviour of 316l Stainless Steel in Acetic Acid Solutions.* Corrosion Science 2003. **45** (5): p. 1051-1072.

111. Liang, Bin, Gong, Jian-Ming; Tu, Shan-Dong, *Corrosion Behaviour of 316l and Saf 2205 Stainless Steels in Acetic Acid Solution Containing Br Ion.* Materials for Mechanical Engineering, 2006. **30**(1): p. 56-59,.

112. G.Q. Liu, Z.Y. Zhu, W. Ke, E.H. Han, and C.L. Zeng, *Corrosion Behavior of Stainless Steel and Nickel-Based Alloys in Acetic Acid Solutions Containing Bromide Ions.* Corrosion 2001 **57**(8): p. 730-738.

113. M. C. Li , C. L. Zeng , H. C. Lin ,C. N. Cao, British Corrosion Journal, 2001. **36**(3): p. 179-183.

114. EunAe Cho, SeJin Ahn and HyukSang Kwon, *Effects of Edta on the Electronic Properties of Passive Film on Fe-20cr in Ph 8.5 Buffer Solution.* Electrochimica Acta, 2005. **50**(16-17): p. 3383-3389.

115. Y.X. Qiao, Y.G. Zheng , W. Ke and P.C. Okafor, *Electrochemical Behaviour of High Nitrogen Stainless Steel in Acidic Solutions.* Corrosion Science, 2009. **51**(5): p. 979-986

116. C. O. A. Olsson , D. Landolt *Passive Films on Stainless Steels : Chemistry, Structure and Growth.* Electrochimica Acta 2003. **48** p. 1093 -1104.

117. V. Maurice, W. P. Yang, and P. Marcus, *Xps and Stm Investigation of the Passive Film Formed on Cr (110) Single-Crystal Surfaces.* Journal of Electrochemical Society, 1994. **141**(11): p. 3016-3027.

118. V. Maurice, W. P. Yang, and P. Marcus, *Xps and Stm Study of Passive Films Formed on Fe-22cr (110) Single-Crystal Surfaces.* Journal of electrochemical. Soc, 1996. **143**(4): p. 1182-1200.

119. Strehblow, P. Keller and H.-H., *Xps Investigations of Electrochemically Formed Passive Layers on Fe/Cr-Alloys in 0.5 M H_2so_4.* Corrosion Science 2004. **46** p. 1939-1952.

120. P. Marcus , I. Olefjord, *Electrochemical and Aes/Esca Characterization of the Passive Films on Fe-Cr and Fe-Cr-Mo Alloys.* Corrosion Science, 1988. **28**(6): p. 589- 602.

121. I. Olefjord, B. Brox, and U. Jelvestam, *Surface Composition of Stainless Steels During Anodic Dissolution and Passivation Studied by Esca.* Journal of Electrochemecal Society, 1985. **132**: p. 2854 - 2861.

122. I. Olefjord , L. Wegrelius, *Surface Analysis of Passive State.* corrosion science, 1990. **31**: p. 89-98.

123. C. R. Clayton , Y. C. Lu, *A Bipolar Model of the Passivity of Stainless Steel: The Role of Mo Addition.* Journal of Electrochemical Society, 1986. **133**(12): p. 2465-2473

124. Y. C. Lu, C. R. Clayton and A. R. Brook, *A Bipolar Model of the Passivity of Stainless Steels - Ii: The Influence of Aqueous Molybdate.* Corrosion Science, 1989. **29**(7): p. 863-880.

125. K. Hashimoto, K. Asami and K. Teramoto, *Spectroscopic Study on the Role of Molybdenum.* Corrosion Science, 1979. **19**: p. 3 -14

126. K. Sugimoto , Sawada, *The Role of Molybdenum Additions to Austenitic Stainless Steels in the Inhibition of Pitting in Acid Chloride Solutions.* corrosion Science, 1977. **17**: p. 425-445.

127. A. Pardo , et al. , *Effect of Mo and Mn Additions on the Corrosion Behaviour of Aisi 304 and 316 Stainless Steels in H2so4.* Corrosion Science 2008. **50**: p. 780-794.

128. C. O. A. Olsson , S. E. Hornstrom, *An Aes and Xps Study of the High Alloy Austenitic Stainless Steel 254 Smo Tested in a Ferric Chloride Solution.* Corrosion Science, 1994. **36**(1): p. 141-151.

129. Strehblow, S. Haupt and H., *A Combined Surface Analytical and Electrochemical Study of the Formation of Passive Layers on Fe/Cr Alloys in 0.5 M H_2so_4* Corrosion Science, 1995. **37**(1): p. 43-54.

130. H. Hoppe, S. Haupt, H. Strehblow, *Combined Surface Analytical and Electrochemical Study of the Formation of Passive Layers on Fe/Cr Alloys in 1 M Naoh.* Surface and Interface Analysis, 1994. **21**(8): p. 514-525.

131. C.T. Liu, J.K. Wu *Influence of Ph on the Passivation Behaviour of 254smo Stainless Steel in 3.5% Nacl Solution.* Corrosion Science 2007. **49**: p. 2198-2209.

132. S. Mischler, A. Vogel, H.J. Mathieu and D. Landolt, *The Chemical Composition of the Passive Film on Fe---24cr and Fe---24cr---11mo Studied by Aes, Xps and Sims* Corrosion Science, 1991 **32**(9): p. 925-944

133. L. Wegrelius, I. Olefjord, in *12th International Corrosion Congress.* 1993, NACE: Houston, TX. p. 3887.

134. Atrens, S. Jin and A., *Esca-Studies of the Structure and Composition of the Passive Film Formed on Stainless Steels by Various Immersion Temperatures in 0.1 M Nacl Solution* Applied Physics A Solids and Surfaces 1988. **45**(1): p. 83-91.

135. I. Sekine, T. Kawase, M. Kobayashi, M. Yuasa, Corrosion Scienc, 199. **32, Issue**(8): p. 815-825.

136. X. Q. Cheng, X. Li, and C. F. Dong, *Study on the Passive Film Formed on 2205 Stainless Steel in Acetic Acid by Aas and Xps.* International Journal of Minerals, Metallurgy and Materials, 2009. **16**(2): p. 170-176.

CHAPTER THREE
EXPERIMENTAL TECHNIQUES AND INSTRUMENTATION

3 Experimental Techniques and Instrumentation

3.1 *Introduction*

The primary motivation of the experimental work was to draw comparisons and characterise the corrosion behaviour of the two austenitic stainless steel alloys, 316L and 254SMO, when immersed in different concentrations of HAc solutions (11.9M and 15.3M) containing bromide ions (18.7mM) at 90°C.

The experimentation and instrumentation that were employed in this research can be grouped as:

1) Electrochemical measurements (open circuit potential, linear polarization resistance and potentiodynamic polarization),

2) Weight loss measurements,

3) Scanning electron microscopy (SEM) and energy-dispersive X-ray (EDX spectroscopy), and

4) X-ray photoelectron spectroscopy (XPS).

3.2 *Electrochemical Measurements*

When a corrosion process proceeds by an electrochemical mechanism, electrochemical methods can be applied in addition to other methods. Generally, the aims of electrochemical measurements are numerous and can be characterized as follows [7, 8]: determination of electrochemical corrosion rates, assessment of the potential dependence of corrosion reactions,

determination of critical potentials and evaluation of corrosion mechanisms. Details of such techniques, their practical applications and limitations have been presented by many workers [8-10].

The electrochemical measurements that were used in this research consisted of: (1) open circuit potential (OCP), (2) linear polarization resistance (LPR) and (3) potentiodynamic polarization (PDP). All of these measurements were carried out using a three-electrode cell system and a Gill AC Potentiostat from ACM Instruments.

For these measurements 500mL of acetic acid/Br$^-$ solutions of interest were prepared and placed in a round-bottom flask which heated using a heating mantle. The solutions temperature was monitored by a thermometer. In every experiment a water-cooled condenser was connected to the outlet of the flask to avoid loss through evaporation. Working electrodes used in the electrochemical measurements were constructed following a design similar to Stern-Makrides electrode [11]. A schematic diagram of this electrode is shown in Figure 3-1. The potential of the working electrode was referred to a Saturated Calomel Electrode (SCE) which was connected via a Luggin solution bridge to avoid any heating effect. The tip of the luggin probe was placed as close as possible to the working electrode surface. In our study, the platinum electrode was used as a counter (auxiliary) electrode.
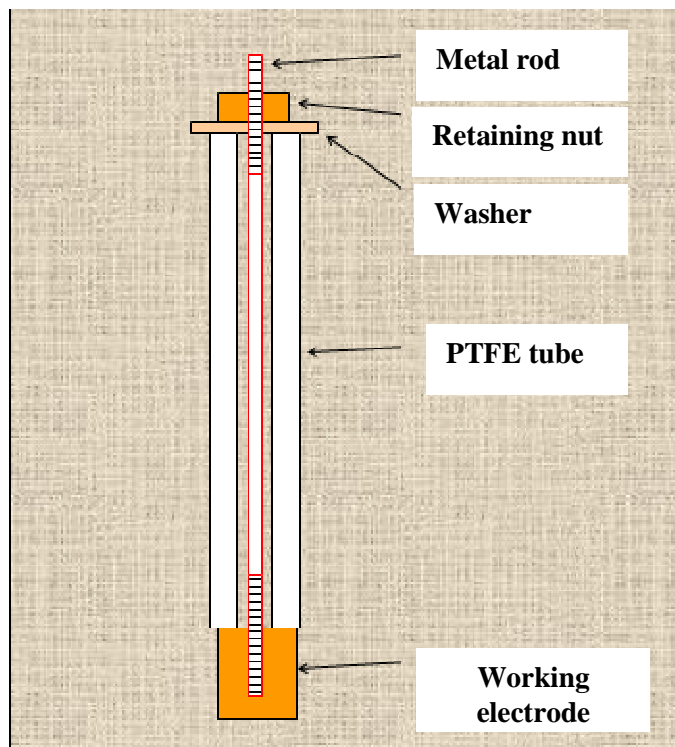
Figure 3-1 Working electrode design similar to Stern-Makrides electrode

The following sub-sections provide more details about the electrochemical measurements utilised in this study.

3.2.1 OCP:

In this technique one simply records the potential of an electrode (the sample) that is not subjected to any external current as a function of time [7]. During such measurements both the anodic and cathodic reactions take place simultaneously on the electrode surface, and are at equilibrium i.e., the two reaction rates are equal (no net current). Thus, the sample is considered at equilibrium potential, which is also known as the free corrosion potential (E_{corr}), or open circuit potential (OCP).

Generally, a more positive OCP indicates that a metal surface is the less prone towards electrochemical dissolution. Thus, OCP can be used to indicate the likely resistance to corrosion of the metal or alloy in any conductive environment.

3.2.2 LPR:

LPR which was developed by Stern and Geary [12], is one of the most widely used techniques for determining instantaneous corrosion rates and its theoretical background is well understood [8, 13, 14].

In LPR, a small potential perturbation, typically the applied range is about $\pm 20mV$, in the vicinity of the corrosion potential is applied while the current is recorded. The voltage range is so small that an approximately linear current-potential curve is obtained as shown in Figure 3-2.

The gradient of the curve is simply volts/current ($\Delta E/\Delta I$) and so is resistance (ohms). For the linear part of the curve this is known as the polarization resistance [5, 15].

$$R_P = (\Delta E/\Delta I)$$

Rp (ohm) is the polarisation resistance of the sample surface. If current density is plotted rather than current, then the unit of Rp is ohm/cm^2. The Stern-Geary equation allows the corrosion current density (i_{corr}) corresponding Rp to be determined [5, 10, 12]:

$$i_{corr} = B/R_p$$

B is the Stern-Geary coefficient in mV/decade. The B value must be determined from separate experiments such as from anodic and cathodic Tafel slopes obtained for PDP curves [16], see the next section. Therefore, the Stern-Geary coefficient can be related to the Tafel anodic (ba) and cathodic (bc) constants in V/ decade as:
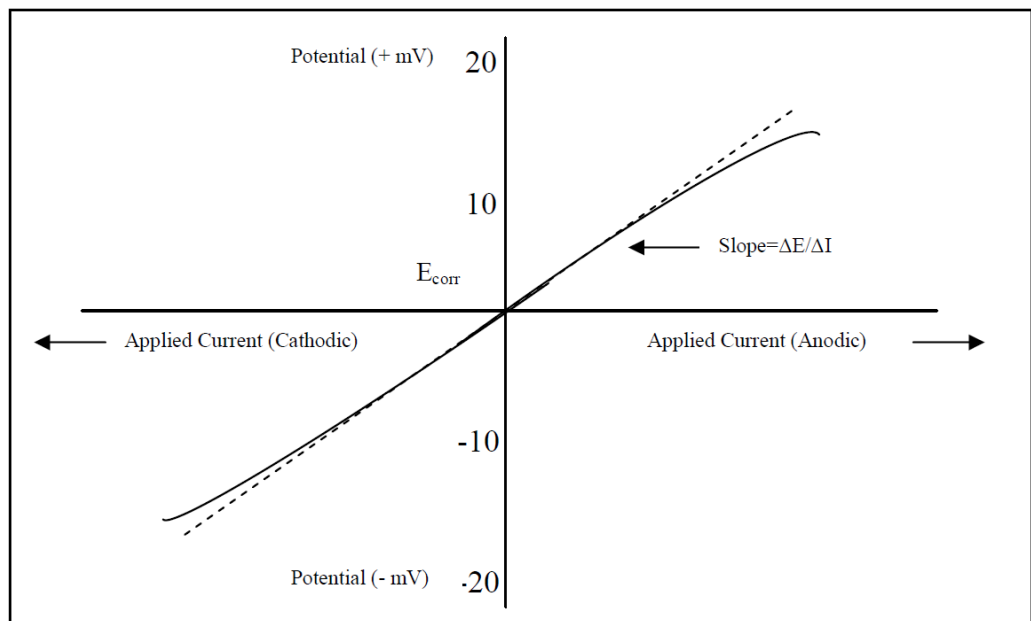
$$B = ba.bc \ / \ [2.3(ba + bc)]$$

Figure 3-2 Theoretical linear polarization plot [5]

Then, by using Faraday's law, the corrosion rate can be calculated as follows [10]:

$$\text{Corrosion rate (mm/year)} = (i_{corr} \times M_W) / (F \times n \times D)$$

where F is the Faraday constant (96485 $C.mole^{-1}.S^{-1}$), D is the density of metal ($g.cm^{-3}$), n is the number of electrons involved in the reaction (in moles of electrons per mole of metal corroded), M_w is the molecular weight ($g.mole^{-1}$) and i_{corr} is the corrosion current density ($A.cm^{-2}$).

In case of non-linear anodic and/or cathodic regions of the polarization curve, B is often assumed to have a value of about 26 mV for activation controlled system or 52mV for a system where the cathodic reaction is limited by diffusion. However, such estimations will almost certainly give errors in corrosion rate, which are often claimed to be less than a factor of about 2-3 of the true value [16, 17].

3.2.3 PDP:

PDP is an electrochemical technique commonly used for corrosion research and testing. The polarization curve displays the relationship between the current and the potential over a relatively wide range.

In a PDP measurement, the electrochemical reactions that occur on the sample surface can be controlled, i.e. to cause it to act independently as either an anode or a cathode. Thus, by studying the anodic and the cathodic processes separately, the corrosion behaviour of the sample can often be further understood.

Generally, the polarisation curves can be determined either by scanning the potential and recording the current or vice versa [16]. Therefore, the corrosion could be predicted by observing the response to a controlled change from steady state behaviour; which is created by application of potential (voltage) or current [18].

If the scanned potential method is adopted, a PDP measurement is performed by slowly scanning the specimen potential through several hundred millivolts from the OCP in either the anodic or cathodic direction, and the potentials are plotted versus the log of the measured current to generate a polarization curve similar to Figure 3-3 [19].

Corrosion current density (i_{corr}) and corrosion potential (E_{corr}) can be estimated from this polarisation curve by Tafel extrapolation (slope of the linear regions) of the anodic and/or the cathodic lines as demonstrated in Figure 3-3. Further details may be derived from the polarization curves. For example, passivity of the metal/alloy due to formation of a thin protective

film on the surface can be indicated from the polarisation curve (dotted lines) displaying a passive limiting current ($i_{passive}$) with increase in potential at the anodic region. Also, break-down of passivity due to either pitting attack or reaching the transpasivity region can be indicated from the polarization curve when the current density increased sharply. Also, an examination of Figure 3-3 reveals that other details can be derived concerning the cathodic processes. For a corroding system under diffusion control, adequate approximations are sometimes possible with limited Tafel behaviour and, i_{corr} is always is equal to the limiting current (i_L).
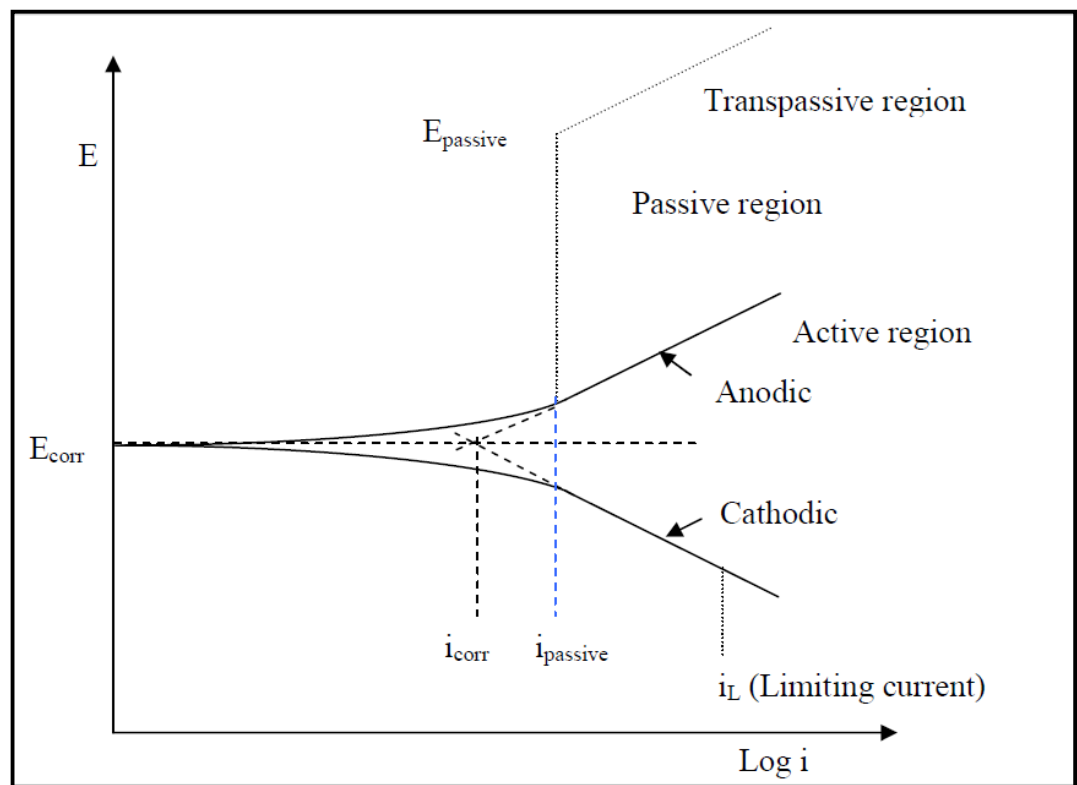

Figure 3-3 Schematic diagram of the polarisation curve demonstrating different anodic and cathodic regions, and showing the Tafel extrapolation method for estimation of corrosion current density (i_{corr}) and corrosion potential (E_{corr}), [19].

Additionally, the potential can be scanned in a cyclic manner from the open circuit potential of the sample to produce a cyclic potentiodynamic polarization curve. The potential of the sample is scanned at slow rate in the anodic direction (forward scan) as before and then the scan direction is reversed when the a pre-determined current or potential is achieved [20]. One important property that can be determined from such cyclic polarization curves is the repassivation potential (E_R, in Figure 3-4) [21], also called critical protection potential. It is defined as the potential at which the current density in the reverse loop equals the current density in the forward loop, the higher the value of repassivation potential is the more resistant the alloy to localized corrosion [20, 22].
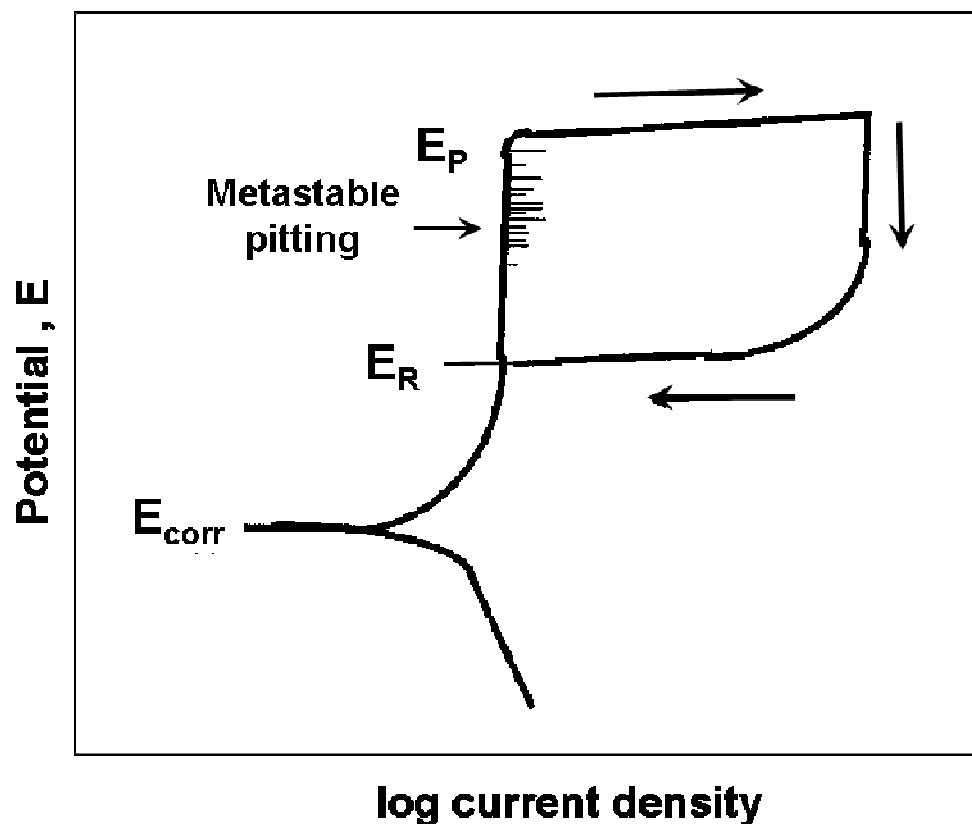

Figure 3-4 Schematic representation of a polarization curve showing pitting potential (E_P), metastable pitting region, repassivation potential (E_R) and, corrosion potential (E_{corr}), [21].

3.3 *Weight Loss Tests*

Weight loss tests are a very widely used corrosion measurement and monitoring technique. They are simple to understand and provide a direct measure of corrosion rate, allow a direct comparison of the relative resistance to corrosion of one sample with another under comparable or standard conditions, and provide a sound basis for estimating the likely active life of process equipment. There are numerous standard techniques for weight loss testing [4, 23].

The samples for these tests are called coupons and may have one of a given number of geometries (usually a small flat rectangular sheet or cylinder). The samples are surface finished, and the surface area determined. Care should be taken to avoid cross-contamination and, for example, new polishing paper should be used to avoid contamination of the metal surface. The coupon is degreased (washed in a suitable solvent) after which it should not be touched directly, dried and accurately weighed. The coupon should then be exposed to the corrosive environment of interest. If the sample is to be stored it should be kept in a desiccator.

Given that surface preparation can be achieved by any one of a number of methods, it is very important that comparisons be made only between coupons that were prepared in a similar manner. Different methods can be used to support the samples when they are in the corrosive medium. These

include plastic wire, glass holders and test racks. Once a coupon is immersed into a corrosive environment, a notable consideration is the length of time that it is left there. Misleading results may be obtained if an incorrect choice is made, due in part to the fact that the initial rate of attack is often greater than the average over a longer period [5]. There are standard procedures that can be used to plan exposure test time, such as ASTM and NACE Standards [4, 23].

Following its immersion in the test solution, a sample should be closely inspected for, e.g. visual signs of localised attacks such as pitting or deposits which can help identify the causes of corrosion. Next, any corrosion products adhering to the sample should be removed from the surface to allow accurate determination of corrosion weight loss.

Cleaning methods are either mechanical (scraping or brushing) or chemical (using solvents). Chemical cleaning is generally preferable, but the solution used will be specific to the metal being cleaned. Normally, the sample undergoes a number of equivalent cleaning cycles with the sample being weighed after each one [4]. Mass loss is plotted against the number of cleaning cycles, see Figure 3-5. Two lines are obtained; AB and BC. The former corresponds to removal of corrosion products, the latter to removal of base metal. The required corrosion mass loss (W) occurs at point B, the

intercept of the two lines [4]. More accurate results will be obtained by testing more than one coupon and averaging the mass lost.
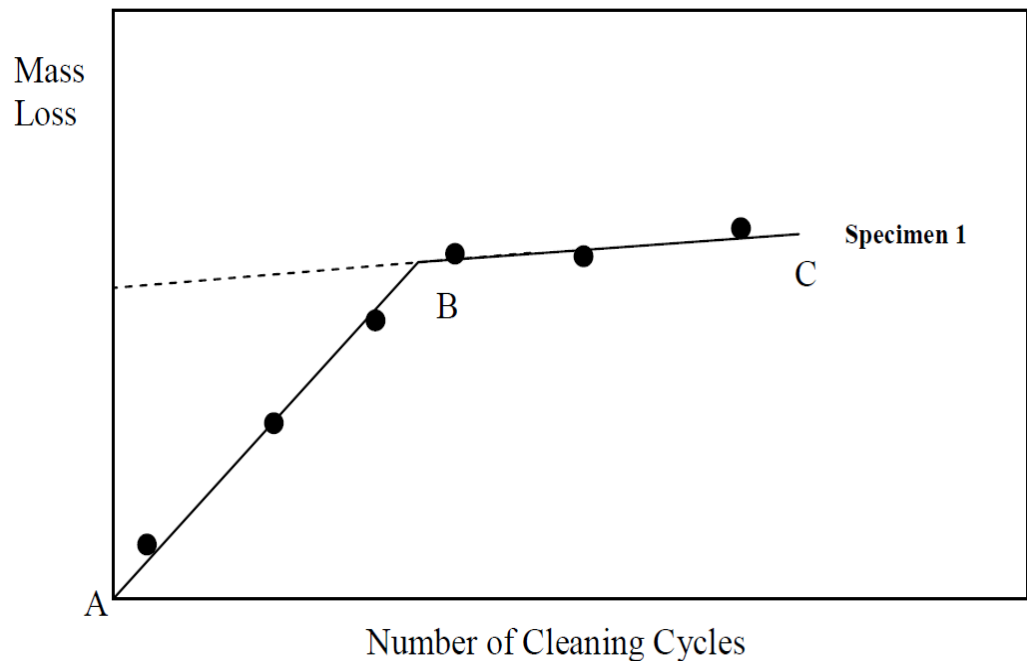

Figure 3-5 Theoretical mass loss of a corroded sample resulting from repeated cleaning cycles [4]

Corrosion rate can be calculated from the measured weight loss as [4, 24]:

$$\text{Corrosion Rate (g/cm}^2.\text{d)} = (K \times W)/ (A \times T \times D).$$

K is a constant [4], W is the mass lost from sample in g, T is the exposure time in days, A is the sample exposure area in cm^2, and D is the sample density in g/cm^3.

Corrosion rate can be expressed in millimetres per year (mm/y), mils per year (mpy) or milligrams per square centimetre per day (mg/cm²d). Conversion between these units can be seen in Table 3-1, [25].

Table 3-1 Conversion factors between some of the units commonly used for corrosion rates [25].

| Unit | mdd | Factor for Conversion to | | | | |
		g/m²/d	μm/yr	mm/yr	mils/yr	in./yr
Milligrams per square decimetre per day (mdd)	1	0.1	36.5/d	0.365/d	1.144/d	0.00144/d
Grams per square metre per day (g/m²/d)	10	1	365/d	0.365/d	14.4/d	0.0144/d
Micrometres per year (μm/yr)	0.0274d	0.00274d	1	0.001	0.0394	0.0000394
Millimetres per year (mm/yr)	27.4d	2.74d	1000	1	39.4	0.0394
Mils per year (mils/yr)	0.696d	0.0696d	25.4	0.0254	1	0.001
Inches per year (in/yr)	696d	69.6d	25400	25.4	1000	1

Note: d is metal density in grams per cubic centimetre (g/cm³).

3.4 SEM and EDX

Figure 3-6 shows a schematic diagram of the major components of the SEM. Generally, a beam of electrons are generated by electron gun (located at the top of the column of the SEM instrument). This electron beam travels through a series of electromagnetic fields and lenses, which focus the electron beam onto the surface of the sample. For stable operation, a high vacuum is normally essential to the SEM. If the SEM contained a gas, the

electron beam could react with it, ionising the gas with the possibility it could react with both the electron beam source causing burn out and contaminate the sample.

The interaction between the beam and the sample surface will result in emission of electrons and photons. The emitted electrons include back scattered electrons (BSE) and secondary electrons (SE), while the emitted photons include X-rays that can be used for elemental analysis (more details given below). Various detectors are employed to record these emissions and the output of these is processed to produce relevant images/data [26, 27].

The backscattered electrons are most valuable for showing variation in surface composition of the analysed sample [27, 28]. The secondary electron is an electron which has escaped from the sample with energy of less than 50 eV. These electrons provide information about the morphology and topography of the sample surface.

If the specimen experiences a net loss or gain of electrons it will gain a positive or negative charge causing image distortion and loss of resolution. Such effects can be overcome simply by earthing the specimen and using an electrically conducting sample or coating the specimen with a gold or carbon [29].

X-rays:

Bombardment of a specimen with high energy electrons produces X-rays; the wavelength of these X-rays depends on the elements that are present in the sample. An electron in the primary beam with sufficient energy can excite an electron in an inner shell of one of the atoms of the sample causing it to leave the atom entirely or move to a higher unoccupied energy level. The hole as a result of this process can be filled by an outer (higher energy) electron, an X-ray photon is emitted of energy equal to the energy difference between the two atomic shells and thus is characteristic of the atom from which the photon was emitted. This is the basis of Energy Dispersive X-Ray Spectroscopy (EDX), which is often used together with SEM [27].

EDX is a useful technique for elemental analysis or chemical characterisation of the sample. EDX can be used for spot analysis in which the electron beam is positioned carefully onto a point of interest on the sample surface. Also, it may be employed for analysis of selected area as well as for line scans.
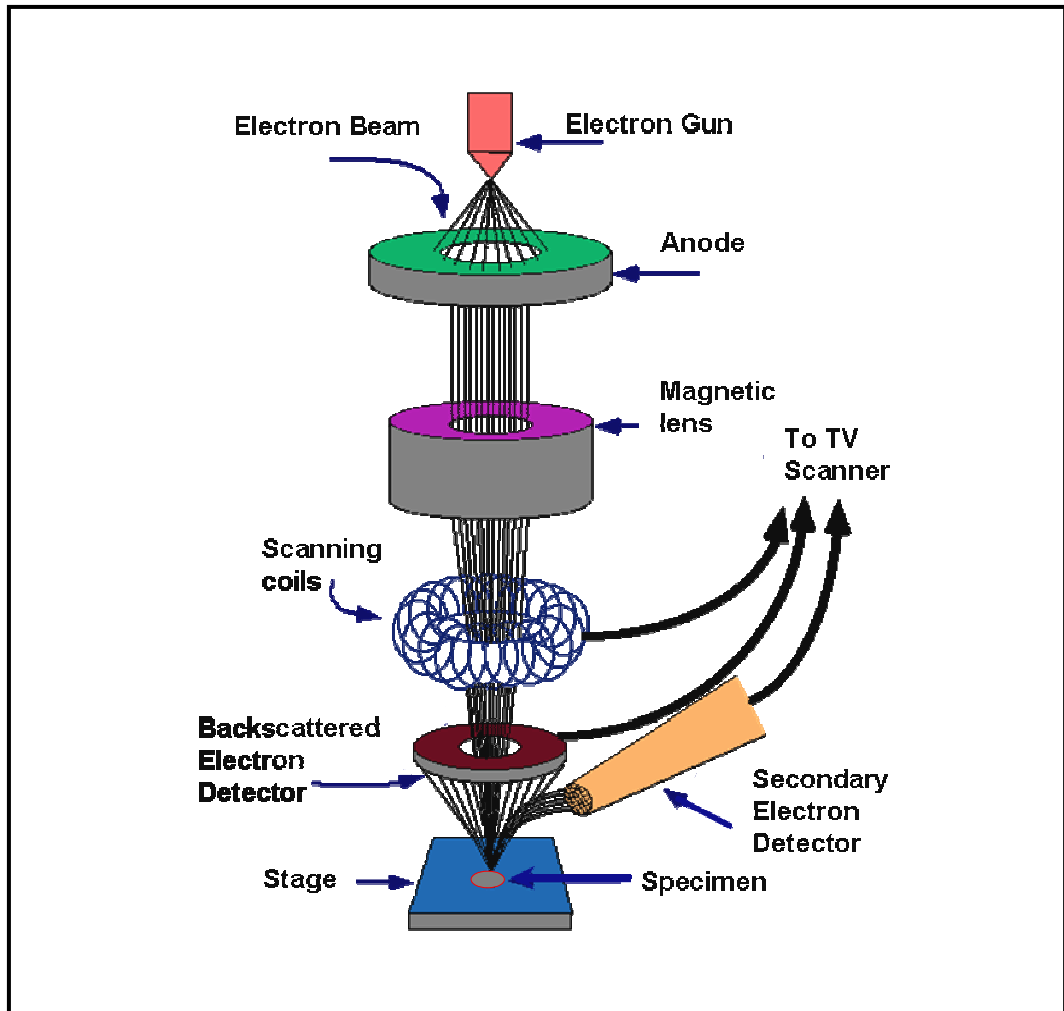
Figure 3-6 Schematic diagram of major components of SEM [3]

3.5 *X-ray photoelectron spectroscopy*

3.5.1 Introduction

X-ray photoelectron spectroscopy (XPS) is also known as Electron Spectroscopy for Chemical Analysis (ESCA). XPS is a surface sensitive technique that is used for providing element/chemical analysis of the

topmost layers of sample ($\approx$ 10nm) [30]. This technique is considered as one of the most useful surface analytical tools since it has the capability to provide quantitative, as well as qualitative information on the elements present in any surface films including the concentration and depth profile of atoms.

XPS is based upon the photoelectric effect first described by Einstein in 1905 i.e. the emission of electrons from a metal surface subject to electromagnetic radiation of sufficiently high frequency. Nordling and Siegbahn reported an experimental spectrometer which measured XPS spectra as long ago as 1957 [31]. Subsequently, Siegbahn's group observed the chemical shift effect of core level binding energies [32] and went on to develop the whole field of XPS during the period 1955-1970. In 1969, the first commercial XPS instrument was produced by Hewlett-Packard in co-operation with Siegbahn [31, 33].

Figure 3-7 shows the basic components of an XPS instrument. These are an X-ray source, electron focusing/collection lenses, and an electron detector/ analyzer [34-36]. A Kratos Axis Ultra X-ray photoelectron spectrometer, Figure 3-8, was used for the present study.
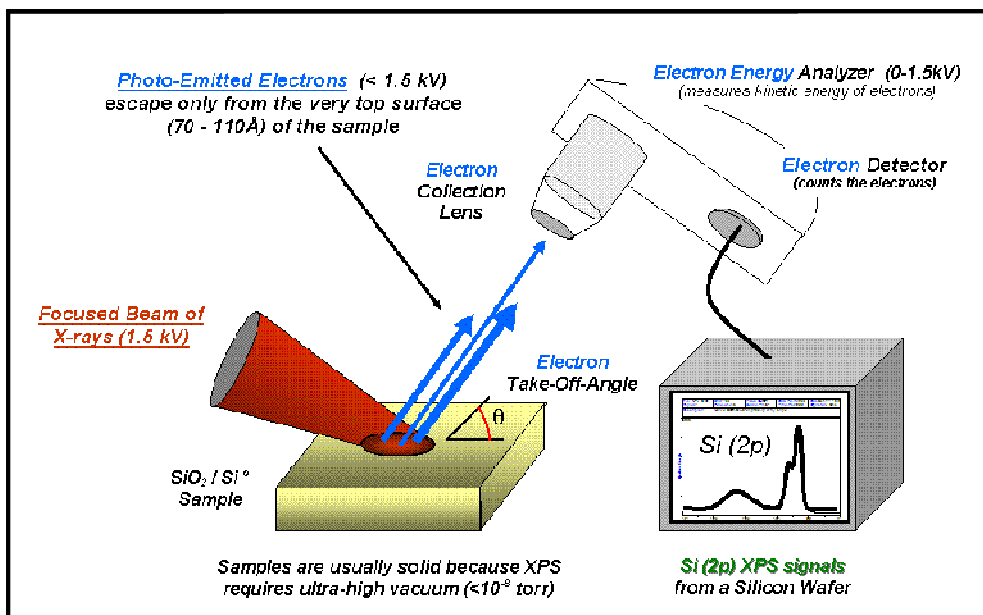
Figure 3-7 The basic components of a monochromatic XPS system [2]

Figure 3-8 Photograph of Kratos Axis Ultra XPS [1]

3.5.2 Principles of XPS

In XPS, a sample is irradiated with a beam of monochromatic X-rays of energy $h\upsilon$, where υ is the frequency of the beam and h is Planck's constant. X-ray photons interact with bound electrons (e.g. in core levels) which, if the energy of the photons is high enough (high enough frequency), will be ejected from the atom and leave the sample surface. This process is called photoemission, Figure 3-9.
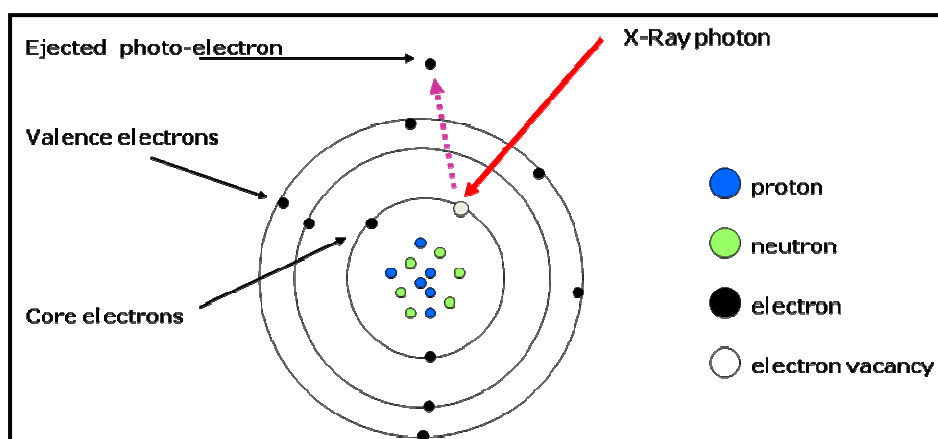

Figure 3-9 Schematic diagram showing the photoelectron

The photoemission process is often envisaged as three stages:

Stage 1

Interaction between the incident photon and the bound electron. The probability of this event is determined by the photoionisation cross section (σ). This parameter is energy dependent and can be defined as the

probability of photoionisation from a particular core level occurring when incident photons interact with atoms that constitute the sample.

Stage 2

This stage is transfer of the electron through the specimen surface. During the movement of the electron, it may have inelastic interactions with neighbouring atoms/electrons, leading to loss of initial information. This inelastic interaction is represented by the inelastic mean free path parameter (λ) which is defined as the depth or distance from which photoelectrons can escape freely without suffering any inelastic collisions.

Stage 3

The final stage is the emission of the photoelectron from the surface with kinetic energy E_K. The relation between the kinetic energy, E_K, of the photoelectron and the binding energy (E_B) of the core electron is give by [35, 37]:

$$E_K = h\nu - E_B - \Phi$$

$h\nu$ is photon energy (for the monochromatic Al source $h\nu$ = 1486.6 eV) and Φ is the work function of the analyser. Usually the work function is found by measurements of well-known standards and then compensated for within the instrument. Thus, Φ may be omitted from above equation.

3.5.3 Notation (Nomenclature)

Photoemission peaks are described by means of their quantum numbers, following the form *nlj*. *n* is the principal quantum number and this takes integer values of 1, 2, 3 etc., *l* is the orbital quantum number which describes the orbital angular momentum of the electron and this takes integer values 0,1,2,3 etc. However, this quantum number is usually given a letter rather than a number (s,p,d,f), *j* is the total angular momentum.

3.5.4 Main Spectral feature of XPS

Detecting and recording the number of emitted electrons (photoelectrons) as a function of their kinetic energy (E_K) will result in a spectrum. Various types of peaks with different features are observed in XPS spectra. An example of XPS spectrum is shown in Figure 3-10. The features appearing in XPS spectra are described below.

3.5.4.1 Core level photoemission peaks

In XPS spectra, the core level photoemission peaks appear as intense narrow peaks similar to those labelled in the Figure 3-10 as O 1s, Cr 2p, Fe 2p, Ni 2p, Mo 3d and C 1s. Tabulation of core level binding energy (E_b) for each of the elements allows one to identify composition of the analyzed surface by simple cross-referencing [19].

3.5.4.2 Auger Peak

In XPS spectra, not all peaks are due to the ejection of electron by a direct interaction with the incident photon. Therefore, there are other peaks than the core level peaks; the most notable peak is the Auger peak which occurs concurrently with photoelectron emission as shown in Figure 3-11.

When an X-ray photon ejects an electron from an inner shell, an electron from an outer shell will move to fill the gap emitting as it does so a photon of energy equal to the difference in energies of the two shells. Sometimes this photon can eject an electron from a shell where the binding energy is less than that of the photon, this is the Auger effect. These Auger electrons will be detected, resulting in Auger peaks which differ from the peaks generated by direct photoelectron emission and whose interpretation is much more complicated than for the direct photoelectron emission [37-39]. An example of an Auger peak is labelled as O KLL in Figure 3-10.
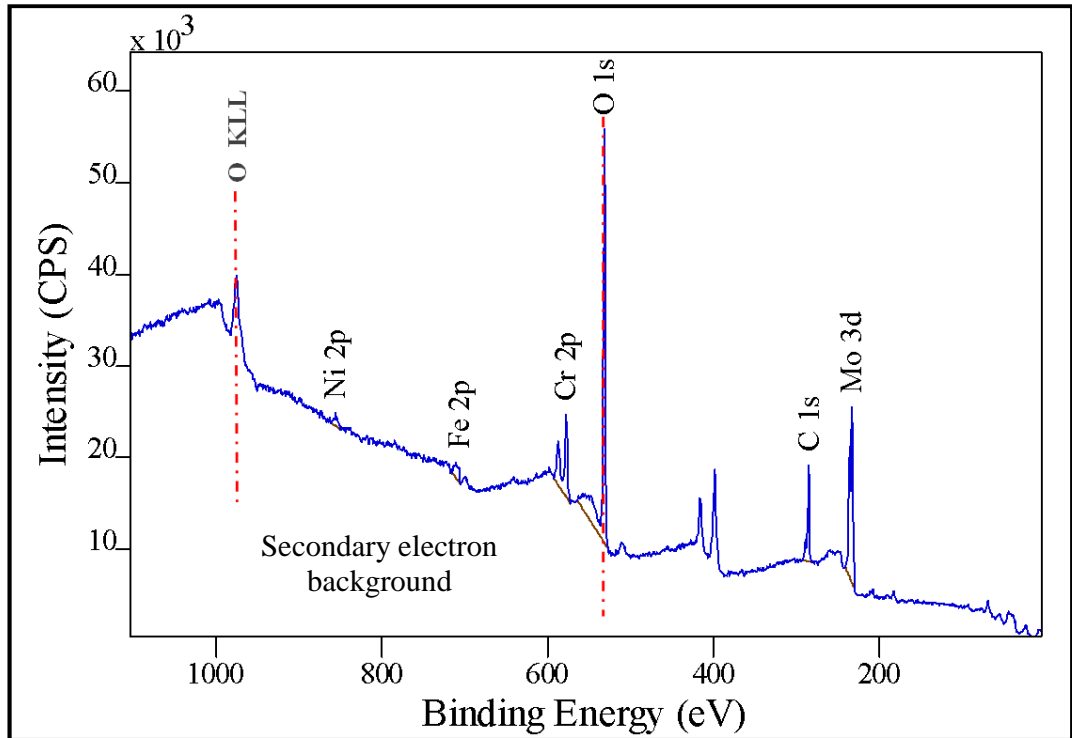
Figure 3-10 Example of an XPS wide scan survey spectrum used in our current research to determine the elements are present in the 316L stainless steel surface.
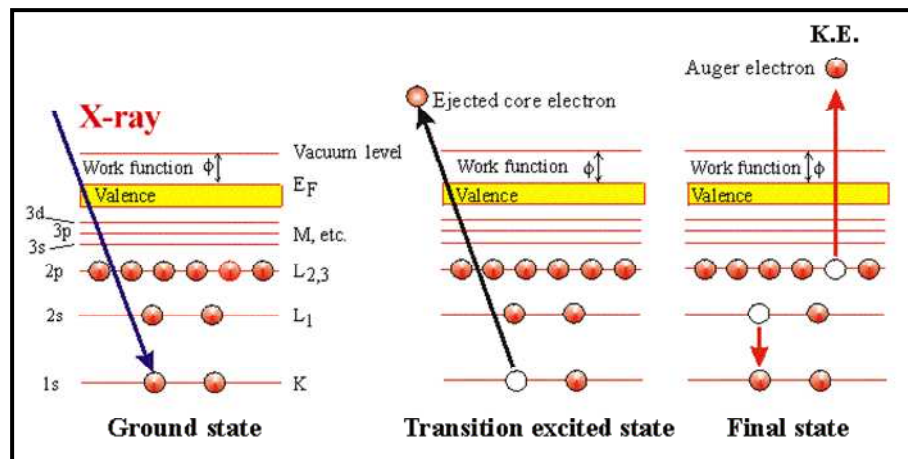

Figure 3-11 Schematic view of the Auger process: Excitation of an electron by X-rays, then photoelectron emission, and finally the auger electron [6]

3.5.4.3 Secondary electron background

The photoelectron and auger peaks sit upon a background of secondary electrons. In Figure 3-10, the background increases in intensity with increasing binding energy. These secondary electrons have undergone energy loss as the result of inelastic collisions with atoms in their path from the point of excitation to the surface [40, 41].

3.5.5 More details:

- **Chemical Shift**

A very important feature of XPS is the chemical information that can be obtained, such as the oxidation states of surface species. The change in the binding energy produced by a change in the oxidation state of an element is defined as the chemical shift. The binding energy of the photoelectrons will increase as the oxidation state increases [42].

- **Spin-orbit splitting**

Spin-orbit splitting is due to coupling between magnetic fields generated by spin (s = ±1/2) and angular momentum (l = 0, 1, 2...) of the electron. The quantum number j, $| l + s |$, indicates this interaction.

This phenomenon is not observed for s core levels where l = 0, but it is seen with p, d and f core levels, which all show characteristic spin-orbit doublets [42]. The binding energy (E_b) of lower total quantum number (j) value in the doublet is higher, $E_b (2p_{1/2}) > E_b (2p_{3/2})$ [37, 42]. An example of such feature is demonstrated in Figure 3-12, where the high-resolution spectrum for Cr 2p

shows the Cr $2p_{1/2}$ and Cr$2p_{3/2}$ spin-orbit split peaks. The intensity ratio of the doublet is determined by 2j+1 [19], as shown in Figure 3-13 [43].
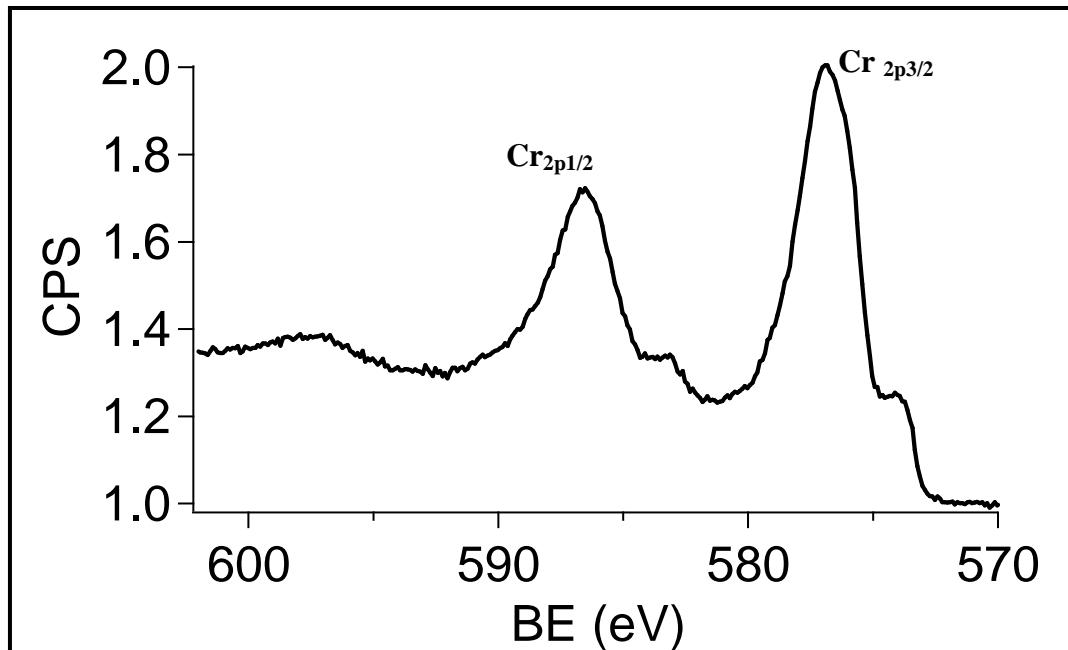

Figure 3-12 Cr$_{2p}$ spectrum acquired during present research, It shows the Cr$_{2p1/2}$ and Cr$_{2p3/2}$ spin orbit split peaks.

Figure 3-13 example of intensity ratios for different electronic orbitals [41].

- **Multiplet Splitting**

Multiplet splitting occurs when an atom contains unpaired electrons. In this case, the unpaired electron left in the core level from where the photoelectron was ejected interacts with the unpaired outer shell electron. This can create a number of final states, which will be noticeable in the photoelectron spectrum [37, 44].

- **Satellite peak**

Satellite peaks can be present in core level XPS spectra due to some of the outgoing photoelectron energy exciting the transition/emission of a valence band electron. As a result, the energy of the outgoing core electron is reduced giving satellite structure at higher binding energy than the main core level line [19, 42].

3.5.6 Quantification and depth profiling in XPS

To derive quantitative information from XPS spectra, peak intensities must be converted to atomic concentrations [36]. These intensities (areas under the curve) provide information on the amount of each element present. Peak intensities are determined via an automated peak-fitting procedure. The most important parameters used in such procedures are peak height, peak background, width, position and line-shape (e.g. Gaussian, symmetric or asymmetric, Weibull, etc., and combinations of these). In this project,

CasaXPS processing software [45] was used to execute all the peak fitting process.

By determining peak areas (suitably corrected for instrumental factors), the concentration of each element detected can be calculated. The equation normally used is [37] :

$$I_{ij} = KT (KE) Lij (\gamma) \sigma ij \int n_i(z)e-z/\lambda(KE)\cos\theta \, dz$$

However, in practice, this equation can be modified according to the application, for example with a homogenous sample it simplifies to [19]:

$$I_{ij} = KT (KE) L_{ij} (\gamma) \sigma_{ij} n_i \lambda (KE) \cos\theta$$

where:

K   is the instrumental constant,

T (KE)   is the transmission function of the analyser,

L$_{ij}$ (γ)   is the angular asymmetry factor for orbital j of element i,

σ_{ij}   is the photo-ionisation cross-section,

$n_i(z)$ is the concentration of element i at a distance z below the surface,

λ (KE)   is the inelastic mean free path length, and

θ   is the take-off angle of the photoelectrons measured with respect to the surface normal.

- **Transmission Function**

Transmission function is the detection efficiency of the electron energy analyzer, which is a function of electron energies. Transmission function also depends on the parameters of the electron energy analyzer, such as pass energy [6].

- **Inelastic Mean Free Path (IMFP):**

The inelastic mean free path (IMFP), λ (KE), of electrons describes the depth or distance from which photoelectrons can escape freely without suffering any inelastic collisions [46]. The IMFP is dependent on the nature of the material being travelled through [47, 48]. Also, the value of IMFP is dependent on the KE of the electron [6]. The good surface sensitivity of XPS and the other surface techniques happen from the fact that the IMFP is typically between $\approx$ 3–50 Å for electron energies between about 10 and 2,500 eV [49].

3.6 *References*

1.   *Instrument Web Pages of X-Ray Photoelectron Spectroscopy, School of Materials, the University of Manchester. .* [cited 2011]; Available from: http://www.materials.manchester.ac.uk/research/facilities/xps.
2.   Wikipedia, Web page of. *X-Ray Photoelectron Spectroscopy , <Http://En.Wikipedia.Org/Wiki/X-Ray_Photoelectron_Spectroscopy>.* [cited.
3.   *Iowa State University Homepage,Department of Materials Science and Engineering, How the Sem Works.* [cited 2011]; Available from: http://mse.iastate.edu/microscopy/home.html.
4.   *Astm Standards G1-03 (Standards Practice for Preparing, Cleaning, and Evaluating Corrosion Test Specimens).* 2003.
5.   M.G. Fontana, *Corrosion Engineering* 3ed. 1987: McGraw-Hill Book Company.

6.   Roger Smart, Stewart McIntyre, Mike Bancroft, Igor Bello. *X-Ray Photoelectron Spectroscopy.* [cited 2011; Available from: *mmrc.caltech.edu/SS_XPS/XPS_PPT/XPS_Slides.pdf.*

7.   Heitz, Ewald, *Dc Electrochemical Methods*, in *Analytical Methods in Corrosion Science and Engineering*, Florian Mansfeld Philippe Marcus, Editor. 2005. p. 435-462.

8.   A.A. Aksüt, W.J. Lorenz, and F. Mansfeld, *The Determination of Corrosion Rates by Electrochemical D.C. And A.C. Methods- Iii. Systems with Discontinuous Steady State Polarization Behaviour* Corrosion Science, 1982. **22**(7): p. 611- 619.

9.   N.G. Thompson, J.H. Payer, and B.C. Syretl,, *Corrosion Testing Made Easy (Dc Electrochemical Test Methods).* NACE International, 1998. **6**.

10.   *Astm Standards G 102-89 (Standards Practice for Calculation of Corrosion Rates and Related Information from Electrochemical Measurements).* 2004.

11.   Milton Stern, A. C. Makrides and *Electrode Assembly for Electrochemical Measurements.* Electrode Assembly for Electrochemical Measurements, 1960. **107**(9): p. 782-782.

12.   Geary, M. Stern and A. L., *Electrochemical Polarization.* Journal of Electrochemical Society, 1957. **104**(1): p. 56-63.

13.   L.L. Shreir, R.A. Jarman, and G.T. Burstein, *Corrosion. Metal/Environment Reactions.* 3 ed. Vol. 1. 1994: Butterworth Heinemann.

14.   Jones, Denny A., *Principles and Prevention of Corrosion* 2ed. 1994: Macmillan Publishing Company.

15.   Scully, John R., *Chapter 4:The Polarization Resistance Method for Determination of Instantaneous Corrosion Rates*, in *Electrochemical Techniques in Corrosion Science and Engineering*, John R. Scully Robert G. Kelly, David W. Shoesmith, and Rudolph G. Buchheit, Editor. 2002, Marcel dekker Inc.

16.   Cottis, R. A., *Electrochemcial Methods*, in *Shreir's Corrosion (Corrosion in Liquids, Corrosion Evaluation)*, M. Graham R. Cottis, R. Lindsay, S. Lyon, T. Richardson, D. Scantlebury and H. Stott, Editor. 2010, Elsevier. p. 1341.

17.   A. Bard , L. Faulkner, *Electrochemical Methods Fundamentals and Applications.* 2 ed. 2001: John Wiley and Sons Inc.

18.   Silverman, David C., *Practical Corrosion Prediction Using Electrochemical Techniques*, in *Uhlig's Corrosion Handbook*, R. W. Revie, Editor. 2000, John Wiley and Sons, Inc: Canada. p. 1179-1225.

19.   Al-Refaie, Abdullah, *Inhibition Mechanisms of Molybdate and Nitrite (Phd Thesis)*, in *School of Materials, Corrosion and Protection Centre*. 2009, The University of Manchester.

20.   Silverman, David, *Tutorial on Cyclic Potentiodynamic Polarization Technique*, in *Corrosion* 1998, NACE International: San Diego Ca .Paper No. 98299

21.   Szklarska-Smialowska, Z., *Characteristics of Pitting Potentials* in *Pitting and Crevice Corrosion.* 2005, NACE International. p. 7.

22.   Nacera S. Meck , Paul Crook, Raul B. Rebak and S. Daniel Day, *Localized Corrosion Susceptibility of Nickel Alloys in Halide Containing Environments*, in *Corrosion*. 2003, NACE International San Diego Ca. Paper No.: 03682.

23.   *Nace Standards Tm0169-2000, Item No.21200 (Laboratory Corrosion Testing Metals).* 2000.

24. Baboian, Robert *Corrosion Rate Calculation (from Mass Loss)*, in *Corrosion Tests and Standards: Application and Interpretation* 2005, ASTM International. p. 23.
25. *Nace Corrosion Engineering's Reference Book*. 3 ed, ed. Robert Baboian and R. Treseder (in Memorium). 2002,: NACE intenatinal.
26. Goldstein JI , et. al., *Scanning Electron Microscopy and X-Ray Microanalysis* 3rd ed. 2003: Springer, New York.
27. P.J. Goodhew, J. Humphreys, and R. Beanland, *Electron Microscopy and Analysis*. 3rd ed. 2001, London, UK: Taylor & Francis Inc.
28. Goodhew.P.J,Humphreys.Jand Beanland.R, *Electron Microscopy and Analysis*. 3rd ed. 2001, London, UK: Taylor & Francis Inc.
29. Watt, I. M., *The Principles and Practice of Electron Microscopy*. 2nd ed. 1997, Cambridge, UK: Cambridge University Press.
30. Zemlyanov, Dmitry, *Introduction to X-Ray Photoelectron Spectroscopy and to Xps Applications*. 2007, Birck Nanotechnology Center. http://nanohub.org/resources/2668.
31. C. Nordling, E. Sokolowski, K. Siegbahn, , *Precision Method for Obtaining Absolute Values of Atomic Binding Energies.* Physical Review 1957. **105** p. 1676-1677.
32. Michelangeli, Ela, *Local Surface Crystallography and Electronic Structure of Adsorbates on Metal-Oxide Substrates*, in *The Faculty of Science and Engineering*. 2004, the University of Manchester: Manchester.
33. *X-Ray Photoelectron Spectroscopy or Esca - Electron Spectroscopy for Chemical Analysis by the Surface Analysis Forum*. [cited 2011]; Available from: http://www.uksaf.org/tech/xps.html.
34. Hüfner, S., *Photoelectron Spectroscopy: Principles and Applications*. 2nd ed. 1996: Springer-Verlag, Berlin.
35. Vickerman, J.C., *Surface Analysis - the Principal Techniques*. 1997: John Wiley & Sons Ltd.
36. Briggs, D., *Handbook of X-Ray and Ultraviolet Photoelectron Spectroscopy*. 1977: Heyden & Son Ltd.
37. John Watts and John Wolstenholme, *An Introduction to Surface Analysis by Xps and Aes*. 2003: John Wiley & Sons Ltd.
38. Linsmeier, Ch, *Auger Electron Spectroscopy.* Vacuum, 1994. **45**(6-7): p. 673 - 690.
39. R. A. Bartynski, E. Jensen, S. L. Hulbert and C. -C. Kao, *Auger Photoelectron Coincidence Spectroscopy Using Synchrontron Radiation* Progress in Surface Science, 1996(2-4): p. 155-162.
40. Sigmund, Peter, *Inelastic Background Signal in X-Ray Photoelectron Spectroscopy.* Physical Review B 1988. **38**(16): p. 11140-11146.
41. Sigmund, Sven Tougaard and Peter, *Influence of Elastic and Inelastic Scattering on Energy Spectra of Electrons Emitted from Solids.* Physical Review B 1982. **25**(7): p. 4452-4466.
42. Hans-Henning Strehblow , Philippe Marcus, *X-Ray Photoelectron Spectroscopy in Corrosion Research*, in *Analytical Methods in Corrosion Science and Engineering*, Florian Mansfeld Philippe Marcus, Editor. 2006, Taylor & Francis Group, LLC.
43. *Photoelectron Spectroscopy – Principles*. [cited; Available from: www.phy.cuhk.edu.hk/course/surfacesci/mod3/m3_s2.pdf.

44.   M. Biesinger, B. Payne, A. Grosvenor, L. Lau, A. Gerson, R. Smart, *Resolving Surface Chemical States in Xps Analysis of First Row Transition Metals, Oxides and Hydroxides: Cr, Mn, Fe, Co and Ni* Applied Surface Science, 2011. **257**(7): p. 2717-2730

45.   Carrick, N. Fairley and A., *The Casa Cookbook Part 1: Recipes for Xps Data Processing*. 2005: Acolyte Science.

46.   Jablonski, Aleksander, *Quantitative Aes: Via the Inelastic Mean Free Path or the Attenuation Length?* Surface and Interface Analysis, 1990. **15**(9): p. 559-566.

47.   Powell, C.J., *Attenuation Lengths of Low-Energy Electrons in Solids.* Surface Science, 1974. **44**(1): p. 29-46.

48.   Spicer, I. Lindau and W. E., *The Probing Depth in Photoemission and Auger-Electron Spectroscopy* Journal of Electron Spectroscopy and Related Phenomena 1974. **3**(5): p. 409-413

49.   Jablonski, C. J. Powell and A., *Evaluation of Calculated and Measured Electron Inelastic Mean Free Paths near Solid Surfaces.* Journal of Physical and Chemical 1999. **28**(1).

CHAPTER FOUR

CORROSION OF 316L AND 254SMO STAINLESS STEEL ALLOYS IN ACETIC ACID SOLUTIONS CONTAINING BROMIDE

4 Corrosion of 316L and 254SMO stainless steel alloys in acetic acid solutions containing bromide

4.1 Introduction

Acidic conditions are commonly encountered in chemical production and processing, necessitating careful material selection to avoid equipment failure. Stainless steels are often the material of choice for such environments, and much work has been performed to determine their performance [1-5]. Here, we contribute to this body of knowledge through examining the corrosion of two austenitic stainless steels, namely 316L and 254SMO, in concentrated acetic acid (HAc) solutions. More specifically, we assess their functionality in the presence of a small concentration of added Br^- anions, which are known to significantly increase system corrosivity [3]. Technologically, this work is directly motivated by its relevance to the industrial synthesis of terephthalic acid, a precursor for polyethylene terephthalate (PET), where HAc is employed as a solvent and Br^- as a catalytic promoter [6-8].

To date, there have been a number of studies of the corrosion of stainless steels in HAc solutions [3-5, 8, 9]. Most pertinently, Turnbull *et al.* have examined the corrosion behaviour of 316L alloy in HAc solutions (11.9 M - 15.3 M) at 90⁰C, containing 18.7 mM (1500 ppm) Br^- anions [5]. Their study focused upon the influence of the addition of Cl^- anions to such solutions.

Significant corrosion rates (> 0.1 mm/year) were found for all of the solutions, both with and without Cl⁻, with the most aggressive comprising 11.9 M acetic acid, 18.7mM Br⁻, and 42mM Cl⁻. Liang *et al.* [4] have also studied the corrosion of 316L stainless steel in acetic acid, probing the impact of several environmental parameters, including temperature and Br⁻/Cl⁻ concentration. Notably, in sharp contrast to Turnbull *et al.* [5] who observed no localised corrosion, they demonstrate that surface degradation includes significant pitting.

In this part of the thesis, we examine the corrosion of 316L and 254SMO stainless steel alloys in two different concentrations of HAc, namely 11.9 M and 15.3 M, with both solutions containing 18.7 mM Br⁻; henceforth these two solutions will be referred to as 11.9M-HAc-Br⁻ and 15.3M-HAc-Br⁻, respectively. Corrosion rates are assessed both by weight loss, and linear polarisation resistance (LPR). Interfacial corrosion chemistry is further characterised by open circuit potential (OCP) and potentiodynamic polarization (PDP) measurements. Substrate morphology is elucidated with optical microscopy, including 3D surface profiling, and scanning electron microscopy (SEM).

4.2 Material and Methods

Commercially produced 316L and 254SMO stainless steels were employed for this study. The nominal elemental compositions of these two alloys are

listed in Table 4-1. Prior to measurements, all samples were cleaned by rinsing sequentially in acetone, ethanol and deionised water, and then stored in a dessicator. 11.9 M and 15.3 M acetic acid solutions were prepared from glacial acetic acid (99.8% purity) and deionised water. Mimicking Ref.[5], Br⁻ anions were introduced into these solutions through the addition of NaBr (8.7 mM) and HBr (10 mM) i.e. a concentration of 18.7 mM of Br⁻ in total. All of the experiments were carried out with the solutions maintained at 90⁰C, under stagnant, aerated conditions. Experiment set up for both weight loss and electrochemical measurements are shown in Figure 4-1.

Table 4-1 Elemental compositions of 316L and 254SMO alloys (at.%).

Alloy	Fe	Cr	Ni	Mo	Mn	Cu	Co	Si	C	P	S	N
316L	67.95	17.93	9.484	1.157	1.839	0.279	0.104	0.790	0.079	0.054	0.048	0.289
254SMO	56.26	20.18	17.32	3.531	0.514	0.613	0.000	0.704	0.056	0.036	0.002	0.790

For the weight loss measurements, 25 mm x 12.7 mm x 1.6 mm corrosion coupons of 316L and 245SMO, which had relatively smooth surface finishes (600 grit), were used Figure 4-2b. Following determination of their initial weights (± 0.0001 g, two coupons were immersed in each solution of interest (0.5 L in a glass round-bottom flask) for a period of 96 hours. Latterly, for selected solutions, weight loss measurements were also undertaken following immersions of 48 and 240 hours. PTFE wire was used to suspend the coupons. To determine weight loss due to corrosion, a standard procedure was applied to remove adhered corrosion products [10, 11], which involves chemical cleaning with 10 vol% nitric acid at 60⁰C for 20 minutes

prior to weighing.   Corrosion rates and associated errors were calculated from the average weight loss of the two coupons in each solution.

OCP, LPR, and PDP measurements were carried out in a round-bottom glass cell, containing 0.5 L of solution. A typical three-electrode arrangement was employed, comprising the working electrode, platinum counter electrode, and a saturated calomel electrode (SCE) as reference electrode.   Working electrodes (exposed area 3.93 cm^2) were cylindrical rods, polished with SiC paper to 4000 grit. Following a design outlined in Milton Stern and A. Makrides work [12], each had a tapped hole in one end to enable attachment to a threaded steel rod, which was insulated from the cell environment by means of a PTFE sleeve, Figure 4-2a. A tight seal between the PTFE sleeve and working electrode was maintained to avoid the occurrence of crevice corrosion. However, the samples were checked after each test and if any crevice was notice the test results were excluded. The reference electrode was located in a separate glass vessel connected to the primary cell through a salt-bridge containing the acetic acid solution under study; the reference electrode unit was not explicitly maintained at 90 ^{0}C. A computer-controlled potentiostat (Gill AC 930) was used to acquire the electrochemical data**.** OCP and LPR measurements were performed at intervals of one hour, with the sample being left open-circuit between measurements. PDP data, anodic branch only, were acquired by scanning to + 700 mV relative to the rest potential at a rate of 10mV/min, and then reversing the scan direction.

Given the large resistance of the solutions under investigation, PDP and LPR data have been IR-drop corrected subsequent to acquisition. Details of solution resistance (R_s) and examples of IR drop corrections can be seen in appendix I.

Following weight loss and electrochemical measurements, substrate morphology was assessed with optical microscopy, including 3D surface profiling using white light interferometric microscopy (ContourGT, Bruker), and SEM supported by energy dispersive X-ray spectroscopy (EDX). Substrates were imaged both parallel to the surface plane and in cross section. For the optical 3D imaging, TalyMap Platinum software [13] was used for data processing.
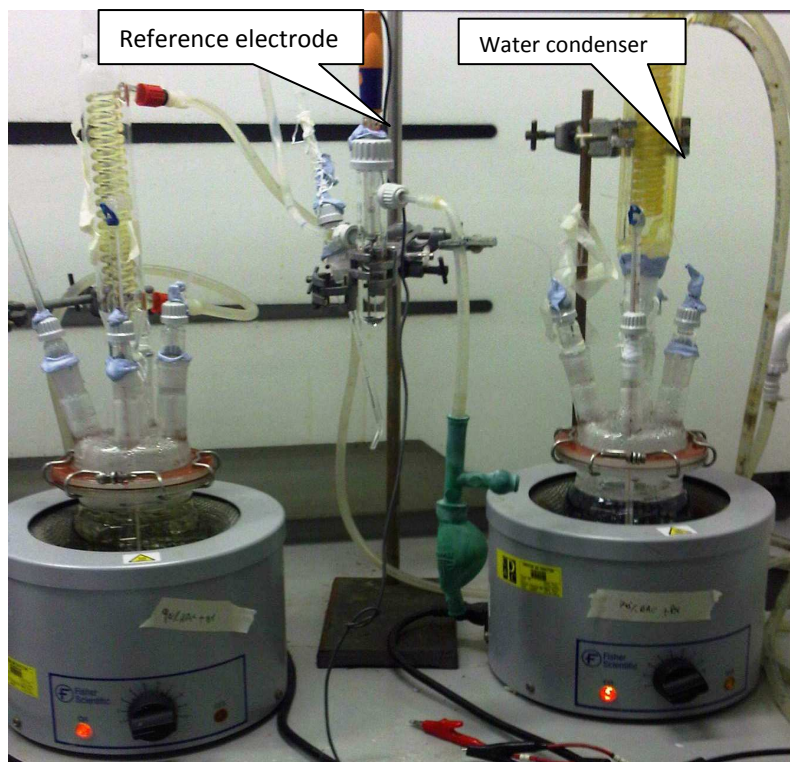

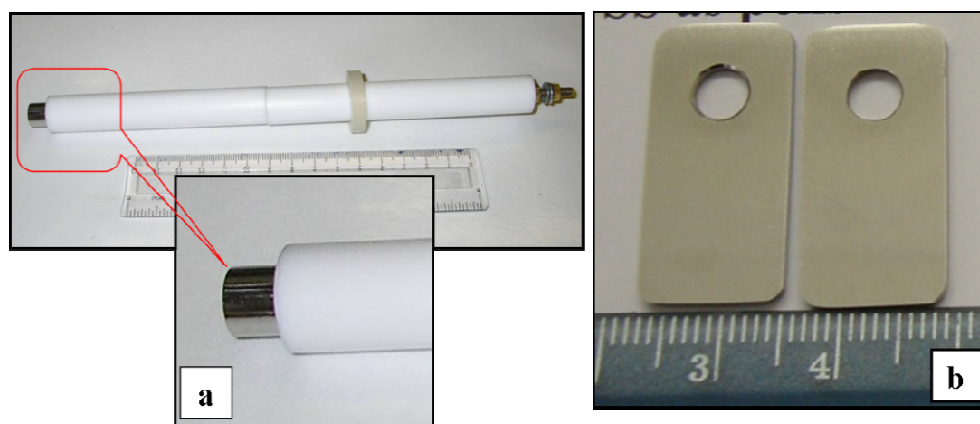Figure 4-1General view of the experiment setup both electrochemical measurement and immersion test

Figure 4-2 Examples of the electrode used in electrochemical measurements and the coupon samples used in this work.

4.3 Results

Table 4-2 lists corrosion rates derived from weight loss measurements for both 316L and 254SMO, following immersion in either 11.9M-HAc-Br⁻ or 15.3M-HAc-Br⁻ for 96 hours. These data indicate that, with the exception of 316L exposed to 15.3M-HAc-Br⁻, corrosion rates were not significant. The 2.3 mm/y corrosion rate exhibited by 316L in 15.3M-HAc-Br⁻ was accompanied by a change in solution colour, transforming from clear to dark red. There was also a yellowing of the solution for 254SMO in 15.3M-HAc-Br⁻, suggesting some dissolution of substrate material. On the basis of previous work [14, 15], the origin of the colour changes is most probably formation of ferric acetate. No colour changes were observed for either alloy in 11.9M-HAc-Br⁻. The change in the solution colour following each test is shown in Figure 4-3.

Table 4-2 Corrosion rates calculated from the weight loss of 316L and 254SMO, following immersion in either 11.9M-HAc-Br- or 15.3M-HAc-Br- for 96 hours.

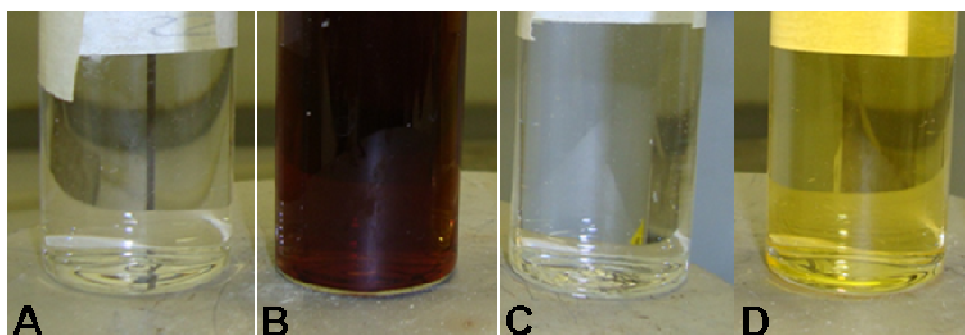|	Corrosion Rate (mm/y)	
	11.9M-HAc-Br⁻	15.3M-HAc-Br⁻
316L	0.007 ± 0.001	2.27 ± 0.02
254SMO	0.005 ± 0.001	0.012 ± 0.001

Figure 4-3 Change in the test solutions colour after the weight loss experiments A) 316L in 11.9M HAc B) 316L in 15.3M HAc C) 254 SMO in 11.9M HAc D) 254 SMO in 15.3M HAc. All these were with 18.7mM Br⁻.

Corrosion coupons of 316L and 254SMO, subsequent to immersion in 15.3M-HAc-Br⁻ for 96 hr, are displayed in Figure 4-4 (a) and (b), respectively. For 316L, exposure to this solution has apparently resulted in significant localised corrosion in the form of pits. An optical micrograph of this coupon is shown in Figure 4-4 (c). This image exhibits dark circular features, of the order of 200 µm in diameter, which can simply be ascribed to pitting. In addition, the remainder of the surface is apparently roughened, indicating that substrate degradation is not restricted to pit formation. Cross-sectional

SEM revealed that these pits are essentially hemispherical in profile, with some displaying a subsurface lateral extent greater than their entrance diameter, i.e. there is undercutting of the substrate (Figure 4-4 (e)). The possibility of intergranular corrosion, initiated at pit walls, was assessed by etching cross-sectioned samples in oxalic acid solution to reveal the grain structure surrounding pits. No evidence of such attack was apparent.

In sharp contrast to 316L, no pitting of 254SMO is evident in either the photograph of the corrosion coupon in Figure 4-4 (b), or the corresponding optical micrograph (Figure 4-4 (d)), where observed features are simply a result of surface preparation. However, a higher lateral resolution SEM image of this surface (Figure 4-4 (f)) does indicate the removal of some substrate material through the appearance of micron size angular surface cavities exhibiting apparently well-defined facets. It should be noted that there was no evidence of surface degradation for either alloy following immersion in 11.9M-HAc-Br$^-$ for 96 hours at 363 K.

Figure 4-5 (a) and (b) display PDP scans acquired from 316L and 254SMO, respectively, in 11.9M-HAc-Br$^-$. To probe the evolution of the substrate corrosion chemistry with time, data have been collected following immersion for 0.5 hr, as well as 96 hr. Despite weight loss measurements and substrate analysis indicating no significant corrosion after 96 hr, it is clear that there are still differences in the PDP scans both as a function of alloy and time. For 316L (Figure 4-5 (a)), the OCP (starting point of scan) is -

240 mV after 0.5 hr of immersion, and increasing anodic polarisation leads initially to a peak in current density (4×10^{-2} mA cm^{-2} at -200 mV). This feature is strongly indicative of the substrate undergoing a transition from the active to passive state within this potential range. Passivity is maintained until approximately 0 mV, as demonstrated by the relatively low value of current density that is largely independent of applied polarisation. Further polarisation leads to a steady rise in current density (3×10^{-3} mA cm^{-2} to 0.4 mA cm^{-2}) until a potential of +200 mV is reached. Here, there is a sudden step increase in current density, which can be attributed to + 200 mV being the critical pitting potential (E_c). After 96 hr of immersion, the OCP of 316L has risen to -50 mV, and no active-passive transition feature is apparent in the PDP curve upon anodic polarisation. Comparison with the PDP data acquired from 316L after 0.5 hr of immersion suggests that the substrate is already in a passive state at this value of OCP. Furthermore, both PDP profiles are rather similar above -40 mV, including the value of E_c and the degree of hysteresis displayed upon reversing potential scan direction. For both reverse scans, the protection potential (E_P), where pits become passivated, is ~ -30 mV.

Figure 4-5 (b) displays the two PDP curves for 254SMO in 11.9M-HAc-Br⁻. After 0.5 hr of immersion, in contrast to 316L, the profile of the forward scan, which quickly becomes near vertical as potential is swept away from OCP (– 70 mV), indicates that the substrate is in a passive state at OCP. Above +390

mV, the current density increases steadily until E_c (+520 mV) is reached. After 96 hr of immersion OCP is +180 mV, which is also consistent with the surface being in a passive state, with E_c being located at +550 mV. For both curves, there is again a significant hysteresis in the polarisation profile upon reversal of the scan direction.

The OCP of each alloy in 11.9M-HAc-Br- is plotted as a function of time up to 96 hr in Figure 4-5 (c). Focussing on 316L, OCP increases from -230 mV to -130 mV within the first three hours of immersion. From examination of the PDP data in Figure 4-5 (a), this change in OCP can be assigned to surface passivation. OCP increases further to -50 mV during the following 23 hr of immersion, most likely due to thickening of the passive film. Subsequent to this period of time, OCP remains approximately constant, indicating that the 316L surface has achieved a steady state after 23 hr of immersion. Unlike 316L, the OCP of 254SMO does not plateau, but rather increases continuously, initially more rapidly, from - 130 mV to +150 mV over the 96 hr of immersion. This range of OCP is consistent with the steel being in a passive state throughout immersion (see Figure 4-5 (b)). The continuous increase in potential can simply be interpreted as arising from film thickening.

Figure 4-5 (d-f) display results equivalent to those in Figure 4-5 (a-c), but for the two alloys in 15.3M-HAc-Br-, which has been shown to be more aggressive. Figure 4-5 (d) shows PDP data for 316L in 15.3M-HAc-Br- after

- 114 -

0.5 hr and 96 hr of immersion. Both curves exhibit an immediate steep rise in current density as the substrates are anodically polarised away from OCP. These profiles may be interpreted as a lack of surface passivity, i.e. the surfaces are undergoing active dissolution throughout the anodic sweep. OCP is -180 mV and -30 mV, after 0.5 hr and 96 hr of immersion, respectively. This change is consistent with the plot of OCP versus immersion time in Figure 3 (c), where there is a sudden increase in OCP after 65 hr.

PDP data from 254SMO in 15.3M-HAc-Br$^-$ after 0.5hr and 96 hr of immersion are depicted in Figure 4-5 (e). Beginning with the shorter immersion time, the PDP curve exhibits a peak in current density (2×10^{-1} mA cm^{-2} at - 100 mV) characteristic of a transition from an active to passive surface state. This passive state is maintained up to +230 mV, at which point the current density rapidly rises. Notably, reversing the potential sweep direction does not result in any hysteresis, suggesting that the steep current density increase above +230 mV is not associated with archetypal pit formation processes. In contrast, such hysteresis is observed in the PDP data acquired following immersion for 96 hr, with E_c being +660 mV. However, there is no evidence of passivity in the forward anodic sweep, rather simply a steady increase in current density until E_c is attained. Furthermore, OCP has increased to +310 mV; it was -130 mV after 0.5 hr of immersion. This variation in OCP agrees with that exhibited Figure 4-5 (f), where OCP is graphed as a function of time of immersion. In this plot there is a step

change in OCP after 14 hours of immersion, which can be ascribed to the onset of surface passivity.

To aid further interpretation of the profiles of the PDP data acquired after 0.5 hr of immersion in 15.3M-HAc-Br$^-$, SEM images have been acquired subsequent to PDP measurements. Figure 4-6 (a) shows a typical image for 316L. As expected on the basis of the PDP curve after 0.5 hr immersion (Figure 4-5 (d)), the surface has undergone general dissolution as evidenced by the overall etched appearance. In addition, micron-sized facetted pits are apparent, indicating localised corrosion is also occurring. EDX data acquired from these pits (not shown) suggest that MnS inclusions are apparently nuclei for this pit formation. A SEM image of 254SMO following PDP after 0.5 hr of immersion in 15.3M-HAc-Br$^-$is is shown in Figure 4-6 (b). Unlike, 316L, no general dissolution is observed, but facetted pits are again observed. It should be noted that the lack of general dissolution does not indicate that the surface is passivated at OCP, but rather is a result of anodic polarisation inducing passivation. EDX indicates that the near surface alloy composition within the pits differs significantly from that of the remaining surface. Specifically, the concentrations of Ni and Mo are reduced, 20.3 at.% to 6.7-13.0 at.% and 2.5 at.% to 0.3 at.%, respectively, whilst that of Cr is increased, 23 at.% to 37- 41 at.%.

Given that the PDP and OCP data (e.g. steps in OCP versus time profiles in Figure 4-5 (f)) suggest that the corrosion exhibited by both 316L and 254SMO in 15.3M-HAc-Br$^-$ may be time dependent, temporal variation has been further investigated through weight loss measurements. Table 4-3 lists the corrosion rates of 316L and 254SMO in 15.3M-HAc-Br$^-$ obtained from weight loss after 48, 96, and 240 hours of immersion. As already established gravimetrically for an immersion period of 96 hours (see Table 4-2), the corrosion rate of 316L is much greater than that of 254SMO for all three immersion periods. Furthermore, whereas for 316L the corrosion rate apparently simply fluctuates with time (±10%); there is a 60% reduction in the corrosion rate of 254SMO over the same period. This systematic reduction of the corrosion rate as a function of time for 254SMO is most likely due to surface passivation after some period of immersion. From the OCP plot for 254SMO in 15.3M-HAc-Br$^-$ (Figure 4-5 (f)), it is most likely that such passivation coincides with the sudden increase in OCP after 14 hr. We note that the similar positive step, although smaller in amplitude, in OCP for 316L immersed in 15.3M-HAc-Br$^-$ cannot be attributed to achievement of surface passivity, as there is no corresponding decrease in corrosion rate at 240 hr of immersion.

To confirm that the sudden increase in OCP for 254SMO is coincident with surface passivation, LPR is employed to determine the variation with time of the instantaneous corrosion rate. Figure 4-7 shows the OCP plot from Figure

4-5 (f) for 254SMO in 15.3M-HAc-Br⁻, together with LPR corrosion rate data acquired at the same time. Clearly, the sharp increase in OCP corresponds to a sudden decrease in corrosion rate, verifying the origin of the OCP step. It should be pointed out the corrosion rates determined from LPR are significantly higher than those obtained from weight loss. Partially, this may be attributed to uncertainty in the estimation of the Tafel constants; values of b_a = 120 mV/decade and b_c =40 mV/decade were employed. In addition, it has been reported that for systems where the solution phase displays low conductivity, as is the case here, application of LPR can result in overestimation of the corrosion rate, particularly when the real corrosion rate is very low [16]. Notably, although the reported LPR corrosion rates may be too high, this systematic error does not detract from the veracity of the correlation between the steps in the OCP and LPR plots in Figure 4-7.
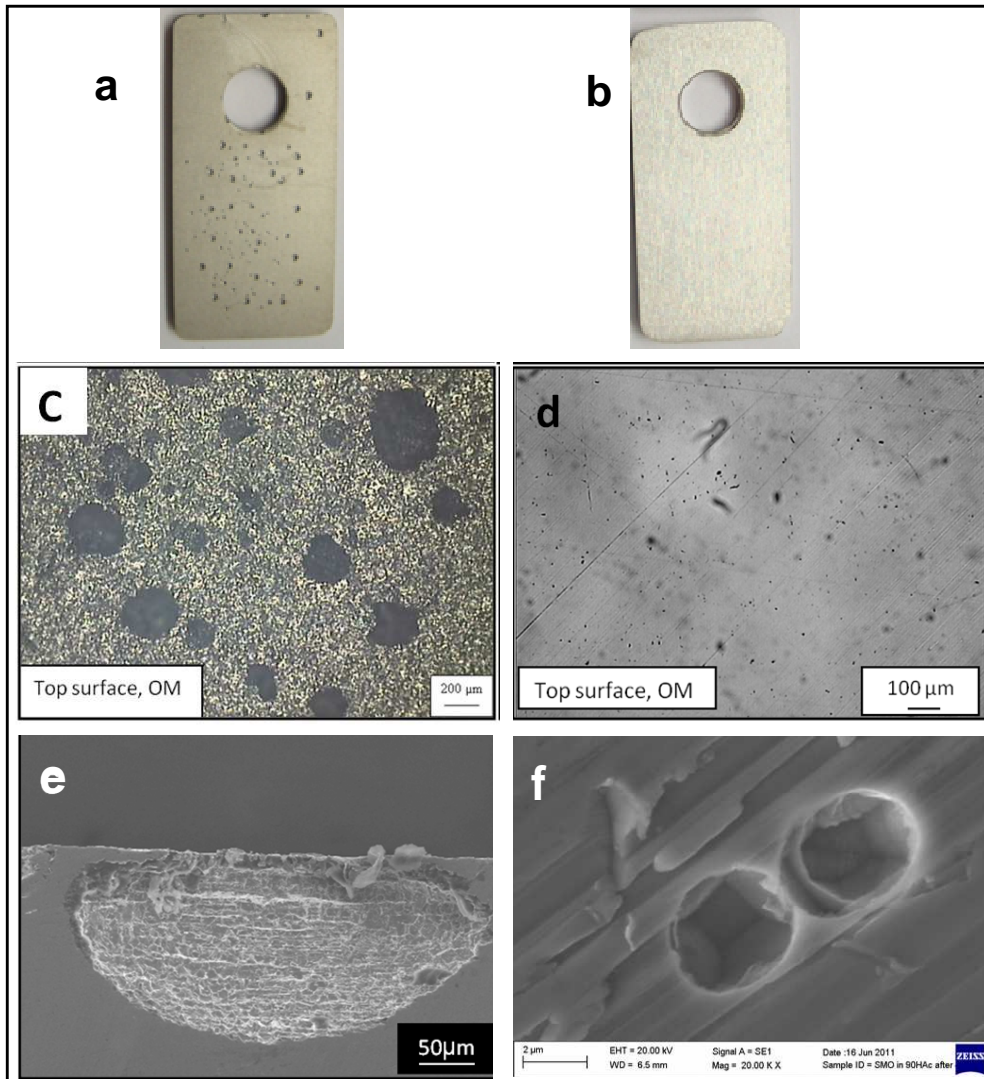
Figure 4-4 Images of 316L and 254SMO samples acquired subsequent to the immersion in 5.3M-HAc-Br⁻ for 96hr. (a) and (b) photograph of coupons of 316L and 254SMO, respectively. (c) and (d) Optical micrographs for face of the corrosion coupons of the 316L and 254SMO, respectively. (e) Cross-sectional SEM of the pit in 316L. (f) SEM of the 254SMO sample.
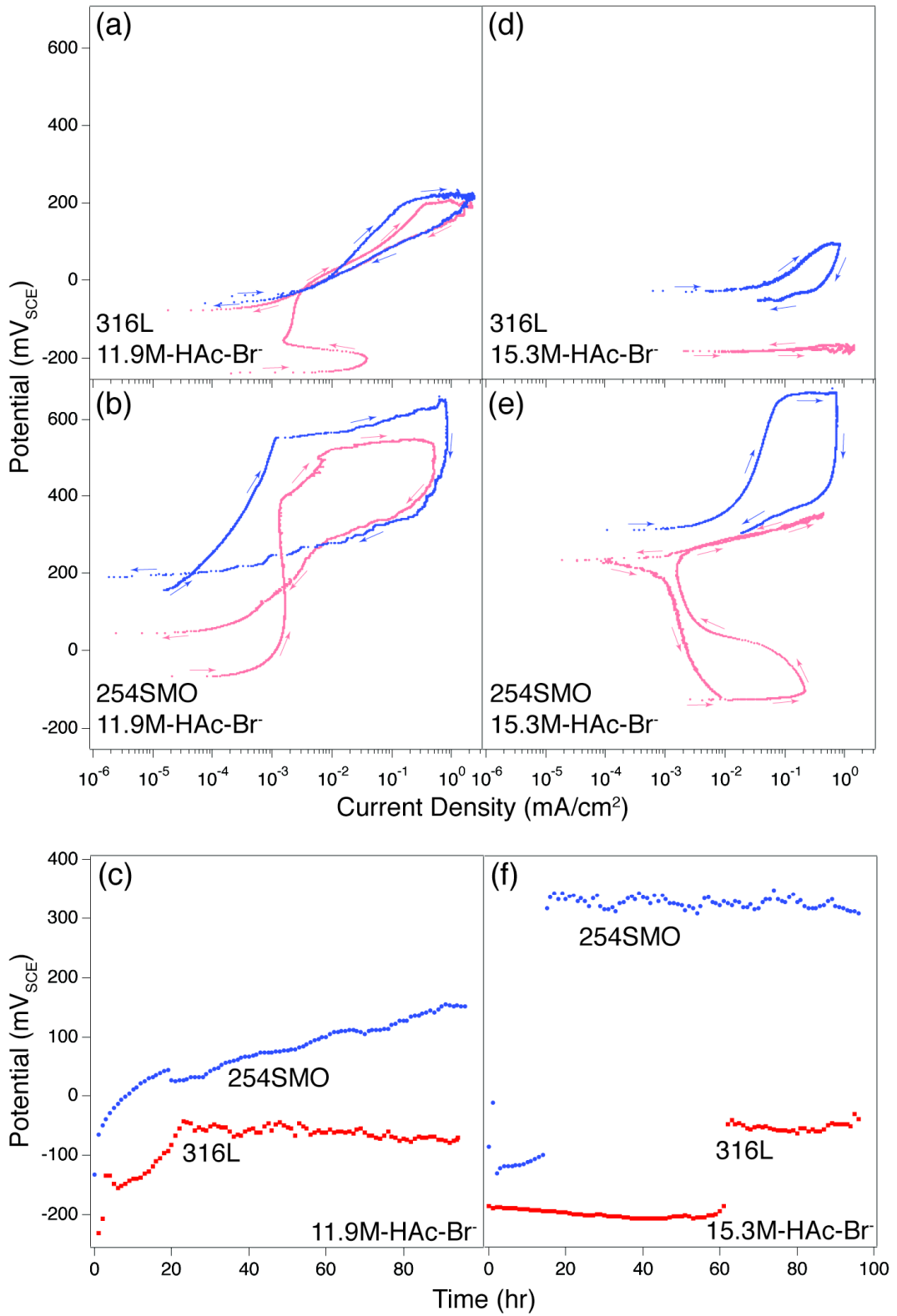
Figure 4-5 PDP scans after 0.5hr (red) and 96hr (blue) and OCP acquired from 316L and 254SMO immersed in 11.9M-HAc-Br⁻ (a-c) and in 15.3M-HAc-Br⁻ (d-f)
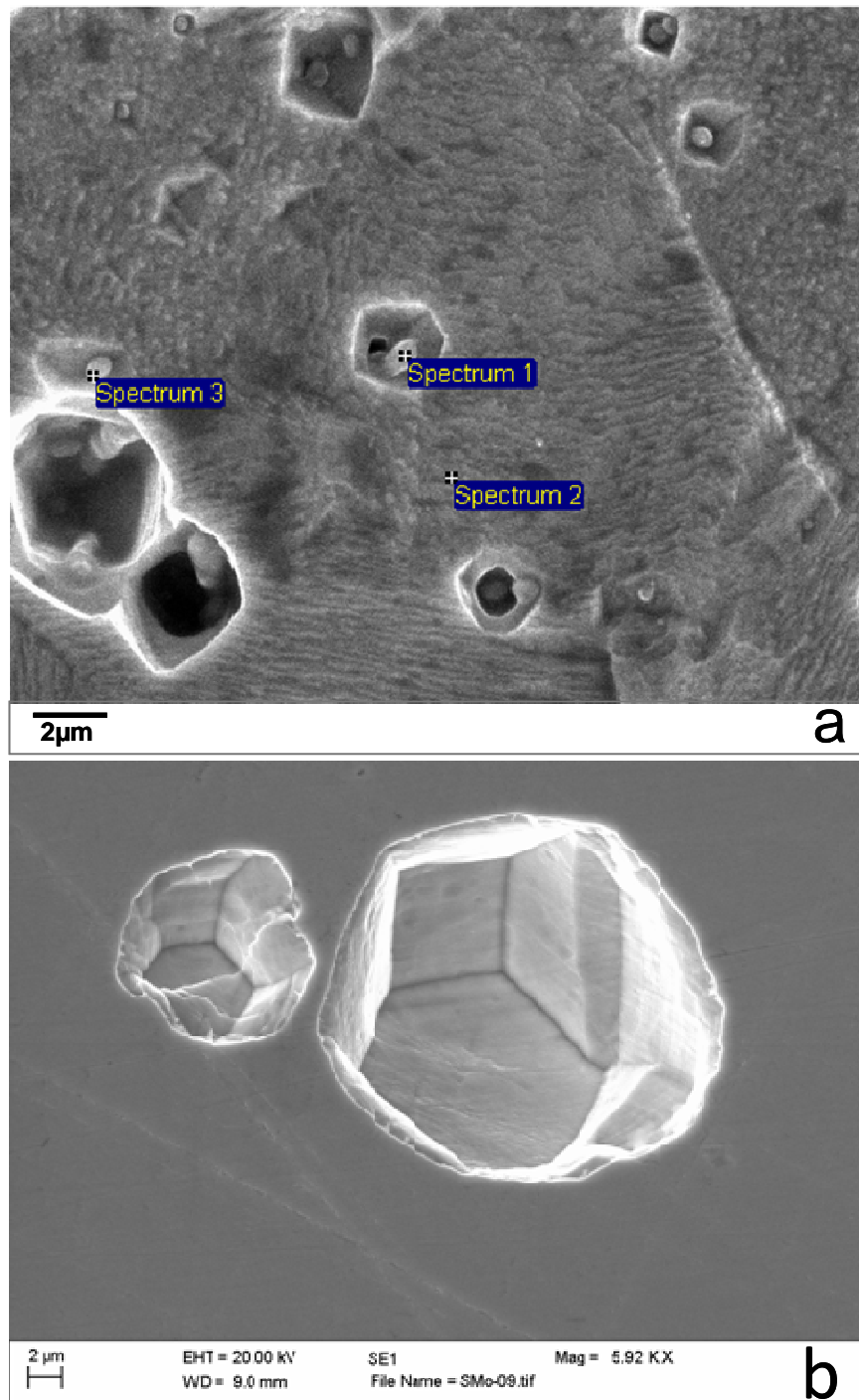
Figure 4-6 SEM images for 316L (a) and 254SMO (b) after 0.5 hour of immersion in 15.3M-HAc-Br⁻ and then anodically polarised as displayed in Figure 2 (d) and (e).

Table 4-3 Corrosion rates calculated from the weight loss of 316L and 254SMO, following immersion in 15.3M-HAc-Br- for 48, 96, or 240 hr.

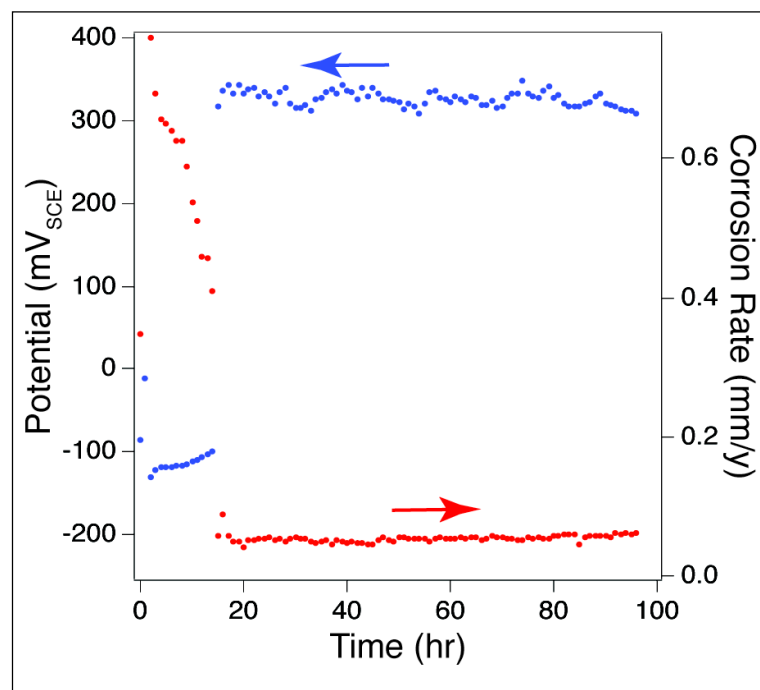|	Corrosion Rate (mm/y)	
Immersion time (hr)	316L	254SMO
48	2.51 ± 0.03	0.020 ± 0.002
96	2.27 ± 0.02	0.012 ± 0.001
240	2.73 ± 0.04	0.008 ± 0.001

Figure 4-7 plot showing the variation with the time in the OCP and corrosion rate (mm/year) calculated by LPR (after IR correction) for 254SMO stainless steel immersed in 15.3M-HAc-Br- for 96hours

Finally, as the images of 316L in Figure 4-4 indicate the occurrence of both pitting and uniform corrosion in 15.3M-HAc-Br-, an attempt has been made to estimate the relative importance of these two processes in terms of material loss. For this work 3D surface profiling, using white light

interferometry, has been employed to get an estimate of the amount of material lost from within pits compared to the overall gravimetric weight loss. Effort has focussed on a coupon of 316L immersed in 15.3M-HAc-Br⁻ for 240 hr. Figure 4-8 shows the 3D profile of the two faces and four sides of the 316L coupon. Pits are apparent as depressions in the images.

To calculate the total volume of the pits, the material ratio curve (Abbott Firestone curve) that represents the areal material ratio of the surface as a function of its depth was employed [13]. Such an approach has been recently been employed successfully for determining the volume of surface voids on processed aluminium alloy [13, 17]. Prior to pit volume calculation the circular hole for coupon suspension and serial number imprinted on one face were masked to avoid error in pit volume calculation. Table 4-4 shows the output of this analysis, including the area occupied by pits, volume of pits, amount of material lost, and pitting corrosion rate. Besides listing values for the entire coupon (Total), data are also provided for each of the four edges and the two faces (see labelling in Figure 4-8). Evidently, the highest pitting corrosion rates, 2.3 - 3.9 mm/y, are observed for the coupon edges. Most likely, this phenomenon is associated with induced stress during sample machining. More importantly, the pitting corrosion rate of the entire coupon (Total) was determined to be 1.7 mm/y, which is a considerable fraction (~ 0.6) of the uniform + pitting corrosion rate, 2.73 ± 0.04 mm/y, obtained from weight loss of 316L following immersion for 240 hr. Thus pitting contributes

significantly to the mass loss of the sample under these conditions. It should

be noted that mass loss due to pitting, determined from 3D surface profiling,

is systematically underestimated to a certain extent due to some pits

undercutting the substrate (e.g. Figure 4-4 (e)), which is not detected by this
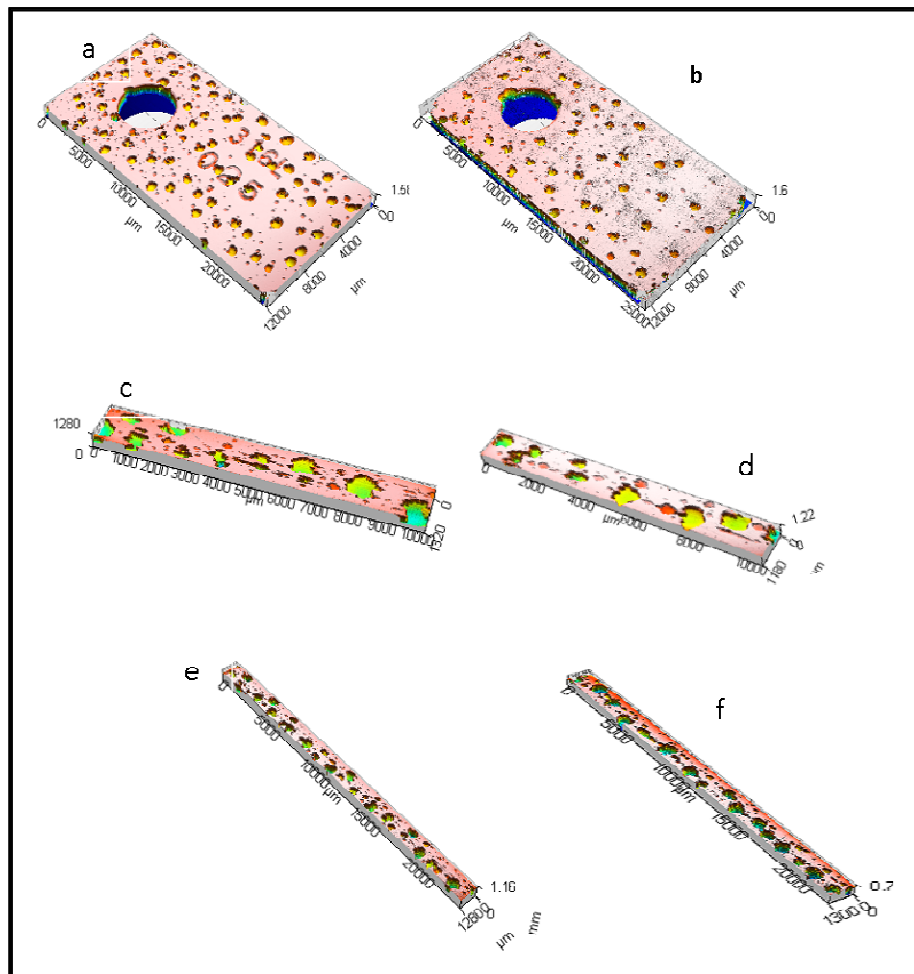
technique.

Figure 4-8 3D surface profile of 316L stainless steel coupon sample immersed in 15.3M HAc-Br$^-$ for 240hr. These were acquired by white light interferometry: a) face 1, b) face 2, c) side 1, d) side 2, e) side 3 and f) side 4.

Table 4-4 Area occupied by pits, volume of pits, amount of mass lost, and pitting corrosion rate obtained from analysis of 3D surface profiling images (Figure 4-8) of a 316L sample subsequent to immersion in 15.3M-HAc-Br for 240 hr. Labels in Figure 4-8 provide a key to the relative locations of the faces and edges.

	Surface Area of pits (cm²)	Surface Area (cm²)	Volume of pits ($\mu m^3/\mu m^2$)	Mass lost (mg/cm^2)	Pitting Corrosion rate (mm/y)
Face 1	0.51	2.99	50	40	1.8
Face 2	0.37	3.16	38	31	1.4
Side 1	0.04	0.14	108	86	3.9
Side 2	0.08	0.30	64	51	2.3
Side 3	0.09	0.30	87	69	3.2
Side 4	0.04	0.13	90	72	3.3
Total	1.13	7.02	49	39	1.7

4.4 Discussion

On the basis of the above data, it has been demonstrated that the corrosion performance of austenitic stainless steels, namely 316L and 254SMO, in concentrated acetic acid solutions containing bromide at 90^0C depend upon length of exposure and alloy identity. It was found that 316L and 254SMO steels have good corrosion resistance and low corrosion rates, 0.007 mm/y and 0.005 mm/y, respectively, in 11.9M-HAc-Br⁻. Increasing acid concentration to 15.3 M led to a dramatic increase in corrosion rate of 316L to 2.7 mm year^{-1} with clear evidence of uniform and pitting corrosion proceeding simultaneously. The presence of pitting is similar to previously reported findings where 316L suffered from pitting corrosion in 86% (15.3M) HAc with 1000ppm Br⁻ ions in a terephthalic acid (TA) production plant [18]. Additionally, presence of Br traces in 87% acetic acid at 124°C significantly increase the pit depth of the type 300 series stainless steels [18]. Furthermore, it was reported by both Ashiru *et al.* [8] and Gon *et al.* [6], during materials failure investigations that pitting corrosion of 316 stainless steel equipments in TA plant failed in an environment of acetic acid and either bromide or chloride ions.

The open circuit potential (OCP) measurements, supported by potentiodynamic polarisation and substrate imaging, were particularly useful in assessing condition of changes with time. Notably, the step increase in OCP for 316L steel and 254SMO during immersion in 15.3M-HAc-Br⁻

solution indicates sudden changes in corrosion activity of the steels. A similar step increase in potential from -250 mV to 20 mV was observed in the work by Alan Turnbull *et al*. [5] for 316L in 11.9 M HAc with Br⁻, whilst the same alloy showed no step in 15.3 M HAc with Br ions. Generally, it is assumed that such a remarkable shift in the OCP toward more noble potentials is indicative of formation of a film offering some degree of protection against corrosion. This explanation is appropriate for 316L in 11.9M-HAc-Br⁻, although the OCP is more gradual. It is also the applicable for OCP step seen for the 254SMO in 15.3M-HAc-Br⁻. However, the step increase in the OCP observed for 316L in 15.3M-HAc-Br⁻ is not associated with a signifcant decrease in corrosion rate. An alternative explanation is that the step coincides with an increase in the importance of pitting due to the evolving surface structure.

Focusing on the pits on 254SMO, their origin is possibly due to presence of a small amount of sigma-phase. The composition of this phase is strongly dependant on annealing temperature. Generally, the most important alloying elements in the sigma-phase composition are Cr, Ni and Mo [19]. The increased level of chromium in sigma phase results in chromium de-alloying of the steel in the vicinity of the phase followed by localised attack of those areas. It is known that some level of sigma phase remains in properly treated 254SMO steel; additionally, the amount of the sigma-phase can increased under applied cold deformation and high temperature aging

during fabrication [19]. The EDX analysis taken within the pits indicates reduced level of Ni and increased level of Cr compared with analysis taken from the steel surface and further verifies presence of the phase.

4.5 Summary

- Corrosion behaviour of austenitic 316L and 254SMO stainless steels at 90^0C changes significantly with increase in acetic acid concentration in the presence of bromide. Both steels show excellent corrosion resistance in 11.9M-HAc-Br$^-$. In contrast, both steels corrode to some extent in 15.3M-HAc-Br$^-$, with 316L displaying a much greater corrosion rate.

- During immersion in 15.3M-HAc-Br$^-$ 254SMO steel passivates after approximately 14 hours, whilst 316L continues to dissolve.

- Crystallographic pits are revealed on the surface of both steels after immersion in 15.3M-HAc-Br$^-$.

- Intensive localised attack is evident on the surface of 316L, and is associated with presence of manganese sulphide inclusions.

- Localised attack of 254SMO steel is possibly associated with the presence of a small amount of sigma-phase.

- The correlation between the up/down steps in OCP and corrosion rate by LPR observed for 254SMO is indicative of passivation.

- The 316L steel experiences uniform and pitting corrosion in 15.3M-HAc-Br⁻. The contribution of the pits to the total weight loss was at least 60 % after 10 days of immersion.

4.6 References

1. A. Pardo M. Merino, A. Coy, F. Viejo, R. Arrabal and E. Matykina, *Effect of Mo and Mn Additions on the Corrosion Behaviour of Aisi 304 and 316 Stainless Steels in H_2so_4.* Corrosion Science, 2008. **50**(3): p. 780-794

2. E. A. Ferreira, R. D. Noce, C. S. Fugivara, and A. V. Benedetti, *Evaluation of 316l Stainless Steel Corrosion Resistance in Solution Simulating the Acid Hydrolysis of Biomass.* Journal of The Electrochemical Society, 2011. **158**(4): p. C95-C103.

3. G.Q. Liu, Z.Y. Zhu, W. Ke, E.H. Han, and C.L. Zeng, *Corrosion Behavior of Stainless Steels and Nickel-Based Alloys in Acetic Acid Solutions Containing Bromide Ions.* Corrosion, 2001. **57**(8): p. 730-738.

4. Liang bin , Gong Jian-ming and TU shan-dong, *Corrosion Behavior of Aisi316l and Saf2205 Stainless Steel in Acetic Acid Solution Containing Br Ion.* Materials for Mechanical Engineering, 2006. **30**(1): p. 56-59.

5. Alan Turnbull, Mary Ryan , Anthony Willetts and Shengqi Zhou *Corrosion and Electrochemical Behaviour of 316l Stainless Steel in Acetic Acid Solutions.* Corrosion Science, 2003. **45**: p. 1051–1072.

6. Y. Gong, J. Cao, X.-H. Meng and Z. G. Yang, *Pitting Corrosion on 316l Pipes in Terephthalic Acid (Ta) Dryer.* Materials and Corrosion 2009. **60**(11): p. 899-908.

7. G.R. Pophali, R. Khan, R.S. Dhodapkar, T. Nandy, S. Devotta, , *Anaerobic-Aerobic Treatment of Purified Terephthalic Acid (Pta) Effluent; a Techno-Economic Alternative to Two-Stage Aerobic Process. , .* Journal of Environmental Management, 2007. **85**(4): p. 1024-1033.

8. O. Ashiru , A. Al Refaie. *Pitting Corrosion Problems of Stainless Steels in Pta Plant,.* in *NACE international* 2007. Nashville, Tennessee. Paper No. 07196.

9.   M. Adeli, K. Raeissi , and M.A. Golozar, *Corrosion Inhibition of 2205 Duplex Stainless Steel in Acetic Acid Solution by Nitrite Anions.* Corrosion 2010. **66**(7).

10.   ASTM Standard G1-03 Standard Practice for Preparing, Cleaning, and Evaluating Corrosion Test Specimens, ASTM International, DOI: 10.1520/G0001-03.

11.   Baboian, Robert, *Corrosion Rate Calculation (from Mass Loss)*, in *Corrosion Tests and Standards: Application and Interpretation.* 2005, ASTM International. p. 23.

12.   Makrides, Milton Stern and A. C., *Electrode Assembly for Electrochemical Measurements.* Journal of Electrochemical Society, 1960. **107**(9): p. 782-782.

13.   B. Rivett and E.V. Koroleva , F.J. Garcia-Garcia, J. Armstrong, G.E. Thompson, P. Skeldon, *Surface Topography Evolution through Production of Aluminium Offset Lithographic Plates.* Wear, 2011. **270**(3-4): p. 204-217.

14.   Z. F. Yin , W. Z. Zhao , W. Tian , Y. R. Feng and C. X. Yin, *Pitting Behavior on Super 13cr Stainless Steel in 3.5% Nacl Solution in the Presence of Acetic Acid.* Journal of Solid State Electrochemistry 2009. **13**: p. 1291 - 296.

15.   *Wikipedia, the Free Encyclopedia.* last modified on 29 December 2010 [cited January, 2011; Available from: http://en.wikipedia.org/wiki/Iron(III)_acetate.

16.   Hilbert, L.R., *Monitoring Corrosion Rates and Localised Corrosion in Low Conductivity Water.* Corrosion Science, 2006. **48**(12): p. 3907-3923.

17.   Lunder, Borge Holme and Otto, *Characterisation of Pitting Corrosion by White Light Interferometry.* Corrosion Science 2007. **49**(2): p. 391- 401.

18.   Koch, G.H., *Localised Corrosion in Halides Other Than Chlorides, Mti Publication,Materials Technology Institute of the Chemical Process Industries* Vol. 41. 1995: by NACE Int. Houston, TX

19.   T. Koutsoukis, E. G. Papadopoulou, S. Zormalia, P. Kokkonidis and G. Fourlaris, *Precipitation Sequences in Cold Deformed Superaustenitic Stainless Steels.* Materials Science and Technology, 2010. **26**(9): p. 1041-1048.

CHAPTER FIVE

X-RAY PHOTOELECTRON SPECTROSCOPY OF 316L AND 254SMO STAINLESS STEEL ALLOYS: IMPACT OF IMMERSION IN ACETIC ACID SOLUTIONS

5 X-Ray Photoelectron spectroscopy of stainless steel alloys: Impact of immersion in acetic acid solutions

5.1 Introduction

High corrosion resistance of stainless steels is achieved due to the formation of a thin protective, passive, surface film. However, stainless steel alloys are not completely inert and do suffer corrosion problems in aggressive environments. The passive film formed on the surface of steel changes with the surrounding environment thus , it can grow or dissolve, and may adsorb anions [1]. One of the important factors controlling the characteristics (composition, protectiveness, thickness) of the passive film that forms on any steel surface is the composition of the steel.

Many studies characterising these passive films on different types of stainless steels exposed to various environments have already been reported [2-14]. As a general agreement in most of previously done researches, chromium (Cr) and molybdenum (Mo) play the significant influence on the stainless steel passive film formation compared to the other alloying elements. However, there are few numbers of studies concerning the corrosion behaviours of stainless steels and their surface films in acetic acid environments. Sekine et al. [15, 16] worked on the corrosion performance of stainless steels in acetic and formic acids. From these studies, the main conclusion was that mainly, the Cr and Mo contributed to corrosion

resistance in aqueous acid solution. Alan Turnbull [17] noticed an increase in the corrosion potential to more noble value after some time of immersion in the test solution for 316L stainless steel in 11.9M acetic acid solution containing bromide ions at 90 °C . It was concluded that, this observation was due to a formation of a protective film and passivation. Different stainless steels and nickel-based alloys were tested in 50 % acetic acid solutions containing 0.29M Br⁻ [18]. Alloys with higher Mo content showed excellent pitting resistance. In their study, It was found that a protective film of Cr oxide (Cr_2O_3) and Mo dioxide (MoO_2) was formed which protecting the materials from the attack of aggressive ions. Furthermore, in 60% acetic acid solution containing chloride ions at 85 °C, the passive film formed on 2205 stainless steel was studied by X. Q. Cheng [19]. It was found that , about 50% of the top surface of the passive film was Cr cations when the potential is in the passive region while if potential is higher than the trans-passive potential, the Mo content accounted about 45% of the metal cations in the near-surface region.

In the present research, the two examined austenitic stainless steel, 316L and 254SMO, showed a satisfactory resistance to any type of corrosion damage in 11.9M HAc-Br⁻ at 90°C while in 15.3M HAc-Br⁻ solution, only alloy 254SMO showed a sufficient corrosion resistance. These results had been illustrated in the preceding chapter of this thesis (chapter 4) by corrosion weight loss and electrochemical measurements. So far, there is no previous studies

characterized the surface film formed on the 254SMO while, there is only a limited studies done for 316L alloy in acetic acid environment specifically. Also, to gain further insight into the quite different corrosion performances of 316L and 254SMO in concentrated acetic acid, 15.3M, containing bromide anions, a systematic XPS study has been undertaken. Spectra have been acquired from both alloys as a function of immersion time to evaluate surface composition.

5.2 Material and Methods

In this study, rectangular coupon samples (2.5cm x 1.5cm) of 316L and 254SMO stainless steel alloys were used. Chemical compositions of these alloys are presented in Table 5-1. All the samples surfaces were mechanically polished using SiC papers up to 4000 grit, Figure 5-1. After that, the samples were rinsed with acetone, ethanol and washed by deionised water and then allowed to dried in air. The samples kept in a desiccator for at least 24 hours before the test. 15.3M acetic acid (HAc) solution with 18.7mM bromide ions was utilized as the test solution. All reagents chemicals used in this study were analytical grade.

Initially, XPS analysis was performed for as mechanically polished samples that had not been exposed to any test solution. Then, in order to prepare an appropriate range of the alloys substrates for XPS analysis and to investigate the variations in the surface film composition with the immersion time, samples were immersed in 15.3M-HAc-Br⁻ solution (1/2 L in a glass beaker)

for a period of 48 and 96 hours. All of the immersion tests were carried out at $90^{\circ}C$ temperature, under stagnant and open to atmosphere conditions. Once the sample removed from solution, it was gently rinsed by deionised water to remove any possible salt from the surface and then dried in air prior to XPS measurements.

The XPS was performed in a Kratos Axis Ultra instrument (base pressure ~ 2 x 10-9 mbar) equipped with a load lock system for sample introduction. Monochromated Al Kα X-rays (hv = 1486.6 eV, Δhv ~ 0.6 eV) were employed as the photon source. Emitted photoelectrons were collected using a 165 mm hemispherical energy analyser incorporating a delay line detection system. Regions for analysis, not containing any pits within the analysed area ~ 0.3 mm x 0.7 mm, were selected using the optical microscope. Data were acquired at analyser pass energy of 80 eV for wide energy scan overview spectra, and 20 eV for short higher energy resolution spectra of single core levels. Two photoelectron emission angles (θ_E), namely 0° (emission along the surface normal) and 60°, were utilised during the measurements. The angle subtended by the X-ray beam and the entrance lens of the analyser was 60°, and the sample holder's rotation axis was perpendicular to the plane containing these two elements. To prevent any vertical differential charging due to the presence of oxide surface films, samples were mounted using vacuum compatible double-sided adhesive tape. Charge accumulation

during data collection was compensated by exposing samples to a flood of low energy electrons ($\leq$ 3 eV).

Table 5-1 Elemental compositions of 316L and 254SMO alloys (at.%).

Alloy	Fe	Cr	Ni	Mo	Mn	Cu	Co	Si	C	P	S	N
316L	67.95	17.93	9.484	1.157	1.839	0.279	0.104	0.790	0.079	0.054	0.048	0.289
254SMO	56.26	20.18	17.32	3.531	0.514	0.613	0.000	0.704	0.056	0.036	0.002	0.790
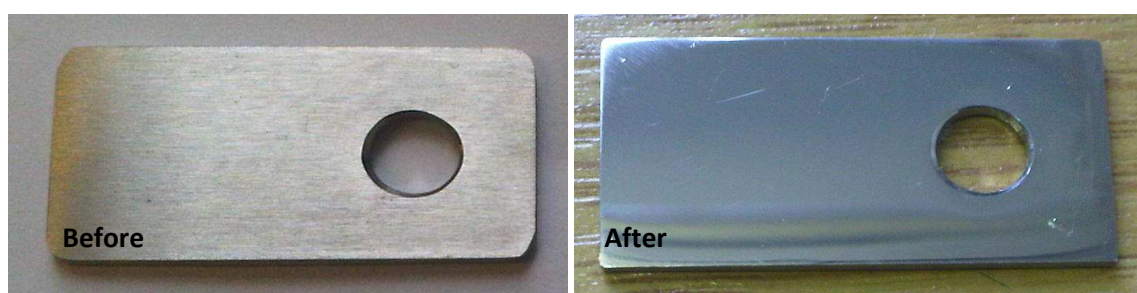
Figure 5-1 Example of the sample used for XPS analysis before and after the mechanical polishing (4000 grit).

5.3 Results and Discussion

Focusing initially upon surface composition prior to immersion in 15.3M-HAc-Br⁻, Figure 5-2 displays overview XPS spectra ($\theta_E = 0°$) from 316L and 254SMO following polishing. Spectral features are labelled. From this annotation, it is clear that both samples exhibit prominent peaks due to O, and C. Features assigned to Fe, Cr, Ni, and Mo, the primary metallic components of both alloys (see Figure 5-2), are also apparent. In addition, there are peaks ascribed to Na, Ca, and S. These species presumably primarily arise through surface contamination during processing, although S is also a minor component of both alloys. Binding energy (BE) scales were

calibrated by assigning a BE value of 285 eV to the C1s hydrocarbon component of adsorbed adventitious carbon [20], and confirming that the oxide oxygen (O^{2-}) O 1s peak is located at 530.1 ± 0.2 eV [21, 22].
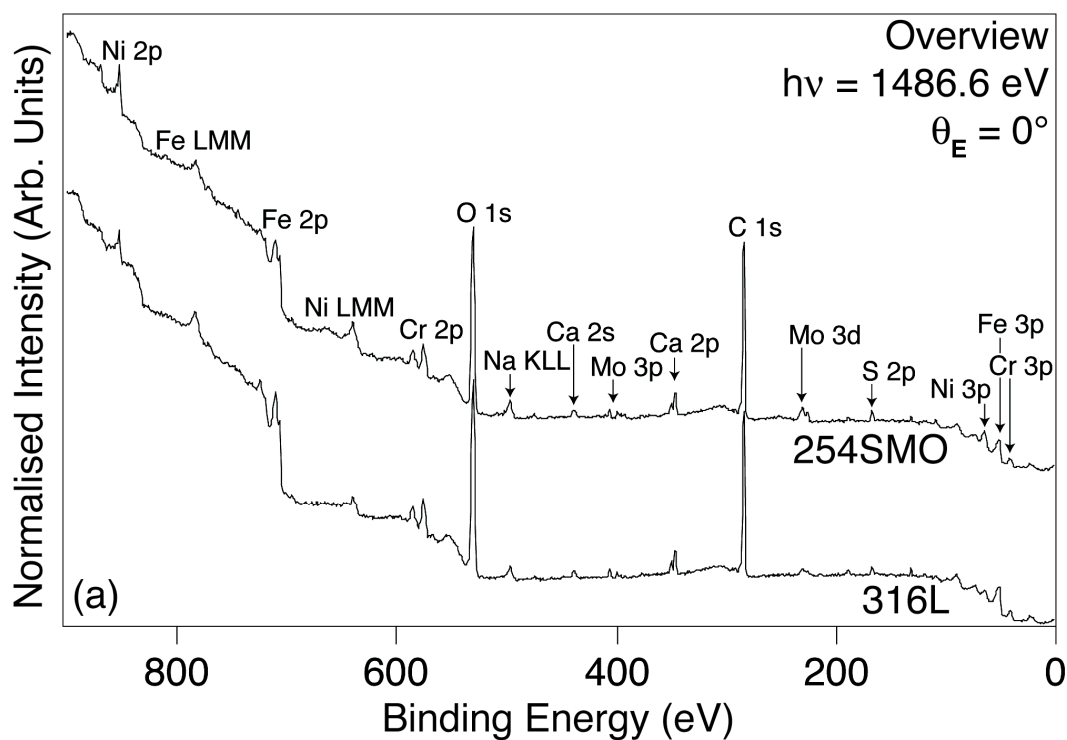

Figure 5-2 Overview XPS spectra recorded from 316L and 254SMO stainless steels following polishing. The spectra have been normalised to have a maximum (minimum) intensity of 1 (0).

Higher resolution XPS spectra (θ_E = 0°) of selected core levels from Figure 5-2, namely, Ni $2p_{3/2}$, Fe $2p_{3/2}$, Cr $2p_{3/2}$, O 1s, and Mo 3d, are displayed in Figure 5-3. The lower and upper rows of spectra, acquired from 316L and 254SMO, respectively, exhibit very similar profiles. This resemblance is underlined by the least squares best fits to the experimental data, also shown in Figure 5-3, which were performed using the CaxaXPS software [23]. Gaussian-Lorentzian (G-L) line shape functions (30 % Lorentzian) were

employed to model all of the photoelectron peaks, except for zero oxidation state metal components (e.g. Fe^0), where asymmetric Doniach-Sunjic (D-S) line shapes were used. Inelastically scattered background electrons were described with Shirley-type functions [24]. Following the approach of previous work, only the $2p_{3/2}$ components of the 2p core level spectra of Fe, Cr, and Ni were fitted [25, 26]. Table 5-2 lists best fit BEs and full width at half maximums (FWHMs) for each of the spectra in Figure 5-3. The Ni $2p_{3/2}$ profiles were fitted using a procedure previously adopted for oxide-free nickel metal [27]. A D-S line shape function for Ni^0, along with two G-L functions to account for satellite features, were employed. Both fits are satisfactory. On this basis, it is concluded that there is no appreciable amount of non-metallic nickel at the surface of either alloy subsequent to polishing. It should be noted that given the non-ideal signal-to-noise ratios, the presence of a small fraction of nickel in another oxidation state cannot be entirely ruled out.

Concerning the Fe $2p_{3/2}$ spectra in Figure 5-3, the leading peak (BE ~ 707 eV) can be attributed to the Fe $2p_{3/2}$ core level of metallic iron (Fe^0) [28]. Higher BE features, in the range 707 < BE < 720 eV, originate from Fe^{2+} and Fe^{3+} [28, 29]. As regards fitting of these Fe $2p_{3/2}$ spectra, a single D-S line shape function has been employed for Fe^0. For the features arising from oxidised iron, two multiplet envelopes consisting of 3 and 4 G-L functions for Fe^{2+} and Fe^{3+}, respectively, along with two broader G-L functions for satellite

peaks, have been utilised [28, 30]. From this fitting, it is clear that photoemission from Fe^{3+} and Fe^{2+} is similarly significant for both alloys. The residual intensity at BE ~ 720 eV arises from Fe $2p_{1/2}$ states.

To fit the Cr $2p_{3/2}$ data in Figure 5-3, contributions from metallic Cr (Cr^0), a single D-S line shape function (BE = 574.0 eV), and Cr^{3+} species were considered initially. A broad G-L function was employed for hydroxide (Cr (OH)$_3$) Cr^{3+} (Cr_{OH}^{3+}), and a multiplet envelope of 5 G-L functions for oxide (Cr_2O_3) Cr^{3+} (Cr_{oxide}^{3+}) [5, 31-35]. Visual inspection indicates that these components are sufficient to adequately fit both spectra, and that the Cr_{OH}^{3+} peak is dominant. It should be noted that in previous work., it was concluded that one may differentiate chromite ($FeCr_2O_4$) Cr^{3+} ($Cr_{chromite}^{3+}$), another potential surface phase [33], from Cr_{oxide}^{3+}. However, given the presence of Cr_{OH}^{3+} and the rather similar spectral signatures of $Cr^{3+}{}_{oxide}$ and $Cr^{3+}{}_{chromite}$, no attempt has been made to consider $Cr^{3+}{}_{chromite}$ features explicitly. Nevertheless, the possibility that chromite may be formed at the surface of these alloys cannot be ruled out.

Addressing the O 1s data (Figure 5-3), both spectra have been fitted with 4 G-L functions, which have been constrained to have identical FWHMs. As indicated above, the lowest BE peak arises from oxide oxygen (O^{2-}) [22, 36, 37]. The precise origins of the rest of the peaks are somewhat less certain. It is proposed that the feature at BE ~ 531.5 eV corresponds to lattice hydroxyl

(e.g. OH in Cr (OH) $_3$), along with surface adsorbed species containing oxygen bound to carbon (RCxOy) [38, 39]. The other two higher BE peaks, labelled Oa^1 and Oa^2, are both suggested to be due to the presence of adsorbates, most likely OH (Oa^1) and RCxOy (Oa^1 and Oa^2) [22, 39].

Finally, turning to the Mo 3d data in Figure 5-3, both spin-orbit components were displayed, i.e. $3d_{5/2}$ and $3d_{3/2}$. It should be noted that for both spectra a contribution from the S 2s core level has been removed prior to plotting; the intensity and BE of these peaks have been estimated from the S 2p signals in Figure 5-2 The lowest BE feature (~ 227.7 eV) can be attributed to the $3d_{5/2}$ core level of Mo^0. Hence, a doublet of D-S line shapes has been employed to fit this peak and the Mo^0 $3d_{3/2}$ component, with the BE difference and intensity ratios being fixed at expected values [40, 41]. Remaining intensity is assigned to Mo in various positive oxidation states. G-L line shape doublets for Mo^{4+}, $Mo^{5+,}$ and Mo^{6+} have been fitted with keeping the area ratio between Mo $3d_{5/2}$ and $3d_{3/2}$ as 1.5 and the spin-orbit pair intervals set at 3.1eV ± 0.2 [41-44], although given the rather poor signal-to-noise ratio, particularly for the 316L data, there is a degree of conjecture associated with this procedure.
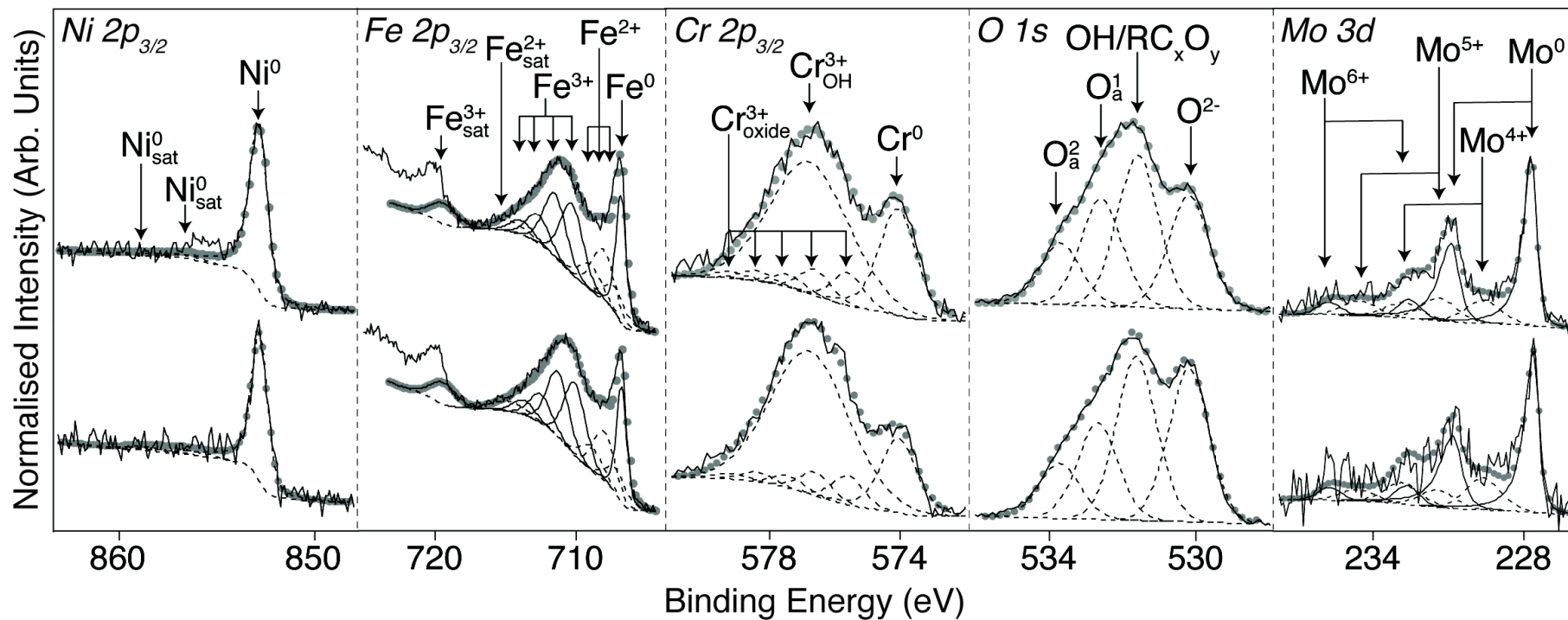
Figure 5-3 High resolution XPS data of selected core levels from Figure 5-2. All these spectra were acquired following polishing of both stainless steels: 316L (lower line) and 254SMO (upper line). All the spectra have been normalized to have maximum (minimum) intensity of 1 (0).

Table 5-2 Optimal Ni $2p_{3/2}$, Fe $2p_{3/2}$, Cr $2p_{3/2}$, O 1s, and Mo $3d_{5/2}$ BEs and FWHMs resulting from fitting of spectra in Figure 5-3. See main text for details of fitting procedures. The values given in italics are for satellite peaks.

Chemical Species	BE(eV) (FWHM (eV))		Chemical Species	BE(eV) (FWHM (eV))	
	316L	254SMO		316L	254SMO
Ni^0	852.8 (1.1)	852.9 (1.1)	Cr^0	574.0 (1.3)	574.0 (1.3)
	856.5 (2.5)	*856.6 (2.5)*	Cr^{3+}_{oxide}	575.6 (1.1)	575.6 (1.1)
	858.8 (2.5)	*858.9 (2.5)*		576.6 (1.1)	576.6 (1.1)
				577.4 (1.1)	577.4 (1.1)
Fe^0	706.8 (0.8)	707.0 (0.8)		578.4 (1.1)	578.4 (1.1)
Fe^{2+}	707.1 (1.8)	707.3 (1.8)		579.2 (1.1)	579.2 (1.1)
	708.0 (1.8)	708.2(1.8)	Cr^{3+}_{OH}	576.8 (2.8)	576.8 (2.8)
	708.9 (1.8)	709.1 (1.8)			
	714.8 (2.8)	*715 ((2.8)*	O^{2-}	530.2 (1.3)	530.2 (1.3)
Fe^{3+}	710.1 (1.8)	710.3 (1.8)	OH/RC_xO_y	531.6 (1.3)	531.5 (1.3)
	711.3 (1.8)	711.5 (1.8)	O_a^1	532.6 (1.3)	532.4 (1.3)
	712.5 (1.8)	712.7 (1.8)	O_a^2	533.6 (1.3)	533.5 (1.3)
	713.7 (1.8)	713.9 (1.8)			
	719.4 (2.1)	*719.5 (2.1)*	Mo^0	227.6(0.5)	227.7(0.5)
			Mo^{4+}	229.6(1.6)	229.6(1.6)
			Mo^{5+}	231.5(1.6)	231.4(1.6)
			Mo^{6+}	232.7(1.1)	232.6(1.1)

To study how the surface film behave/change when the steels were immersed in the acetic acid solution, the XPS was also performed for the two stainless steels surface following immersion in the 15.3M HAc-Br- for different time. The overview scan, Figure 5-4, for both stainless steels showed similar futures as the polished surfaces with disappearance of the contaminations on the surface, Na, Ca. also, it was noticed that the Sulfur peak (S 2p) is not present for all the spectra after the immersion in the acid. Thus, the high resolution spectra of Mo 3d are not influenced by S 1s. However, there was small peak observed at ~ 182eV which is matching the Br 2p core level binding energy [45].
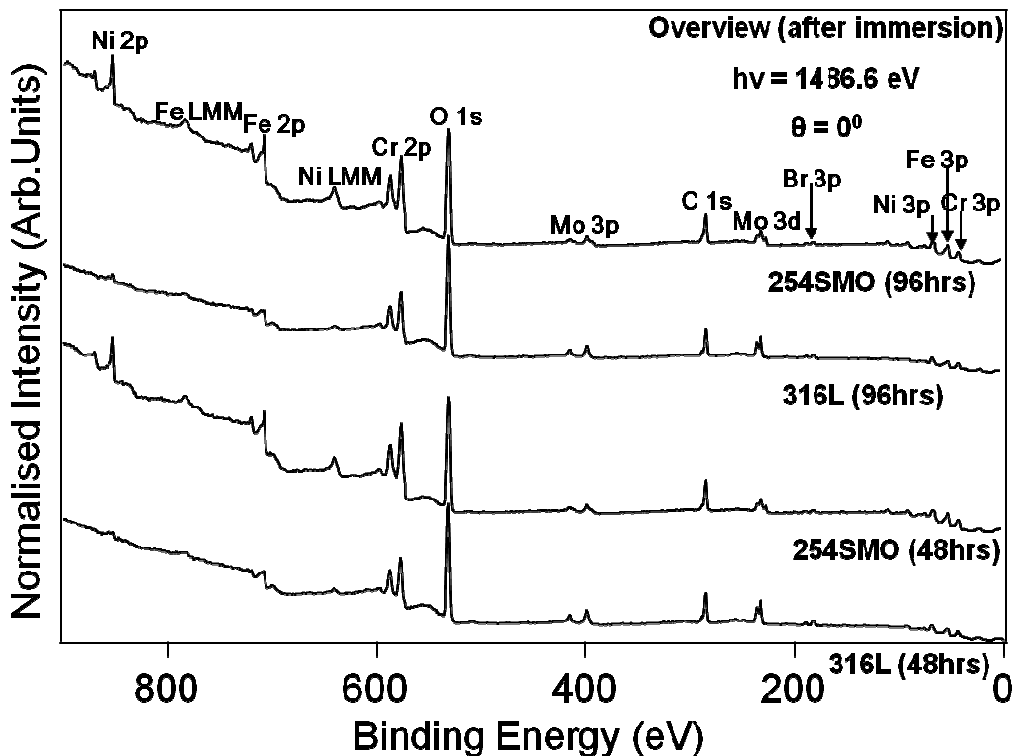
Figure 5-4 Overview XPS spectra recorded from 316L and 254SMO stainless steels following immersion in 15.3M HAc-Br- for 48 and 96 hours. The spectra have been normalised to have a maximum (minimum) intensity of 1 (0).

Figure 5-5 - Figure 5-9 displayed the higher resolution XPS spectra ($\theta_E = 0^0$) of Fe $2p_{3/2}$, Cr $2p_{3/2}$, Ni $2p_{3/2}$, O 1s, and Mo 3d core levels acquired from the two stainless steels, 316L (left column) and 254SMO (right column) with different treatment: as polished surface (lower row), after 48hours (middle row) and 96hours (upper row) of immersion in 15.3M HAc-Br$^-$. All the spectra have been normalized to have maximum and minimum intensity of 1 and 0. Also, the spectra were fitted with same procedure/parameters used for spectra acquired from the polished surfaces and showed satisfactory fits with only variation in the intensity of the signals. However, for the 316L stainless steel immersed in the acid, there was a clear shift to a higher binding energy in the oxide oxygen (O^{2-}) from 530.1 ± 0.2eV to 530.6eV. As constraining the position (BEs) of oxide oxygen in O 1s spectrum at 530.1 ± 0.2eV, a new peak well fitted in position of 530.65 eV, Figure 5-7. Possibly, this change in O 1s spectra fitting could be corresponding to the difficulty faced when fit the Cr $2p_{3/2}$ core level spectra. The Cr^0 was fitted satisfactorily at BE of ~ 574eV however, there was a shift in the Cr^{n+} envelope, which can not be fitted by the similar peaks that were fitted in the as polished surface. Thus, an attempted was made to introduce better spectra fitting for Cr $2p_{3/2}$ in the 316L. After constraining the BE and HWFM of the Cr^{3+} (oxide/hydroxide), as shown in Figure 5-6 (left column), there were new peaks can be fitted in to the spectra, these peaks were at binding energy of 577.4, 576.5 and at 579.5 eV. Potentially, these peaks can be assigned as Cr(III)

acetate [46], $CrBr_3$ and Cr^{6+} [35], respectively. The intensities of these considered peaks were summed to the intensity of Cr 2p actions.

Another important difference between the two stainless steels was observed for the feature of the high resolution spectra of Ni $2p_{3/2}$ core level, Figure 5-9 Low intensity peak of oxide/hydroxide was observed for the 316L immersed in 15.3M HAc for both immersion time, 48 and 96 hours. The peak was at binding energy of ~ 856 eV. This binding energy is found in literature [47, 48] to be possibly attributing for the presence of Ni (OH). In high resolution spectra of Ni 2p, it should be emphasised that, the satellite peak can not be fitted in the Ni 2p spectra due to the very low intensity of the observed hydroxide peak. The ratio of the hydroxide/metal peak was in the range of 0.017-0.027. However, in the case of 254SMO steel where the surface was passive, only metallic nickel at ~ 852.9 eV was found and there was no Ni oxide/hydroxide been observed. This finding is in agreement with other worker when the surface of the steel is passivated [13, 49].

Looking to the Mo 3d core level in the 316L results, Figure 5-8, the XPS spectra after the immersion in 15.3HAc-Br- were fitted mainly with Mo^0 and Mo^{6+} while, the Mo^{4+} and Mo^{5+} peaks exhibited a very low intensities and they were almost neglected. The Mo^{6+} could be due to the oxidation of Mo in the air after removing the sample from the test solutions. However, the spectra of Mo 3d were fitted with Mo^0, Mo^{4+}, Mo^{5+} and Mo^{6+} in the case of

254SMO. All of these Mo oxidation states exhibited similar profiles like the features achieved for the polished surface.
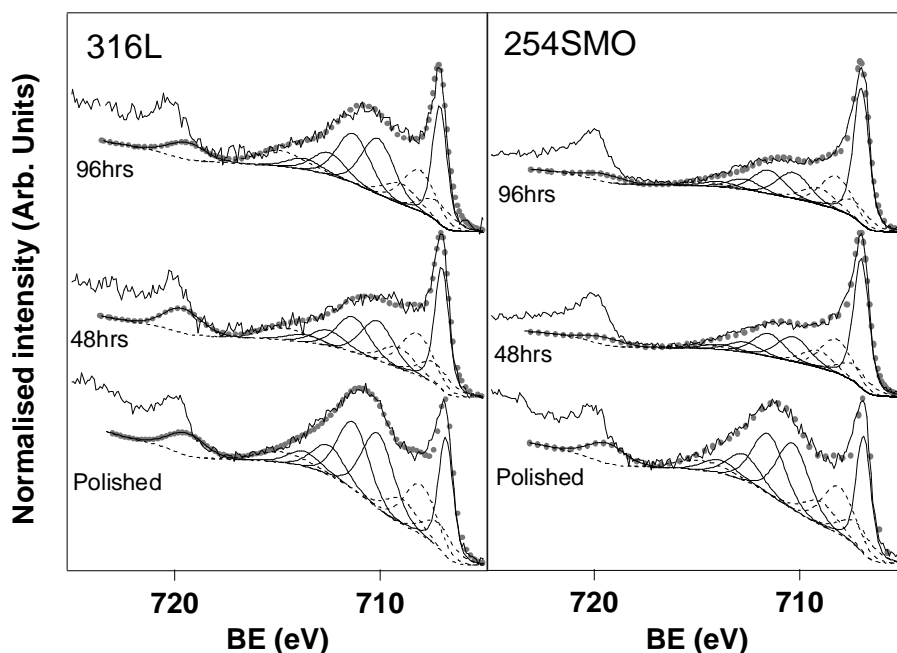

Figure 5-5 High resolution XPS data of the Fe $2p_{3/2}$ core level acquired from the two stainless steels, 316L (left) and 254SMO (right) subsequent to different treatment time: as polished (lower row), after 48hours (middle row) and 96hours (upper row) in 15.3M HAc-Br-.
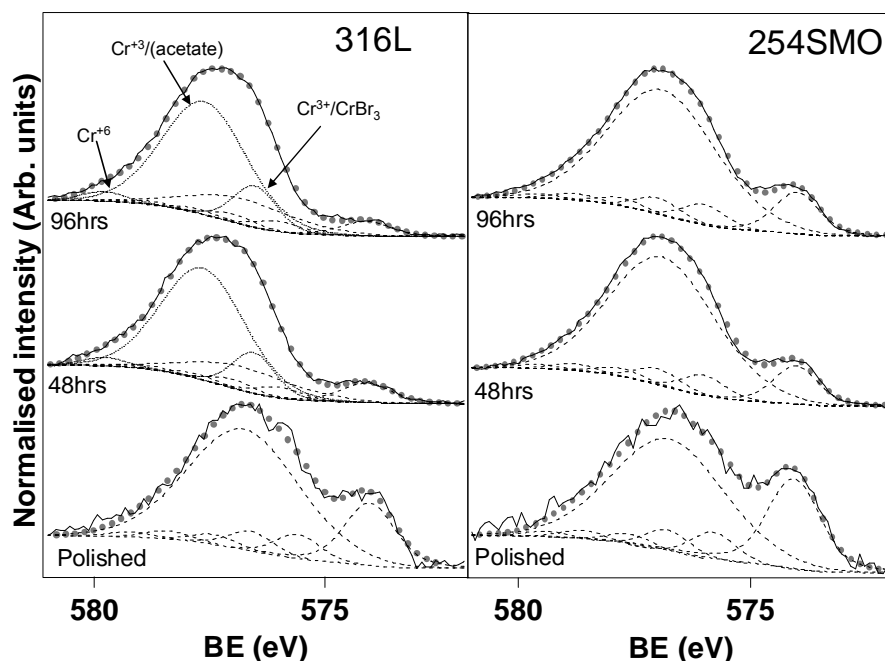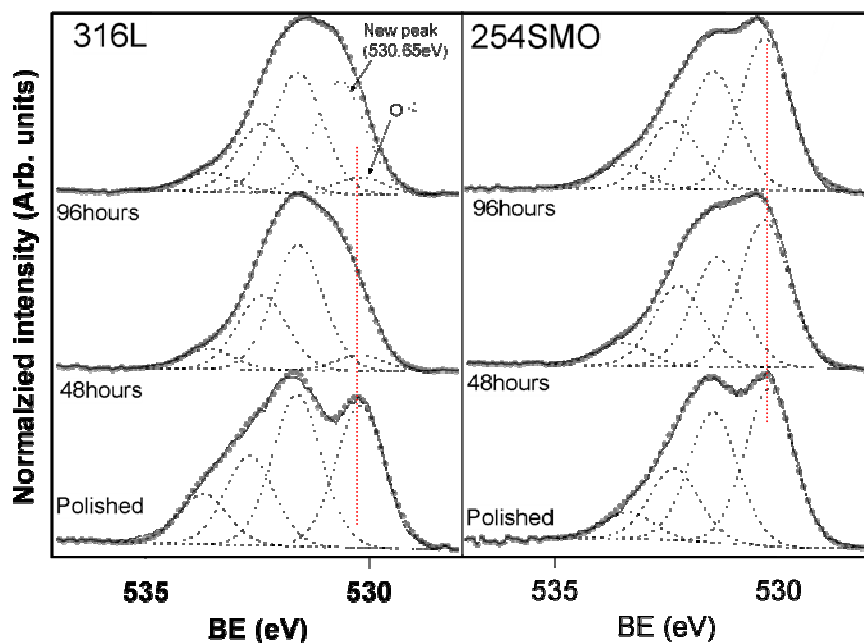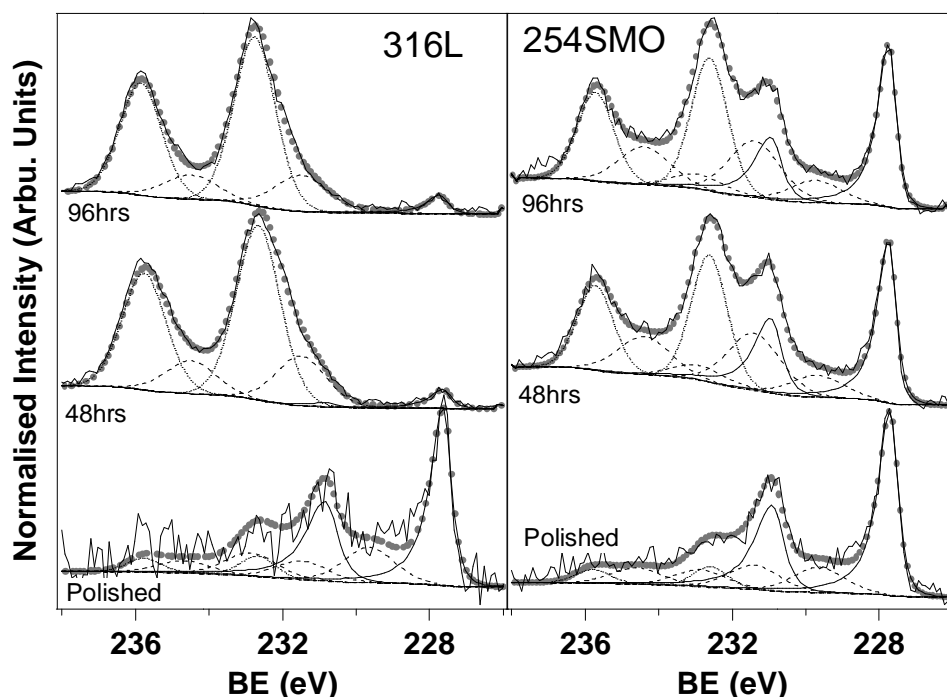

Figure 5-6 High resolution XPS data of the Cr 2 $p_{3/2}$ core level acquired from the two stainless steels, 316L (left) and 254SMO (right) subsequent different treatment time: as polished (lower row), after 48hours (middle row) and 96hours (upper row) in 15.3M HAc-B⁻

Figure 5-7 High resolution XPS data of the O 1s core level acquired from the two stainless steels, 316L (left) and 254SMO (right) subsequent different treatment time: as polished (lower row), after 48hours (middle row) and 96hours (upper row) in 15.3M HAc-Br-.
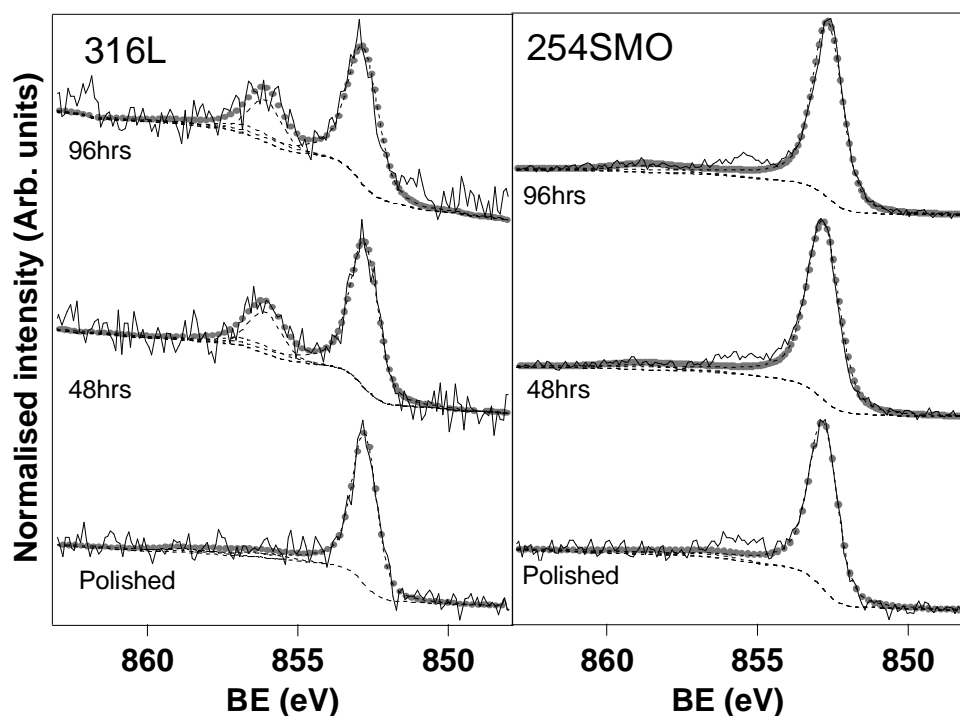

Figure 5-8 High resolution XPS data of the Mo 3d core level acquired from the two stainless steels, 316L (left) and 254SMO (right) subsequent diffferent treatment time: as polished (lower row), after 48hours (middle row) and 96hours (upper row) in 15.3M HAc-Br-

Figure 5-9 High resolution XPS data of the Ni $2p_{3/2}$ core level acquired from the two stainless steels, 316L (left) and 254SMO (right) subsequent deferent treatment time: as polished (lower row), after 48hours (middle row) and 96hours (upper row) in 15.3M HAc-Br⁻.

To gain insight into the depth distribution of the various M^{n+} species within the surface film on each alloy, Table 5-3 lists pertinent XPS core level intensity ratios (e.g. $I(Cr^{3+}_{oxide/OH} \, 2p)/I(Fe^{2+/3+} \, 2p)$) at $\theta_E = 0°$ and $\theta_E = 60°$. Here, the intensities of the various M^{n+} states for a particular element have been summed.

The ratio of Cr to Fe calculated for the polished surface, before any test (0 hour), was less than one, Fe $(I(Cr^{3+}_{oxide/OH} \, 2p) \, / \, I(Fe^{2+/3+} \, 2p) < 1)$ for both steels. However, when the steel was immersed in the 15.3M HAc-B⁻, the ratio

increased sharply for both immersion time, 48 and 96 hours. For example in the case of 254SMO stainless steel, the ratio increased from 0.354 to about 2 for the normal emission angle and from 0.71 to about 3 for the 60° emission angle. The increase in the Cr/Fe ratios definitely is an indication of the enrichment of Cr cation(s) in the surface film. However, observing the change in ratio according to the XPS emission angle, the ratio in 316L steel was not influenced or changed with the XPS emission angle. As for example the ratio was 2.097 for the 0^0 and was 2.069 for the 60^0. While in the 254SMO, the value was approximately 50% more for the grazing angle and this confirmed hat the Cr was located in a surface layer on top of the Fe cation for the 254SMO while it could be homogenously mixed in the same layer on the 316L surface.   In order for the surface film to be enriched in Cr either dissolution of Fe from the existing film occurs or Cr is preferentially oxidised during formation of the film [50]. In the case of 316L immersed in 15.3MHAc-Br-, Fe may dissolve from the film or it may continue to dissolve through the film from the substrate, resulting in Cr enrichment in the substrate/film interface as well as in the film/solution interface. However, for the 254SMO, Cr was preferentially oxidised in the first place which leads to an enrichment of Fe in the substrate/film interface more than the film/solution interface. Also, from the intensity relationship of Cr/Fe with immersion time, the ratio recorded for the 254SMO maintains a stable value over the immersion time (48 and 96 hours). This is an obvious indication for the formation of stable passive film on the surface of the steel.

Similar observations were found for the Mo/Fe intensity ratio as well. For the 0^0 emission angle, the ratio was 0.018 (0.056) for the polished surface and increased to ~ 0.75 (0.25) after the 316L (254SMO) was immersed into the solution. Also, from the grazing angle analysis results, the Mo was located on the top of the Fe layer for the 254SMO. Whereas, the Mo/Fe ratio was decreased with the gazing angle for the 316L steel. It was noticed that, for the 316L steel, when extending the immersion time from 48 hours to 96 hours, the ratio (Mo/Fe) was decreased for the normal emission angle but was increased for the grazing emission angle. This possibly was due to the rough surface produced due to general corrosion/localised attack on the surface of the 316L steel. Consequently, the XPS signal intensity might be affected by such surface roughness, leading to doubt in the quantified values of the intensities.

Evaluating the ratio of Mo to Cr cations in the surface of the two stainless steels, the Mo/Cr ratio was not significantly influenced by the acid in the case of the 254SMO. The ratio for the polished surface was 0.16 and subsequent the immersion, the ratio was in the range of 0.122 - 0.141 for the two immersion time, 48 and 96 hours. However, for the grazing angle, there was a noticeable change since the Mo was decreased with the angle analysis to about 0.08 for the polished surface while after the immersion in the acid, the ratio slightly increased for example from 0.141 to 0.179 for the 96 hour immersion in 15.3M HAc-Br-. This observation may suggest that Mo cations

were enriched in the surface after the immersion in to the acid. Though, the ratio of Mo/Fe was significantly increased at the grazing angle while the ratio of Mo/Cr not. This indicated the Mo was obviously above the Fe layer but it could be mixed with Cr and both in the same layer. As well, there was an enrichment of Mo compared to Cr after the immersion of the 316L in to the acid. However, the ratio decreased with the grazing angle analysis.
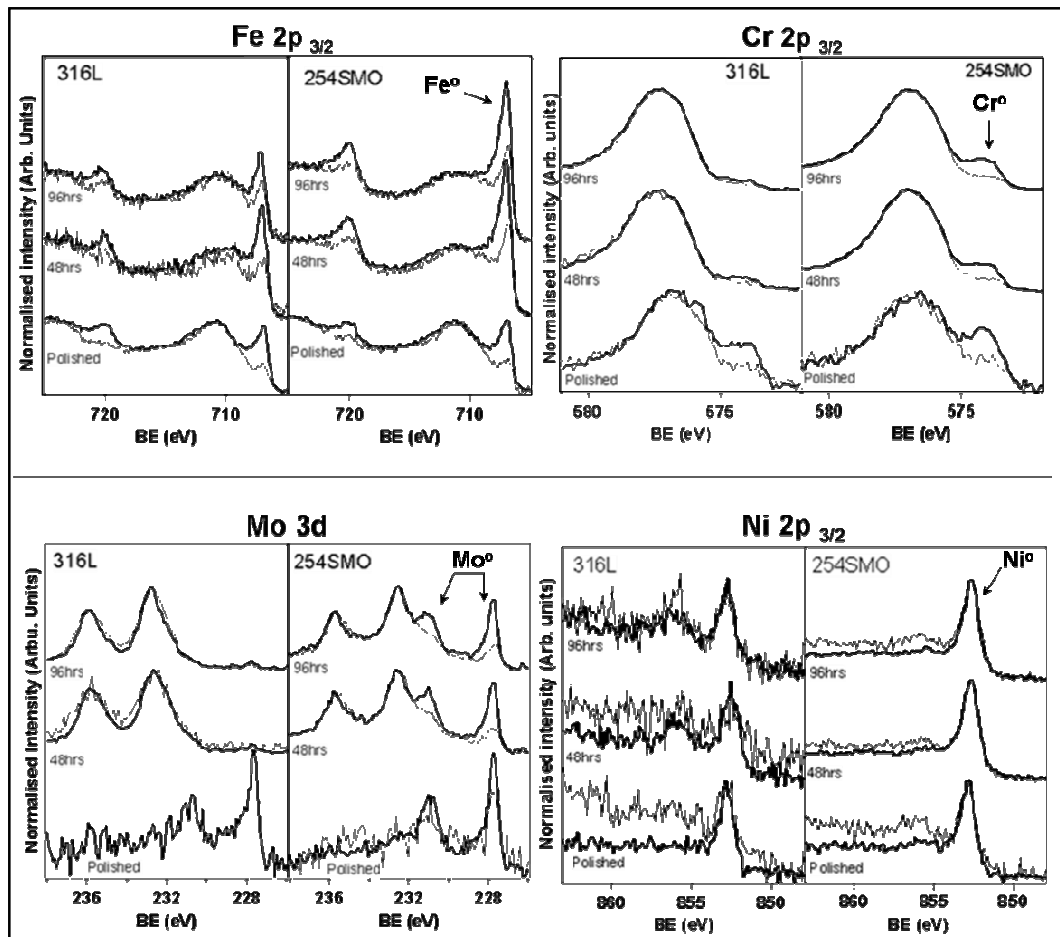

Figure 5-10 Qualitative comparisons between spectra of the core levels, Fe $2p_{3/2}$, Cr $2p_{3/2}$ and Mo 3d, acquired from 316L (left column) and 254SMO (right column). The bold (thin) line spectra were recorded at $\theta_E = 0°$ ($\theta_E = 60°$).

Additionally, depth distribution of the metallic and oxidised species in the surface region of each alloy were assessed by comparing the data recorded at $\theta_E = 0°$ and $\theta_E = 60°$, as the latter are more surface sensitive [51]. Figure 5-10 depicts such a comparison for the Fe $2p_{3/2}$, Cr $2p_{3/2}$, Mo 3d and Ni $2p_{3/2}$ core levels acquired from both stainless steel. The bold (thin) line spectra were recorded at $\theta_E = 0^o$ ($\theta_E = 60^0$). Each pair of spectra has been normalised to maximise overlap in the region associated with M^{n+} features.

For the polished surfaces, this approach results in the peaks assigned to M^0 exhibiting greater intensity at $\theta_E = 0^0$, which is consistent with the formation of films, containing oxidised Fe, Cr, Mo species, atop the alloy substrates. Mo 3d data acquired from polished 316L at $\theta_E = 60^0$ are not shown, as normalisation could not be achieved due to very poor signal-to-noise ratio. Subsequent to the immersion in 15.3M-HAc-Br$^-$, similar features were noticed for the 254SMO. However, the intensity of Cr^0 and Mo^0 recorded from the 316L were completely hampered. This could be due to the continual oxidation of the Cr and Mo near the surface which led to consumption of metallic phase underneath the film whereas the metallic and oxidised Fe peaks were obvious and this is possibly because the Fe is the main constituent of the bulk composition of the alloy.

Table 5-3 M^{n+} XPS core level intensity ratios at $\theta_E = 0°$ and $\theta_E = 60°$ for 316L and 254SMO substrates: polished and after immersed in 15.3M HAc-Br⁻ for 48 and 96 hours.

XPS core level intensity ratio in **316L**	Time(hr)	$\theta_E(°)$	
		0	60
$I(Cr^{3+}_{oxide/OH}\ 2p)/I(Fe^{2+/3+}\ 2p)$	0	0.352	0.349
	48	2.097	2.069
	96	2.268	2.598
$I(Mo^{4+/5+/6+}\ 3d)/I(Fe^{2+/3+}\ 2p)$	0	0.018	0.02
	48	0.787	0.226
	96	0.748	0.425
$I(Mo^{4+/5+/6+}\ 3d)/I(Cr^{3+}_{oxide/OH}\ 2p)$	0	0.051	0.06
	48	0.375	0.109272
	96	0.330	0.164

XPS core level intensity ratio in **254SMO**	Time(hr)	$\theta_E(°)$	
		0	60
$I(Cr^{3+}_{oxide/OH}\ 2p)/I(Fe^{2+/3+}\ 2p)$	0	0.354	0.713
	48	2.018	3.223
	96	1.734	2.740
$I(Mo^{4+/5+/6+}\ 3d)/I(Fe^{2+/3+}\ 2p)$	0	0.056	0.063
	48	0.247	0.473
	96	0.245	0.490
$I(Mo^{4+/5+/6+}\ 3d)/I(Cr^{3+}_{oxide/OH}\ 2p)$	0	0.160	0.088
	48	0.122	0.147
	96	0.141	0.179

5.4 Summary

The above results and discussion can be summarised as:

- Exposure to acetic acid increased the Cr/Fe cations ratio for the two stainless steels, 316L and 254SMO. The higher alloy in terms of its resistance to corrosion attacks (254SMO) exhibit relatively higher Cr/Fe ratios in the outermost layer of the surface whereas in the case of the 316L, it was independent of the emission angle and the Cr and Fe cations were homogenously mixed in the same surface layer.

- The different oxidation states of Mo (Mo^{4+}, Mo^{5+} and Mo^{6+}) were detected in the surface film of the 254SMO, where in the case of 316L, Mo^{6+} state was obviously observed. Also, the Ni $2p_{3/2}$ spectra almost represent a metallic state for the 254SMO whereas; a very weak signal corresponding to $Ni(OH)_2$ is detected in the surface of the 316L following immersion in acid solution.

- Considerable intensity of the metallic sate were recorded for all the core levels, Fe 2p, Cr 2p , Mo 3d and Ni 2p, in the case of the 254SMO. This indicated the formation of stable and thin passive film. In contrast, negligible intensity of metallic state of Cr and Mo were recorded on the 316L surface subsequent to immersion in the acid solution.

5.5 References

1. C. O. A. Olsson , D. Landolt *Passive Films on Stainless Steels : Chemistry, Structure and Growth.* Electrochimica Acta 2003. **48** p. 1093 -1104.

2. V. Maurice, W. P. Yang, and P. Marcus, *Xps and Stm Investigation of the Passive Film Formed on Cr (110) Single-Crystal Surfaces.* J. Electrochem. Soc., 1994. **141**(11): p. 3016-3027.

3. V. Maurice, W. P. Yang, and P. Marcus, *Xps and Stm Study of Passive Films Formed on Fe-22cr (110) Single-Crystal Surfaces.* Journal of electrochemical. Soc, 1996. **143**(4): p. 1182-1200.

4. Strehblow, P. Keller and H.-H., *Xps Investigations of Electrochemically Formed Passive Layers on Fe/Cr-Alloys in 0.5 M H2so4.* Corrosion Science 2004. **46** p. 1939-1952.

5. P. Marcus , I. Olefjord, *Electrochemical and Aes/Esca Characterization of the Passive Films on Fe-Cr and Fe-Cr-Mo Alloys.* Corrosion Science, 1988. **28**(6): p. 589- 602.

6. I. Olefjord, B. Brox, and U. Jelvestam, *Surface Composition of Stainless Steels During Anodic Dissolution and Passivation Studied by Esca. Journal of the Electrochemical Society*, 1985. **132**(12): p. 2854 - 2861.

7. I. Olefjord , L. Wegrelius, *Surface Analysis of Passive State.* corrosion science, 1990. **31**: p. 89-98.

8. C. R. Clayton , Y. C. Lu, *A Bipolar Model of the Passivity of Stainless Steel: The Role of Mo Addition.* Journal of the Electrochemical Society, 1986. **133**(12): p. 2465-2473

9. Y. C. Lu, C. R. Clayton and A. R. Brook, *A Bipolar Model of the Passivity of Stainless Steels - Ii: The Influence of Aqueous Molybdate.* Corrosion Science, 1989. **29**(7): p. 863-880.

10. K. Hashimoto, K. Asami and K. Teramoto, *Spectroscopic Study on the Role of Molybdenum.* Corrosion Science, 1979. **19**: p. 3 -14

11. K. Sugimoto , Sawada, *The Role of Molybdenum Additions to Austenitic Stainless Steels in the Inhibition of Pitting in Acid Chloride Solutions.* Corrosion Science, 1977. **17**: p. 425-445.

12. A. Pardo , et al. , *Effect of Mo and Mn Additions on the Corrosion Behaviour of Aisi 304 and 316 Stainless Steels in H2so4.* Corrosion Science 2008. **50**: p. 780-794.

13. C.T. Liu, J.K. Wu *Influence of Ph on the Passivation Behaviour of 254smo Stainless Steel in 3.5% Nacl Solution.* Corrosion Science 2007. **49**: p. 2198-2209.

14. C. O. A. Olsson , S. E. Hornstrom, *An Aes and Xps Study of the High Alloy Austenitic Stainless Steel 254 Smo Tested in a Ferric Chloride Solution.* Corrosion Science, 1994. **36**(1): p. 141-151.

15. I. Sekine, A. Masucko, K. Senoo, *Corrosion of Aisi316 Stainless Steel in Formic and Acetic Acid.* Corrosion 1987. **43** p. 553-560.

16. I. Sekine, T. Kawase, M. Kobayashi, M. Yuasa, Corrosion Scienc, 199. **32, Issue**(8): p. 815-825.

17. Alan Turnbull a, Mary Ryan b, Anthony Willetts a, Shengqi Zhou a, *Corrosion and Electrochemical Behaviour of 316l Stainless Steel in Acetic Acid Solutions.* Corrosion Science 2003. **45** p. 1051-1072.

18. G.Q. Liu, Z.Y. Zhu, W. Ke, E.H. Han, and C.L. Zeng, Corrosion August 2001 **57**(8): p. 730-738.

19. X. Q. Cheng, X. Li, and C. F. Dong, *Study on the Passive Film Formed on 2205 Stainless Steel in Acetic Acid by Aas and Xps.* International Journal of Minerals, Metallurgy and Materials, 2009. **16**(2): p. 170-176.

20. McCafferty, E. and J.P. Wightman, Surface and Interface Analysis, 1998. **26**: p. 549-564.

21. S. Ningshen, U. Mudali, V. Mittal and H. Khatak, *Semiconducting and Passive Film Properties of Nitrogen-Containing Type 316ln Stainless Steels.* Corrosion Science, 2007. **49**: p. 481-496.

22. R. Cutting , C. Muryn, D. Vaughan and G. Thornton *Substrate-Termination and H_2o-Coverage Dependent Dissociation of H_2o on $Fe_3o_4(111)$.* Surface Science, 2008. **602**(6): p. 1155-1165.

23. Casa-Software-Ltd, *Teignmouth, Devon, Uk. (Www.Casaxps.Com).*

24. Shirley, D.A., Physical Review B, 1972. **5**(12): p. 4709-4714.

25. McIntyre, N.S. and D.G. Zetaruk, Analytical Chemistry, 1977. **49**(11): p. 1521-1529.

26. Grosvenor, A.P.,B.A. Kobe,M.C. Biesingerand N.S. McIntyre, Surface and Interface Analysis, 2004. **36**: p. 1564-1574.

27.   A. Grosvenor, M. Biesinger, R. Smart, N. McIntyre, *New Interpretations of Xps Spectra of Nickel Metal and Oxides.* Surface Science, 2006. **600** (9): p. 1771-1779.

28.   A. P. Grosvenor, B. A. Kobe, M. C. Biesinger and N. S. McIntyre, *Investigation of Multiplet Splitting of Fe 2p Xps Spectra and Bonding in Iron Compounds.* Surface and Interface Analysis, 2004. **36**(12): p. 1564–1574.

29.   G. Bhargava, I. Gouzman , C.M. Chun, T.A. Ramanarayanan and S.L. Bernasek, *Characterization of the "Native" Surface Thin Film on Pure Polycrystalline Iron: A High Resolution Xps and Tem Study.* Applied Surface Science, 2007. **253**(9): p. 4322-4329

30.   Zetaruk, N.S. McIntyre and D.G., *X-Ray Photoelectron Spectroscopic Studies of Iron Oxides.* Analytical Chemistry, 1977. **49**(11): p. 1521-1529.

31.   T Sridhar, K. Suresh and S. Rajeswari, *Electron Spectroscopy for Chemical Analysis (Esca) of Passive Films Formed on Type 316ln Ss in Pulp and Paper Industry.* Transactions of the Indian Institute of Metals, 2004. **57**(3): p. 241-252.

32.   Isao Ikemoto, k. Ishii, S. Kinoshita, H. Kuroda, M. Franco and J. Thomas, *X-Ray Photoelectron Spectroscopic Studies of Cro2 and Some Related Chromium Compounds.* Journal of Solid State Chemistry 1976. **17**: p. 425-430

33.   M. Biesinger, B. Payne, A. Grosvenor, L. Lau, A. Gerson, R. Smart,, *Resolving Surface Chemical States in Xps Analysis of First Row Transition Metals, Oxides and Hydroxides: Cr, Mn, Fe, Co and Ni.* Applied Surface Science, 2011. **257**(7): p. 2717-2730.

34.   M.C. Biesinger, B. Payne, B. Hart , A. Grosvenor , N. McIntryre, L. Lau and R. Smart, *Quantitative Chemical State Xps Analysis of First Row Transition Metals, Oxides and Hydroxides.* Journal of Physics: Conference Series 2008. **100** (012025).

35.   M.C. Biesinger, C. Brown, J. Mycroft, R. Davidson and N. McIntyre, *X-Ray Photoelectron Spectroscopy Studies of Chromium Compounds.* Surface and Interface Analysis, 2004. **36**: p. 1550-1563.

36.   Cutting, R.S.,C.A Muryn,D.J. Vaughanand G. Thornton, Surface Science, 2008. **602**: p. 1155-1165.

37.   Fujii, T.,M.F. de Grootand G.A. Sawatzky, Physical Review B, 1999. **59**(4).

38. L. Martinez, D. Leinen, F. Martín, M. Gabas, J. Ramos-Barrado, E. Quagliata and E. Dalchiele, *Electrochemical Growth of Diverse Iron Oxide (Fe3o4, -Feooh, and -Feooh) Thin Films by Electrodeposition Potential Tuning.* Journal of electroanalytical Society, 2007. **154**(3): p. D126-D133.

39. HAYES, T. YAMASHITA and P., *Analysis of Xps Spectra of Fe2+ and Fe3+ Ions in Oxide Materials.* Applied Surface Science, 2008. **254**(8): p. 2441-2449.

40. W. Crunert, A. Stakheev, R. Feldhaus, K. Anders, E. Shpiro and K. Minachev, *Mo (3d) Spectra of Supported Mo Catalysts.* The Journal of Physical Chemistry, 1991. **95**(3): p. 1323-1328.

41. C. A. Olsson, H.Mathieu and D. Landolt, *Angle-Resolved Xps Analysis of Molybdenum and Tungsten in Passive Films on Stainless Steel Pvd Alloys.* Surface ad Interface Analysis, 2002. **34**: p. 130 -134.

42. Perry A. Spevack , N. S. McIntyre, *Supported Molybdenum Oxide Thin Films 1. Calcination and Reduction Studies.* The Journal of Physical Chemistry, 1993. **97**(42): p. 11020-1 1030.

43. Perry A. Spevack , N. S. McIntyre, *Supported Molybdenum Oxide Thin Films 2. Reactions with Hydrogen Sulfide.* The Journal of Physical Chemistry, 1993. **97**(42): p. 1103 1-11036.

44. A C Lloyd J. Noël, S. McIntyre, D. Shoesmith *Cr, Mo and W Alloying Additions in Ni and Their Effect on Passivity.* Electrochimica Acta 2004. **49**: p. 3015 - 3027.

45. C. Strydom, J R. Staden and H. Sttydom, *1991.* Electroanalysis, An XPS Investigation of the Influence of Bromide and Iodide Solutions on the Surface of Silver Chloride Coated Ion-Selective Electrodes. **3** (3): p. 197-201.

46. Boping Liu, Yuwei Fang and Minoru Terano, *High Resolution X-Ray Photoelectron Spectroscopic Analysis of Transformation of Surface Chromium Species on Phillips Crox/Sio2 Catalysts Isothermally Calcined at Various Temperatures.* Journal of Molecular Catalysis A: Chemical, 2004. **219**(1): p. 165-173

47. B. Kobe, S. Ramamurthy, M.C. Biesinger, N. McIntyre and A. Brennenstul, *Xps Imaging Investigations of Pitting Corrosion Mechanisms in Inconel 600.* Surface and Interface Analysis 2005. **37**: p. 478-494.

48. N.S. McIntyre, T. E. Rummery, M. G. Cook, and D. Owen, *X-Ray Photoelectron Spectroscopic Study of the Aqueous Oxidation of Monei-400.* J. Electrochem. Soc., 1976. **123**(8): p. 1164-1170.

49. Hodgkiess, A. Neville and T., *Study of Passive Film on Stainless Steels and High Grade Nickel Base Alloy Using X-Ray Photoelectron Spectroscopy.* British Corrosion Journal, 2000 **35**(3): p. 183.

50. Marshall, G. Burstein and P., *The Coupled Kinetics of Film Growth and Dissolution of Stainless Steel Repassivating in Acid Solutions.* Corrosion Science, 1984. **24**(5): p. 449-462.

51. Seah, D. briggs and M., *Practical Surface Analysis: By Auger and X-Ray Photo-Electron Spectroscopy.* 2 ed. Vol. 1. 1990: Wiley.

CHAPTER SIX

SURFACE TREATMENT AND CORROSION INHIBITORS

6 Surface treatment and corrosion inhibitors

6.1 Introduction

Unavoidably, any mechanical finishing technique leaves a surface with microscopic irregularities and contaminants, including the polishing abrasive itself that can be ground into the surface. In contrast, ideal electropolishing methods can get rid of the surface irregularities, as well as any disturbed and contaminated material. The surface is left microscopically smooth. Furthermore, compositional in-homogeneities and impurities, such as sulphide inclusions, left by the manufacturing processing or mechanical finishing during the alloys production are removed. In the case of stainless steel, the various elements that make up the alloys are removed at different rates during the electropolishing treatment. Iron and nickel atoms are more easily extracted from the surface than chromium atoms causing a surface rich in chromium. This phenomenon will accelerate and improve the passivitation of electropolished surface [1]. Consequently, these will lead to an enhancement in the corrosion resistance of the metal [2-4].

In addition to the electropolishing methods, acid chemical cleaning is also commonly employed to remove the contaminants from the metallic surface [5], one of often used acids is nitric acid solution. Even if the surface is free from any metallic contaminants, treatment in dilute nitric acid greatly increases the resistance of stainless steel to pitting [6, 7].

Besides the above mentioned surface treatments, the use of corrosion inhibitor is one of the most effective measures for protecting metal surfaces against corrosion, especially in acid environments [8, 9]. The corrosion inhibition of steel and stainless steels in acid solutions with organic compounds containing sulphur, nitrogen or both has been studied by many authors [10-13].

Work presented in this part of the thesis examined the influence of two different electrochemical surface treatments (electropolishing and nitric acid passivation) on the corrosion behaviour of 316L stainless steel immersed in 15.3M HAc with 18.7mM bromide ions at 90 °C. Also, attempts were made to study the performance of three organic inhibitors in the same conditions.

6.2 Corrosion inhibition

One of the most effective methods to prevent metals from corrosion is using proper corrosion inhibitors. Corrosion inhibitors are chemical substances or compounds that, when added in appropriate concentration and state, provide a certain level of protection or reduction in the corrosion rate of particular materials in aggressive environments [14, 15].

Inhibitors have been classified differently by various authors. Some authors prefer to group the inhibitors by their chemical functionality as: Inorganic

inhibitors or organic inhibitors which can be organic anionic or organic cationic [16].

However, the most popular classification system consists of regrouping the corrosion inhibitors in a functionality scheme as: anodic, cathodic, organic, precipitation or volatile corrosion inhibitors [15].

Organic Corrosion Inhibitors

The organic inhibitors affect the entire surface of the corroded metal when present in adequate concentrations. Their effectiveness depends on the chemical composition, their molecular structure and their affinities for the metal surface. Organic inhibitors can control or reduce the corrosion processes by [17-19]:

- Blocking the reaction sites, which will prevent bound metal atom from taking part in corrosion reactions.
- Forming a barrier to diffusion that will reduce the movement or diffusion of ions to/from the metallic surface

Organic inhibitors may also protect or reduce the corrosion rate by participation in electrode reactions and interfering with the usual reaction pathway [18].

Inhibitors will be adsorbed according to the ionic charge of the inhibitor and the charge on the surface. Thus, cationic inhibitors or anionic inhibitors will

be adsorbed preferentially depending on whether the metal is charged negatively or positively.

From the available resource, there were no reports of inhibitors used to control corrosion in acetic acid environments. However, it was reported that inhibitors used for acetic acid are similar to those required for sulphuric acid environments [20]. The three organic corrosion inhibitors that were studied in the present work are: Benzotriazole, Thioura, and 2-mercaptobenzimidazole.

1) **Benzotriazole (BTA):**

Benzotriazole is one of the heterocyclic compounds with the chemical formula of $C_6H_4N_3H$, the chemical structure and molecular weight of BTA are shown in Table 6-1.

It has been reported that triazole type organic compounds are good corrosion inhibitors for many metals and alloys in various aggressive media [21, 22]. As one of this type, BTA is well known inhibitor for copper and has been widely studied as a corrosion inhibitor for stainless steels in acid environments [23, 24].

Inhibition efficiency of different concentrations of BTA on the corrosion behaviour of steel in sulphuric acid has been studied [25]. It was found that

corrosion potential, polarization resistance and the passive region increase with increasing the BTA concentrations while the corrosion current density and the corrosion rate decrease. Maximum inhibition efficiency, 98.5%, was achieved at low concentration, 9.0×10^{-4} M of BTA. Also, the influence of the same inhibitor on the corrosion behaviour for type 304 stainless steel in 2M sulphuric acid water-ethanol (80:20) system had been studied by Rodrigues et al. [26]. The BTA increased the corrosion rate at lower concentrations, 3.0×10^{-6} M. However it provided adequate corrosion inhibition when more than 1.5×10^{-4} M of BTA was used. Also, it was concluded that the BTA acted as a cathodic and anodic inhibitor over the entire range of potentials studied.

2) **Thiourea (TU):**

Thiourea , CH_4N_2S, contains one sulphur and two nitrogen atoms, Table 6-1 , thus, the corrosion of iron and steel in organic and inorganic acids can be controlled or reduced by the addition of TU or its derivatives [27].

The influences of TU as corrosion inhibitor on the corrosion of mild steel [12] and of TU and its derivatives on corrosion behaviours of AISI 410 stainless steel [28] in sulphuric acid were conducted. In both studies, the TU inhibited the hydrogen evolution reaction (HER) rate on steel surface by adsorption and blocking of active sites. However, TU had a maximum in the concentration-efficiency curves, beyond this maximum concentration, TU progressively loses its efficiency due to the decomposition of TU to produce
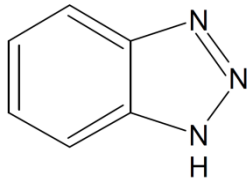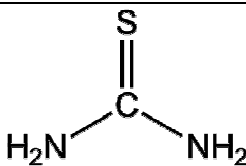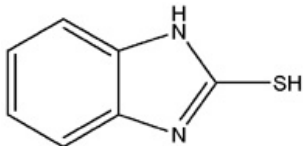
presumably bisulfide ions (HS⁻) which promote the HER and hence the corrosion reaction [12, 27, 28].

TU and two of its derivatives, methyl-thiourea (MTU) and phenyl-thiourea (PTU) were found to be effective inhibitors of corrosion of mild steel exposed to 0.1M sulphuric acid solutions. Replacing the hydrogen atom of the amino group of the thiourea molecule by methyl and phenyl groups caused the increase in percent inhibition efficiencies [29]. Also, diphenyl-thiourea has been investigated as a pickling inhibitor for steel in acetic acid [27]. Moreover, TU and its derivatives behaved as excellent corrosion inhibitors in 20% formic acid. They inhibited the corrosion of mild steel in acid solution by adsorption mechanism. and they behaved as mixed type inhibitors [13].

3) 2-mercaptobenzimidazole (2MBI):

2-mercaptobenzimidazole, $C_7H_6N_2S$, is an organic heterocyclic compound. The chemical structure and molecular weight of the 2MBI can be seen in Table 6-1. Most of the mercapto functional azole compounds showed mixed type corrosion inhibition in acidic solutions for protection of steel [30-34]. In acidic solutions, these inhibitors could be protonated. Then, the protonated species may adsorb on the cathodic sites of the metal surface and decrease the evolution of hydrogen. Also, these compounds could adsorb on anodic sites through N and S atoms, heterocyclic and aromatic rings, which are electron donating groups [30].

Table 6-1 General chemical structure of the three organic inhibitors with their molar mass

Inhibitor	Structure	Abbreviation	Molar mass g/mole
Benzotriazole		BTA	119.12
Thiourea		TU	76.12
2-mercaptobenzimidazole		2MBI	150.20

6.3 Materials and Experiential procedures

Perchloric acid ($HClO_4$) has been frequently used in acetic acid solution as electropolishing electrolyte for many metals [35-37]. In this study, the electropolishing treatment was performed by using a solution of 8% perchloric acid ($HClO_4$) and 92% acetic acid (CH_3COOH) at room temperature.

As shown in Figure 6-1, schematic representation of the experiment set up, the experiment is composed of a glass beaker containing the electrolyte, a

power supply with built-in current and voltage meter, stainless steel sheet and the sample need to be electropolished (316L stainless steel).

The sample was connected to the positive side of the power source (anode) and held in a vertical position in the electropolishing solution. The cathode was a thin sheet made of type 316 stainless steel. In order to ensure uniform material removal from the sample, this sheet was folded in a tube shape. The treatment time was about one minute in the solution with applying 25V.
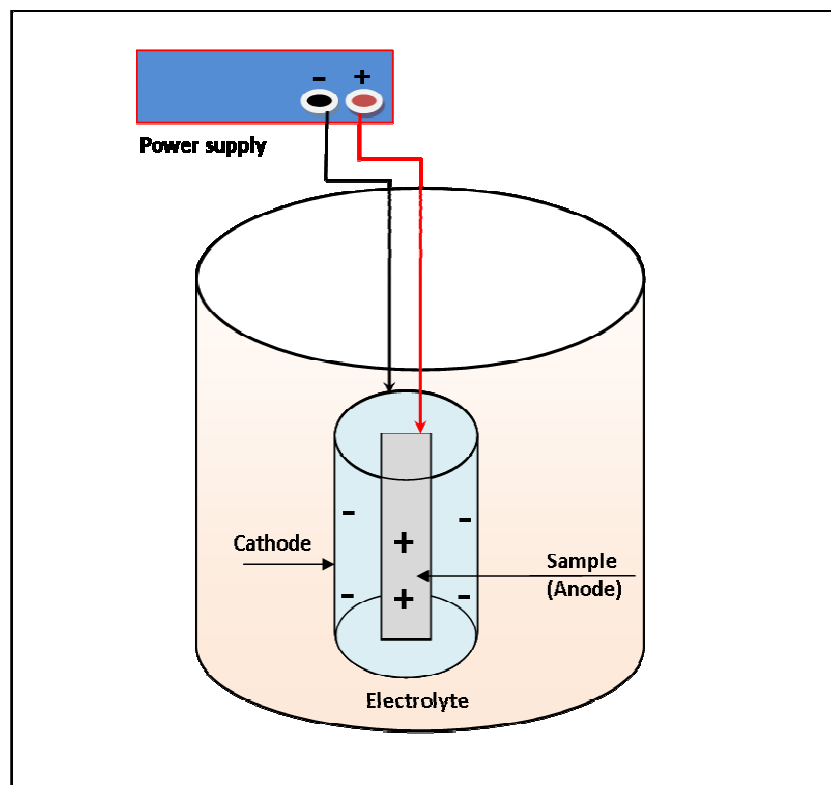
Figure 6-1 Schematic drawing representing the electropolishing experiment

Nitric acid passivation was carried out following ASTM Standard A967-01 [38]. As illustrated in the standard, 20w/V% of nitric acid was used in this treatment. The samples were immersed in the solution at 50°C for 30 minutes. After removing the samples from the passivation solution, they were cleaned and washed with deionized water and kept in the desiccator overnight before being used in the experiments.

After each of the above two treatments, electropolishing and passivation, the treated samples were immersed in the main test solution (15.3M HAc with Br ions at 90°C). Both electrochemical measurements (open circuit potential and corrosion rate and polarization curves) and the corrosion rate calculations by the weight loss method were performed by applying the same procedures described in the previous part of this thesis, chapter 4. In all the corrosion inhibitor evaluation experiments the open circuit potential and corrosion rate were monitored. Visual or microscopic examination of the samples was performed as necessary.

In the present study, the Benzotriazole (BTA) was obtained from high grade commercial reagents, purity (98%) and the required concentration was dissolved in the main test solution, 15.3M HAc with Br ions. Since there was no similar previous study conducted that can guide the optimal inhibitor concentration, a high concentration of BTA, 1M, was initially used, then the concentration was gradually decreased to 0.1M as shown in Table 6-2.

Table 6-2 Concentrations of BTA and pH and conductivity of the solution

BTA Concentration (M)	pH	Solution conductivity (ms/cm²)
1.00 (119.12 g/L)	0.62	0.45
0.50 (59.50 g/L)	0.22	0.31
0.10 (11.91g/L)	< 0	0.29

Concentrations of TU and 2MBI that used in this study are listed in Table 6-3 and Table 6-4. In the TU and 2MBI investigations, severe corrosion was noticed a few hours after immersing the samples into the test solutions, thus, all measurements were executed for **24 hours only**.

Table 6-3 TU concentrations used in this study, pH and conductivity of the solution

TU concentration (M)	pH	solution conductivity (ms/cm²)
0.05 (3.8 g/L)		0.33
0.01 (0.76g/L)		0.34
0.005 (0.38g/L)	< 0	0.30
0.001 (0.076 g/L)		0.29
0.0005 (0.038g/L)		0.29

Table 6-4 2MBI concentrations used in this study, pH and conductivity of the solution

2MBI Concentration (M)	pH	Solution conductivity (ms/cm²)
0.0005 (0.075 g/L)		0.33
0.0001 (0.015 g/L)	< 0	0.30

6.4 Results and discussion

6.4.1 Electropolishing and Nitric acid passivation:

Close examination of the surface of the new mechanically polished 316L stainless steel sample revealed small defects (inclusions) distributed on the surface of the sample as shown in the scanning electron microscopy analysis results Figure 6-2. EDX analysis (point analysis) performed on these inclusions indicate that they are enriched with sulphur (14-19 wt %) and manganese (28-29 wt %) and some amounts of chromium, iron and Ni detected from the base alloy as shown in Table 6-5. These observed inclusions are considered as promoters and preferable sits of the pitting corrosion to initiate. Therefore, electropolishing and passivation were carried out in order to eliminate such defects; these treatments may lead to higher corrosion resistant. Figure 6-3 shows SEM micrographs for the 316L sample after the electropolishing treatment. The result confirmed the presence of these pits without the MnS inclusion since the inclusions supposed to be dissolved during the electropolishing as proven by the EDX analysis Table 6-6. Results of the open circuit potentials (free corrosion potential) that were monitored for 96 hours (four days) for the three differently prepared samples are shown in Figure 6-4. The corrosion potentials were active, more negative at the begining of the test and remained in the same range until the sudden change to more noble, positive, values as for the untreated sample. Also, the electrochemically measured corrosion rate showed the same tendency for

both samples and there were no reduction in the corrosion rate due to the surface treatments. In addition to the electrochemically measured corrosion rate, the corrosion rate was also determined by the weight loss method for all the samples as shown in Table 6-7. Similar results were observed also, and the surface treatments did not affect or improve the alloy surface resistant to the aggressiveness of the solution.
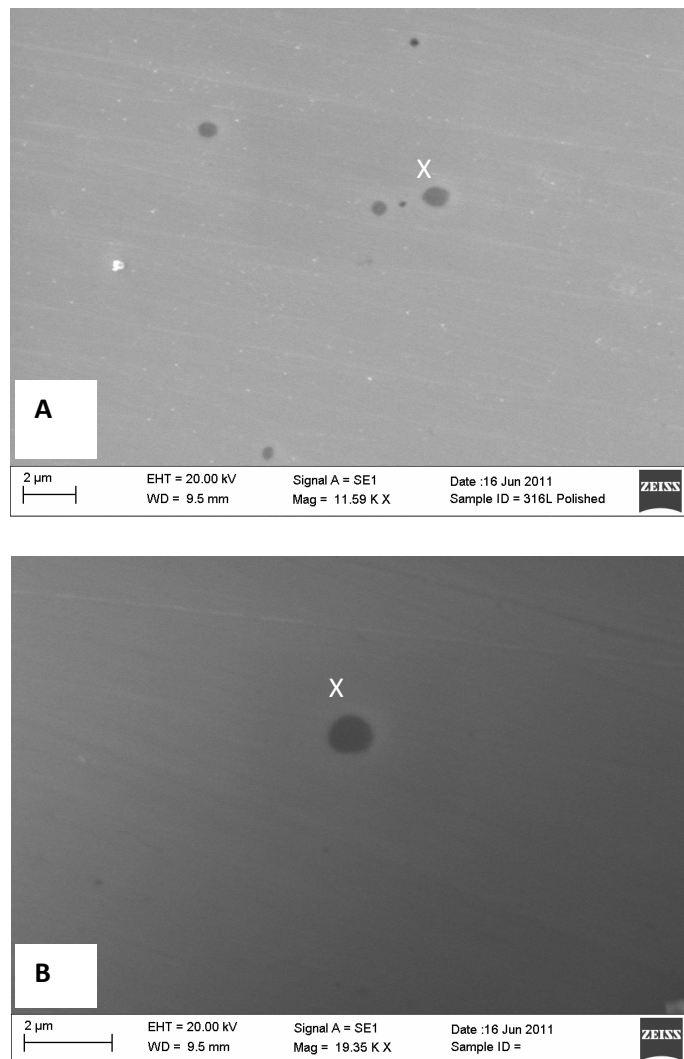

Figure 6-2 SEM micrograhs A and B of mechanically polished 316L stainless steel sample showing MnS inclusins as pointed by X. This confiremd by EDX analysis as belwo.

Table 6-5 EDX analysis results for different points (X) in SEM micrographs, A and B, above confirming the presence of MnS

Element		S	Cr	Mn	Fe	Ni
Weight %	A	19.28	10.05	39.44	27.52	3.70
	B	14.55	12.45	28.37	39.29	5.33
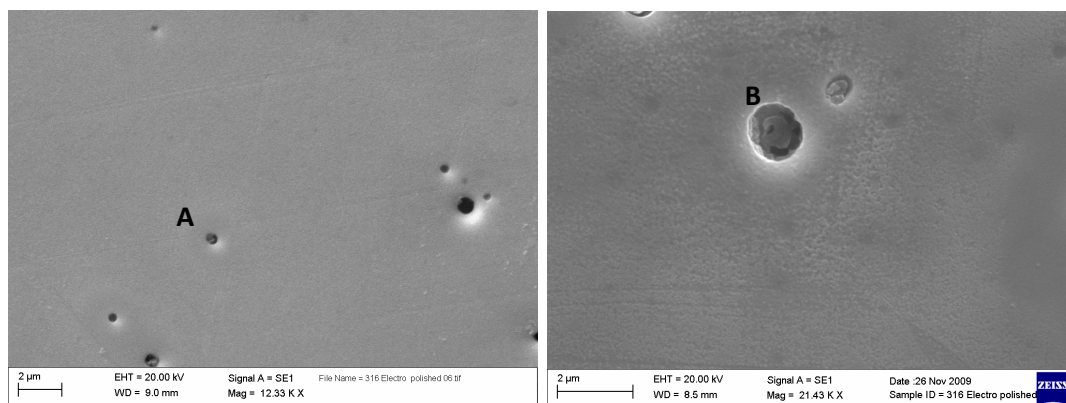
Figure 6-3 SEM of 316L stainless steel sample after electropolishing treatment

Table 6-6 Table 6 6 EDX analysis results acquired from the to points A and B on the above SEM, confirming the weakening of MnS formation after the

Element		S	Cr	Mn	Fe	Ni	Mo	Si
Weight %	A	--	18.23	1.17	69.94	8.61	1.89	0.20
	B	--	18.51	2.00	68.01	9.14	2.34	--
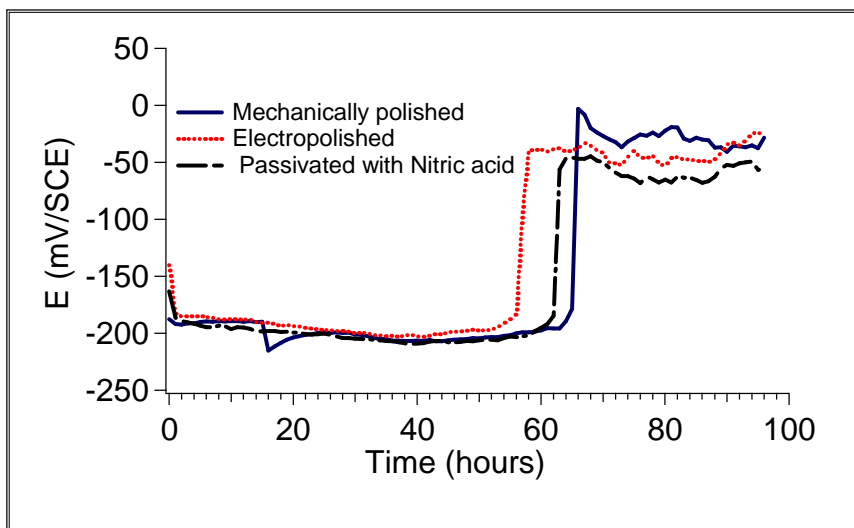
Figure 6-4 OCP of 316L stainless steel samples that tested in 15.3M HAc with 18.7mM Br ions at 90°C for 96 hours, the samples were: mechanically polished, electrochemically polished and passivated with nitric acid prior to the test.
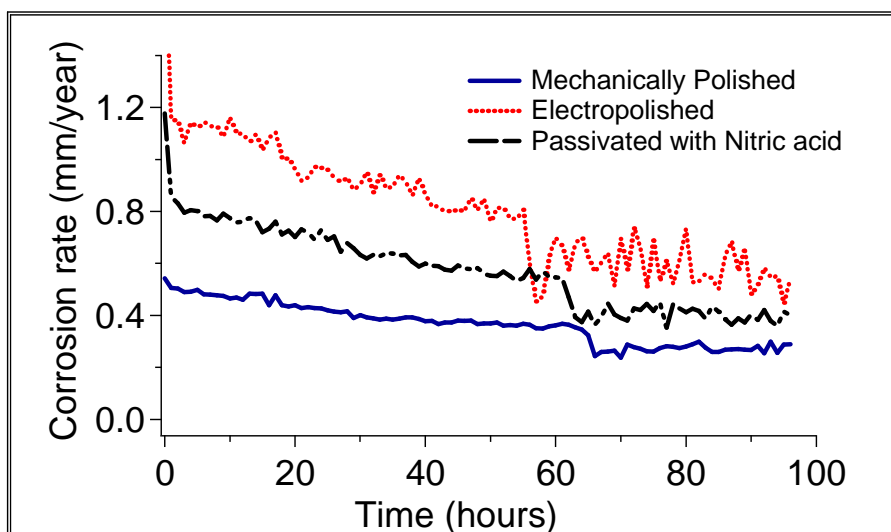
Figure 6-5　Corrosion rate monitored by electrochemical measurement　for 316L stainless steel samples that tested in 15.3M HAc with 18.7mM Br ions at 90°C for 96 hours, the samples were: mechanically polished, electrochemically polished and passivated with Nitric acid prior to the test..

Table 6-7 Corrosion rate (mm/year) for 316L samples determined by weight loss method after immersion in 15.3M HAc with 18.7mM Br ions at 90°C for 96 hours, the samples treated by different methods

Surface Treatment	Corrosion rate (mm/year)
Mechanically polished	2.30
Electro-polished	2.44
Nitric acid Passivated	2.38

6.4.2 Corrosion Inhibitor Results

Results that are shown in Figure 6-6 & Figure 6-7 represent the open circuit potentials and the electrochemically measured corrosion rate respectively after adding BTA to the main test solution (15.3M HAc with Br ions at 90°C). In the case of high concentrations, 1.0M and 0.5M or BTA, the OCP increase immediately to more positive values after immersing in the solution. The values were stable after some time at 300mV$_{SCE}$ and 100mV$_{SCE}$ for 1M and 0.5M of BTA respectively. Similarly, the corrosion rates at these two concentrations, Figure 6-7, decreased from 0.2mm/year to small values with time.

The change in test solution colour from colourless to dark brown was notice after immersing the 316L stainless steel in the main test solution without any corrosion inhibitors due to the corrosion and formation of iron acetate, as discussed in chapter 4. Conversely, there was no colour change in the solution and no sign of corrosion damage noticed in the sample after

introducing the BTA with high concentrations, 1 and 0.5M as revealed in Figure 6-8 and Figure 6-9 respectively.

However, when the concentration of BTA was reduced to 0.1M, the high corrosion rate was notice and the recorded OCP was similar to the one recorded without any inhibitors. Also, a change in the solution colour and severe pitting were observed Figure 6-10. The only dissimilarity was that the change in the OCP to a more positive value happener after a slightly shorter period of immersion (after about 40 hours) in presence of 0.1M BTA while it was after 70 hour if the inhibitor was not used (Figure 6-6).

The pH of the solution increases to more positive value after adding the BTA. Therefore, a possible cause of the reduction in corrosion rate of the alloy was the change in pH when using BTA. Hence, an experiment was carried out by using potassium acetate (CH_3COOK) that can alter the pH to the same value which was recorded for BTA (pH=0.22). This pH was achieved by adding 1.6 g/L (0.13M) of potassium acetate to the main test solution.

The OCP increase immediately to more positive values after immersing the sample into the solution with pH= 0.22 by adding either BTA or acetate, Figure 6-11. Also, from Figure 6-12, the corrosion rate of the alloy was reduced after adding the acetate and this suggests that no inhibitory surface film was formed on the alloy surface due to the absorption of the BAT.
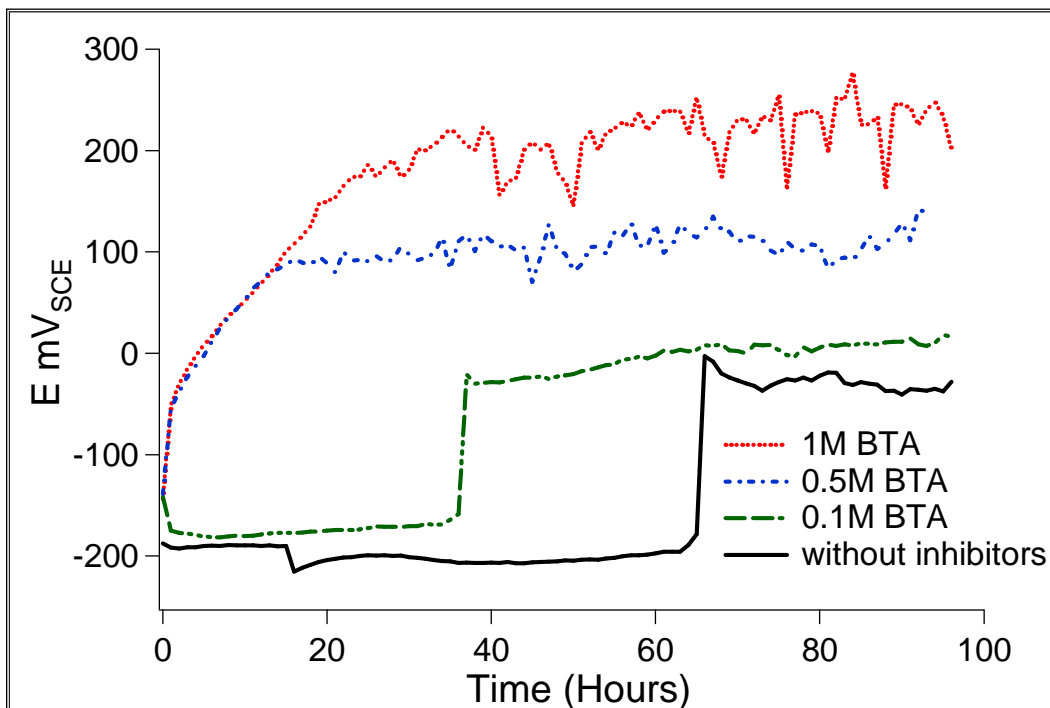
Figure 6-6 OCP for 316L stainless steel samples that tested in 15.3M HAc with 18.7mM Br ions at 90°C for 96 hours, with different concentration of BTA as corrosion inhibitor.
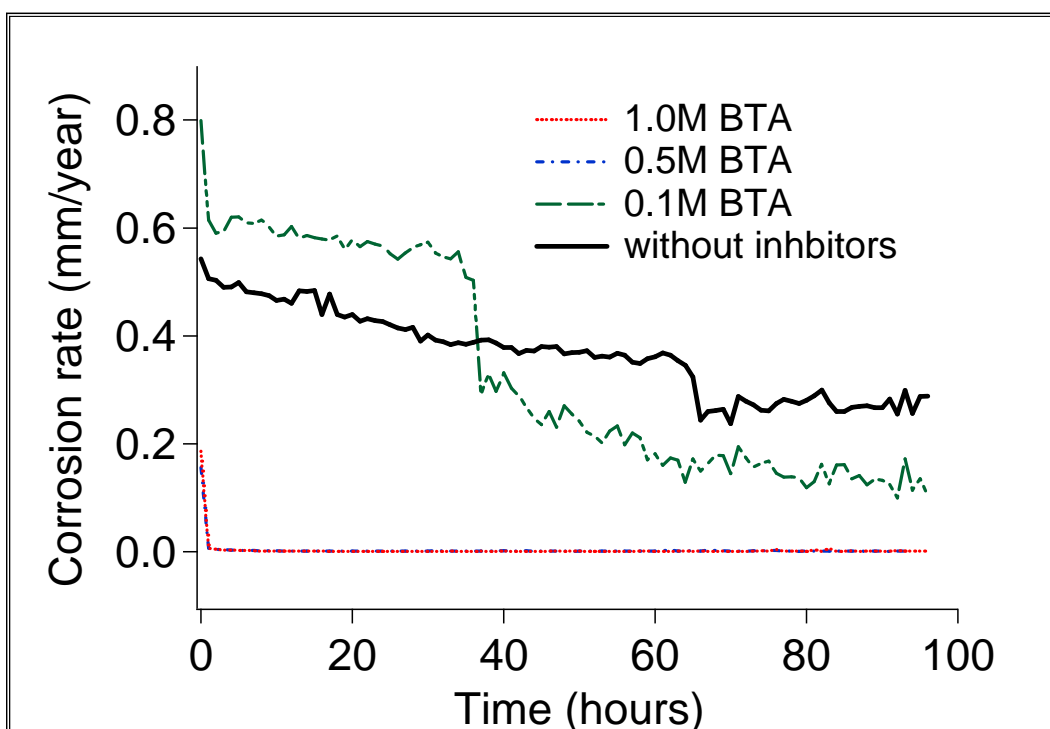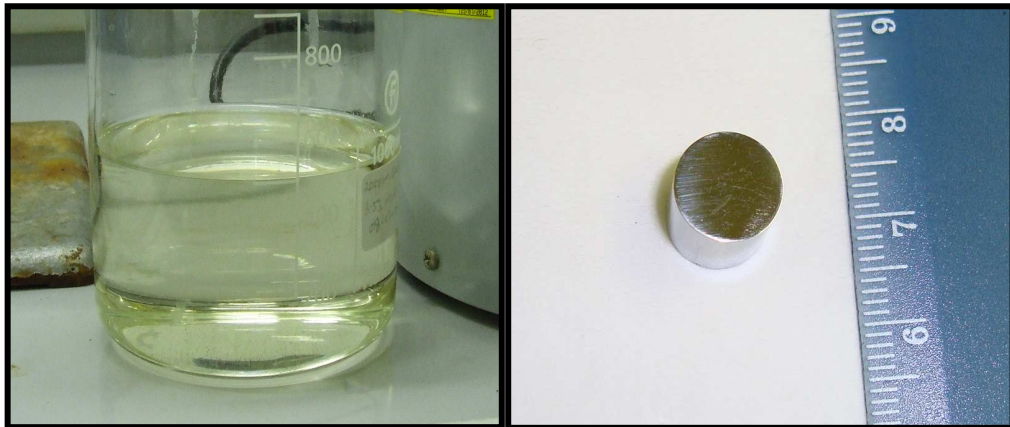

Figure 6-7 corrosion rate for 316L stainless steel samples that tested in 15.3M HAc with 18.7mM Br ions at 90°C for 96 hours, with different concentration of BTA as corrosion inhibitor.

Figure 6-8 Change in the solution colour and the sample general appearance after testing the alloy in 15.3M HAc with Br ions with presence of 1M BTA
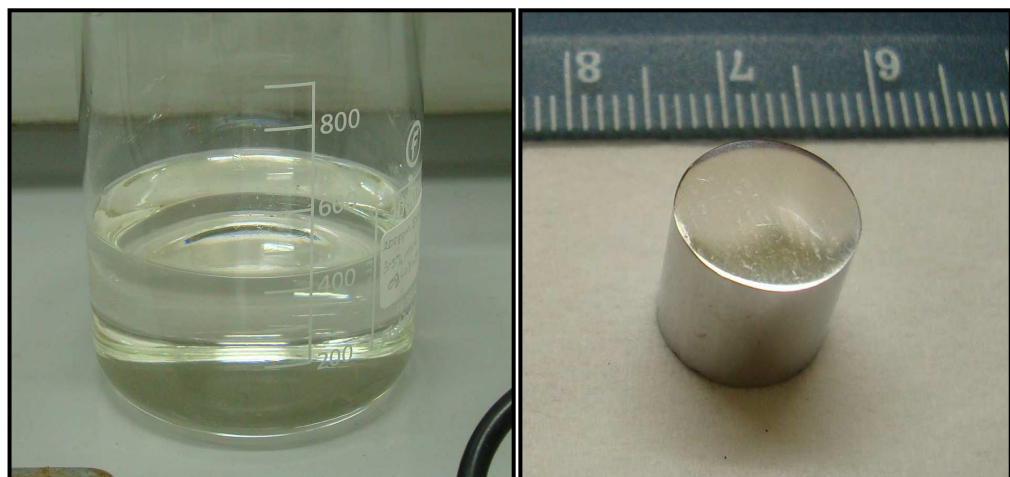
Figure 6-9 Change in the solution colour and the sample general appearance after testing the alloy in 15.3M HAc with Br ions with presence of 0.5M BTA
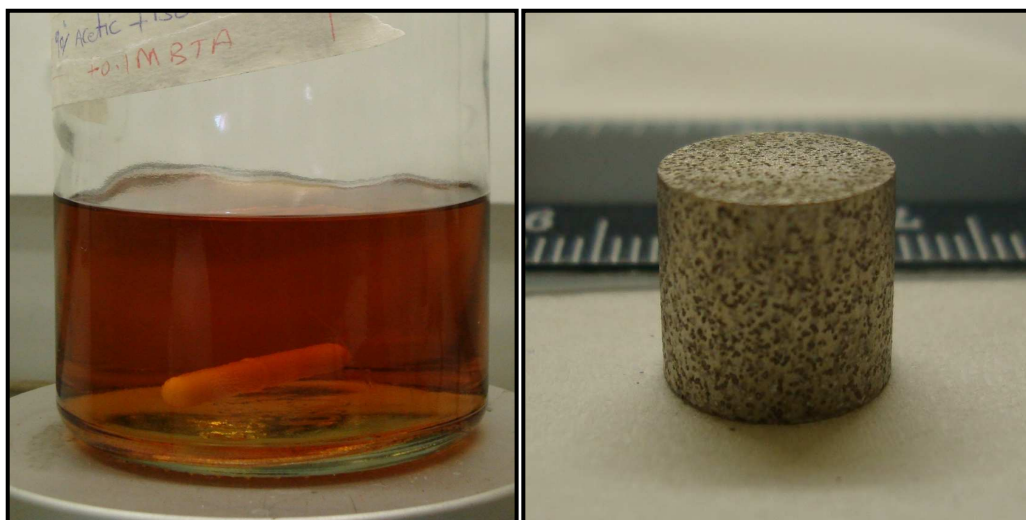

Figure 6-10 Change in the solution colour and the sample general appearance after testing the alloy in 15.3M HAc with Br ions with presence of 0.1M BTA.
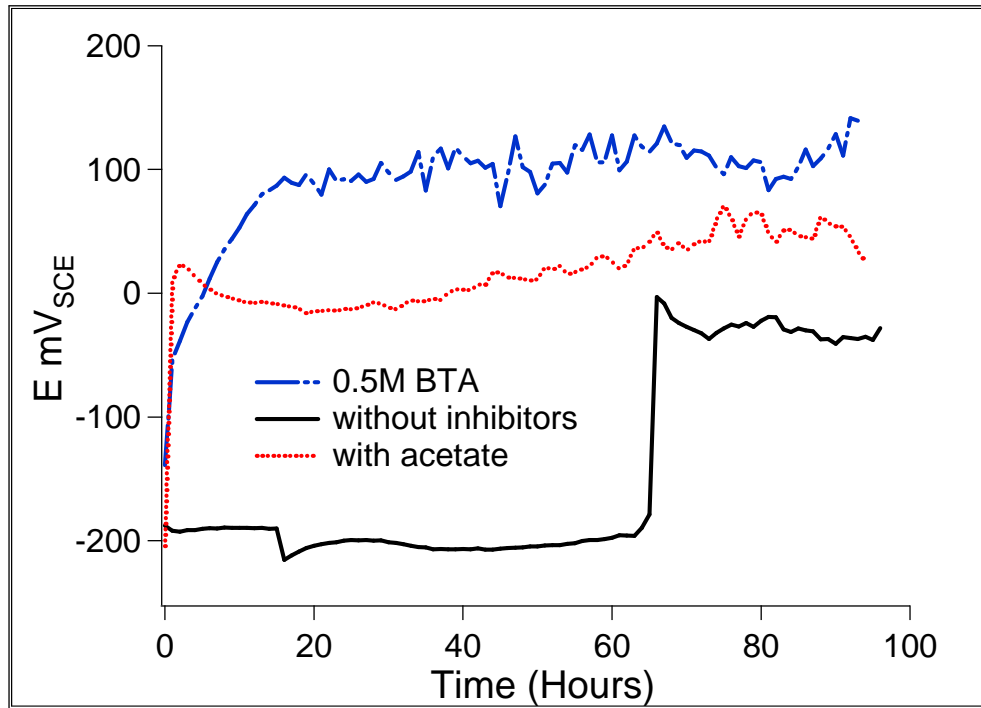
Figure 6-11 OCP for 316L stainless steel samples that tested in 15.3M HAc with 18.7mM Br ions at 90°C for 96 hours, at pH= 0.22 by adding 0.5M of BTA and 0.13M potassium acetate
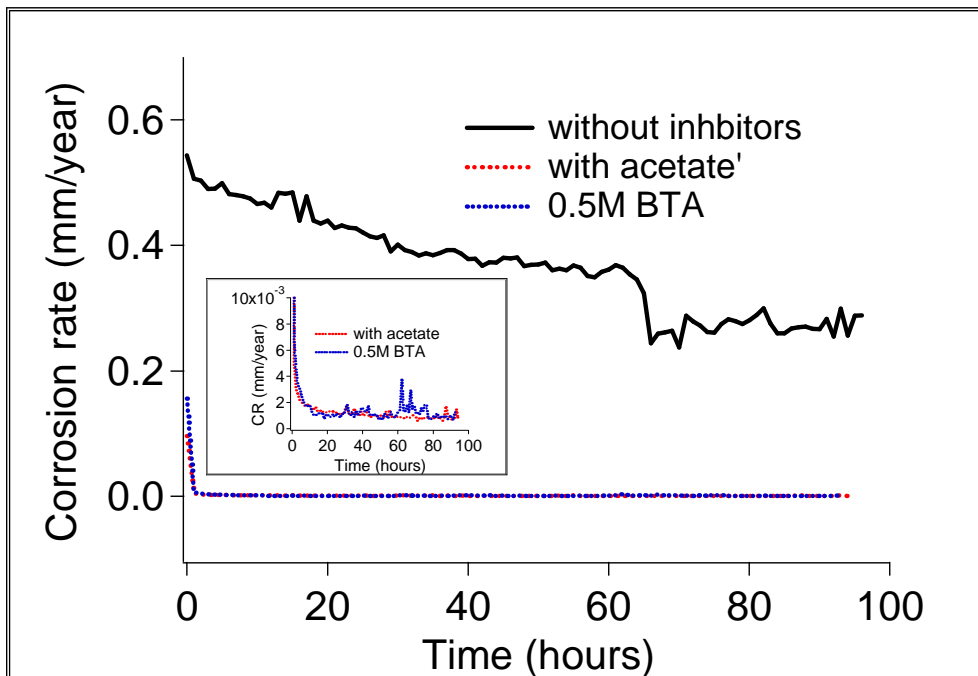

Figure 6-12 corrosion rate of 316L stainless steel samples that tested in 15.3M HAc with 18.7mM Br ions at 90°C for 96 hours, at pH = 0.22 by adding 0.5M of BTA and 0.13M potassium acetate

As mentioned previously, chemical compounds containing either sulphur or nitrogen are suggested to be effective inhibitors for acid corrosion. However, compounds containing both sulphur and nitrogen atoms were found to be better inhibitors than those containing either atom alone [9, 39, 40]. Therefore, TU and 2MBI were tested in this study. In this part of investigations, severe corrosion was noticed few hours after immersing the samples into the test solutions, thus, all measurements were executed for 24 hours only.

With all the concentrations of TU, the OCP were more negative (active potentials) than the OCP for the alloy tested in the main test solution, 15.3M HAc with 18.7mM Br ions, without inhibitors. As demonstrated in Figure 6-13, The OCP was in the range of -250 to -300mV/$_{SCE}$. Also, the monitored corrosion rates were higher than that in the main solution, Figure 6-14. Besides, from the visual observations for all the samples after each test, there was a non-protective (loosely adherent) black corrosion products (it could be iron sulphide) covering the samples, Figure 6-15.

The organic inhibitors containing sulphur have two possible effects on the corrosion of iron and steels. They can chemisorb on the surface of iron and steel and isolate the metal surface from the corrosive environment and therefore control or inhibit the corrosion rate of iron and steel [12, 41, 42]. However, some of these organic sulphur containing inhibitors when adsorbed on the surface of steel might decompose and give out H$_2$S which

can accelerate the corrosion of iron and steel in acid solutions [10, 28, 42]. As reported by Ateya et al. [12], TU and its derivatives could accelerate corrosion and hydrogen evolution probably due to reduction of TU to yield corrosion promoting H_2S or due to protonation of TU on the assumption that the protonated species catalyzes the hydrogen evolution reaction, and hence the corrosion reaction.

Similar to the TU results, also, adding 2MBI as corrosion inhibitors showed the same performance. All the samples showed more negative corrosion potentials and higher corrosion rate as shown in Figure 6-16 and Figure 6-17 respectively. Besides, the samples surfaces were covered by blackish unprotective corrosion products (Figure 6-18).
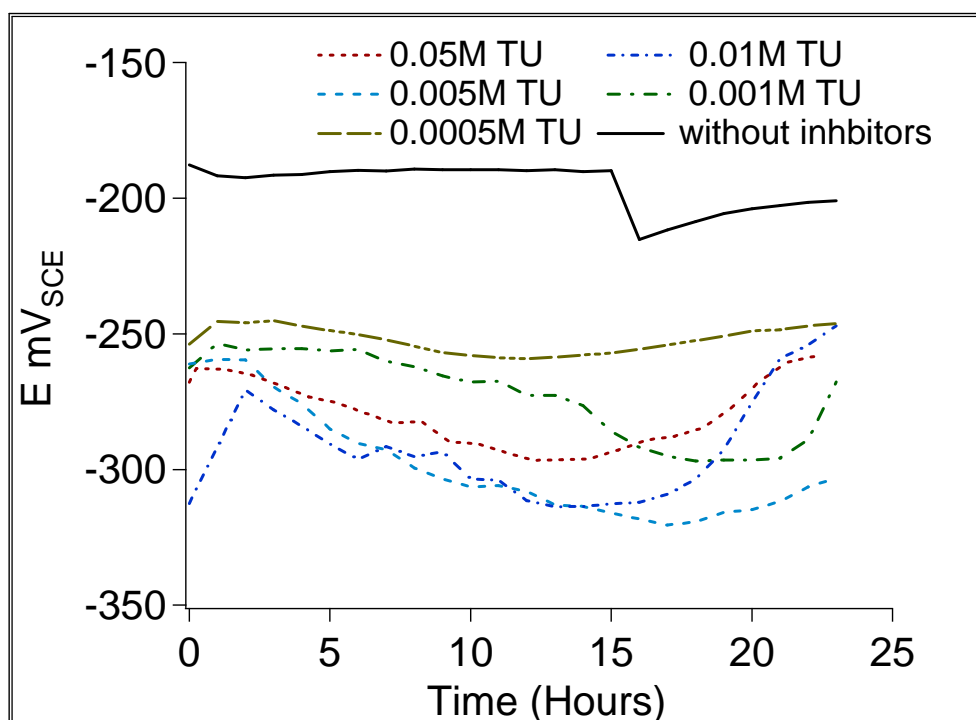

Figure 6-13 OCP monitored for 24 hours for the 316L stainless steel tested in 15.3M HAc with 18.7mM Br ions in presence of different concentrations of thiourea as corrosion inhibitor
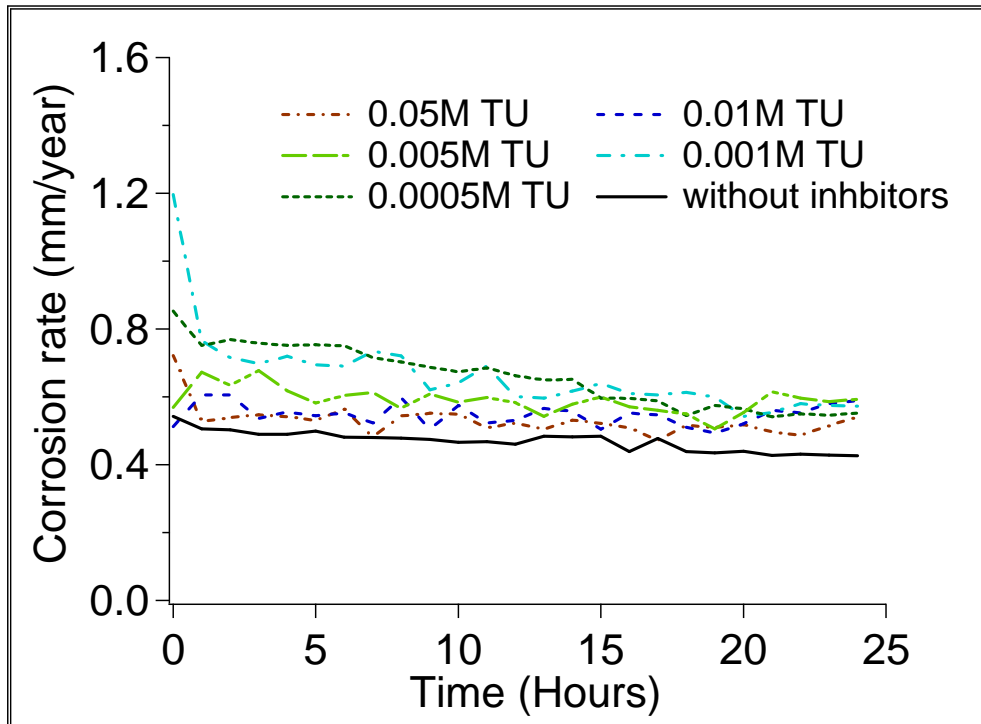
Figure 6-14 Corrosion rate (mm/year) monitored for 24 hours for the 316L stainless steel tested in 15.3M HAc with 18.7mM Br ions in presence of different concentrations of thiourea as corrosion inhibitor
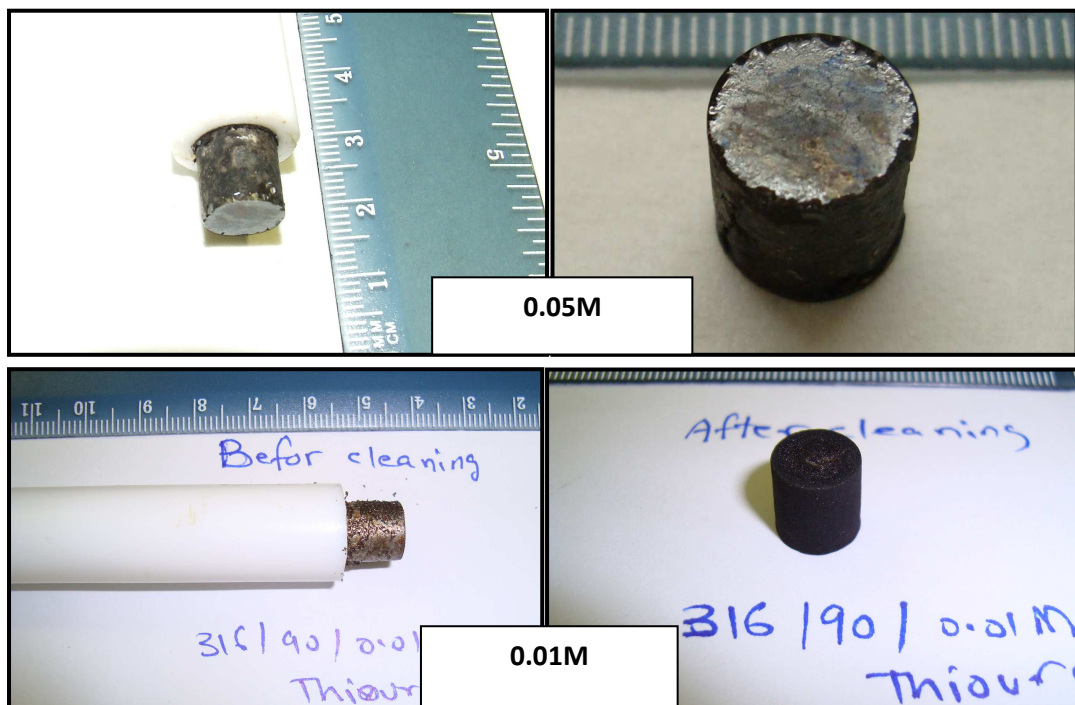

Figure 6-15 General appearance of the 316L stainless steel samples after testing in 15.3M HAc with 18.7mM Br ions and different TU concentrations at 90°C.

0.005M

0.001M
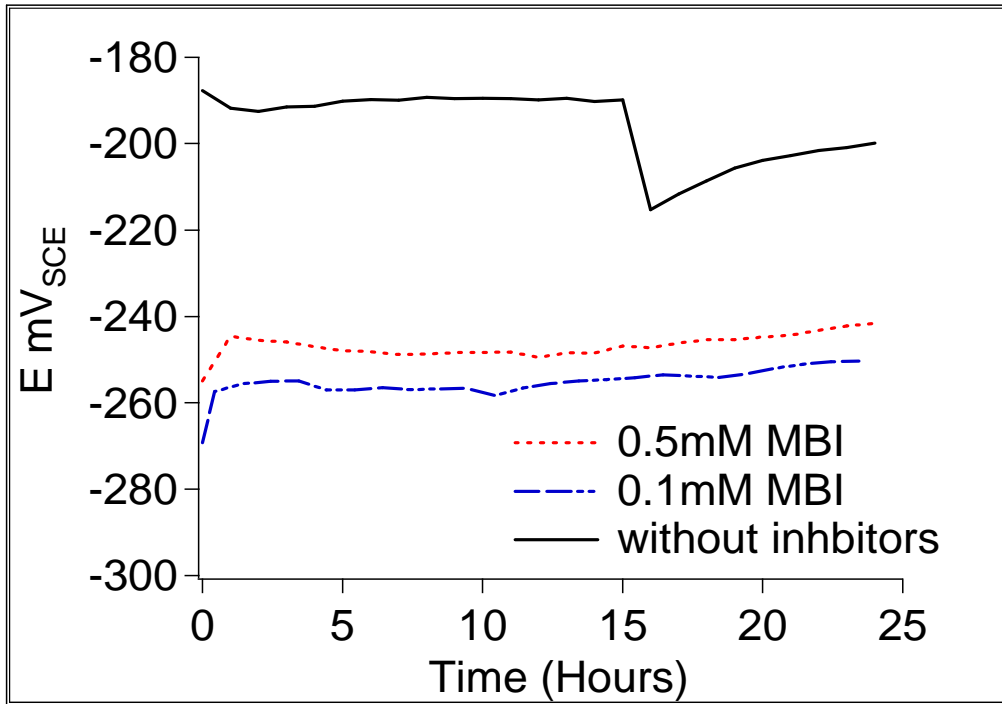
0.0005M

Continue Figure 6-15

Figure 6-16 OCP monitored for 24 hours for the 316L stainless steel tested in 15.3M HAc with 18.7mM Br ions in presence of different concentrations of 2MBI as corrosion inhibitor
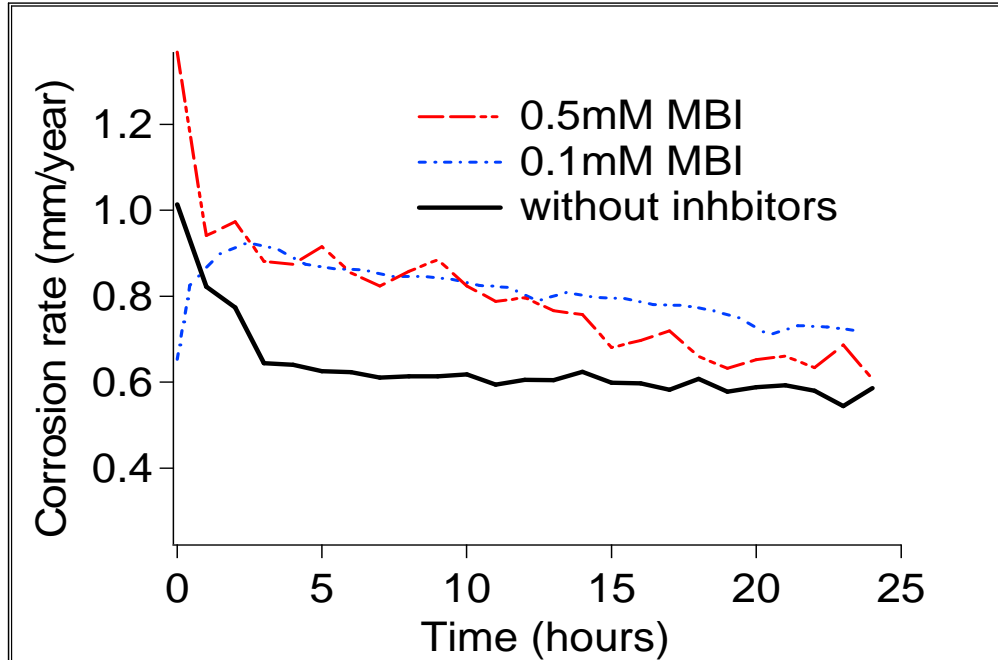

Figure 6-17 Corrosion rate monitored for 24 hours for the 316L stainless steel tested in 15.3M HAc with 18.7mM Br ions in presence of different concentrations of 2MBI as corrosion inhibitor
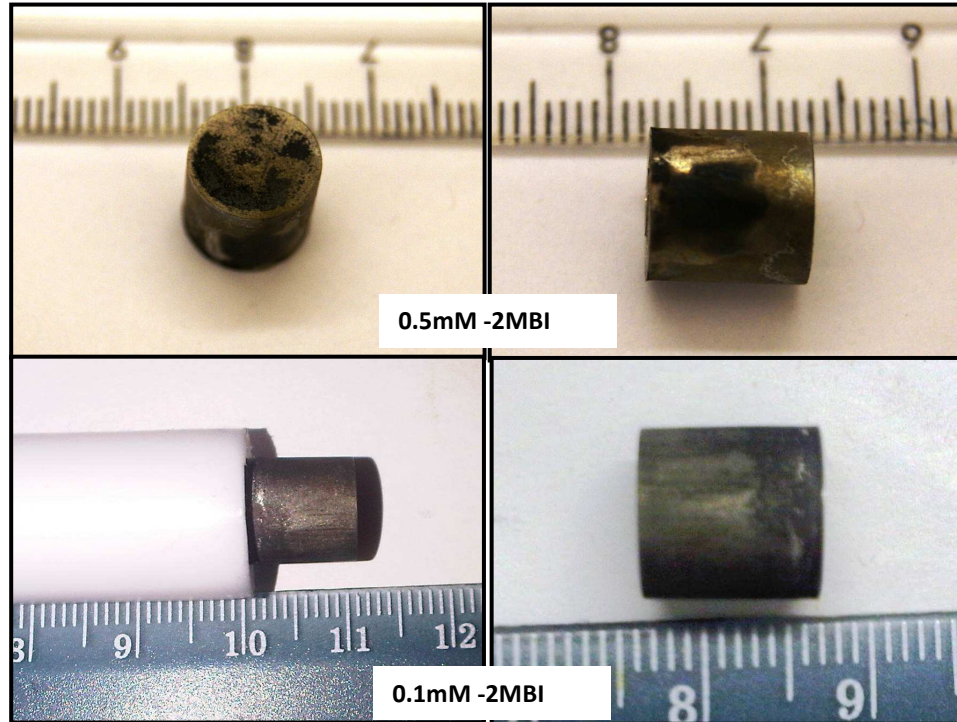
Figure 6-18 general appearance of 316L stainless steel samples after testing in 15.3M HAc with Br ions and different concentrations of 2MBI at 90°C

6.5 Conclusion

The observations concerning the influence of the surface treatment and corrosion inhibitors on the behaviour of the 316L stainless steel alloy in 15.3M HAc with 18.7mM Br ion at 90°C can be summarized as:

- The surface treatments by either electropolishing or nitric acid passivation were not sufficient to give any noticeable protection from the aggressive solution.

- High concentration of BTA inhibited the pitting corrosion of the alloy (0.5M BTA); however this protection was due to the raising in the pH of the solution.

- The organic inhibitors containing both nitrogen and sulphur atoms, TU and 2BMI, increased the aggressiveness of the solution.

- It is suggested that, TU and 2MBI were decomposed and H_2S was produced in the solution which can accelerate the corrosion of alloy.

6.6 References

1. *What Is Electropolishing by Kalamazoo Electropolishing Company.* 2008 [cited 2011; Available from: http://www.kepcoinc.com/?page=serviceselectropolishing.

2. Sutow, Elliott J., *The Influence of Electropolishing on the Corrosion Resistance of 316l Stainless Steel.* Journal of Biomedical Materials Research, 1980. **14**: p. 587-595

3. L. M. Weldon, P. E. Mchugh, W. Carroll, E. Costello, and C. O bradaigh, *The Influence of Passivation and Electropolishing on the Performance of Medical Grade Stainless Steels in Static and Fatigue Loading.* Journal of materials science: materials in medicine, 2005. **16**(2): p. 107- 117.

4. *Electropolishing, a User's Guide to Applications, Quality Standards and Specifications*. January 2003, Delstar metal finishing, INC.: Houston, TX, US.

5. C. Marikkannu, S. Sathiyanarayanan and G. Venkatachari, *Technical Note: Studies on Newer Chemical Passivation Treatment for Stainless Steel* Transactions of the lnstitute of Metal Finishing, 2005. **83**(3): p. 158-160.

6. Barbosa, M.A., *The Pitting Resistance of Aisi 316 Stainless Steel Passivated in Diluted Nitric Acid* Corrosion Science, 1983. **23**(12): p. 1293-1305

7. P. E. Manning, D. J. Duquette and W. F. Savage, *Role of Sulfide Inclusion Morphology in Pit Initiation of Several Type 300 Series Stainless Steels.* Corrosion, 1980. **36**(6): p. 313-319

8. Fouda, S. Abd El-Maksoud and A., *Some Pyridine Derivatives as Corrosion Inhibitors for Carbon Steel in Acidic Medium.* Materials Chemistry and Physics, 2005. **93**(1): p. 84-90.

9. J. Aljourani, K. Raeissi and M. Golozar, *Benzimidazole and Its Derivatives as Corrosion Inhibitors for Mild Steel in 1m Hcl Solution.* Corrosion Science, 2009. **51** (8): p. 1836-1843.

10. X. L. Cheng , H. Y. Ma, S. H. Chen, R. Yu, X. Chen and Z. M. Yao, *Corrosion of Stainless Steels in Acid Solutions with Organic Sulfur Containing Compounds.* Corrosion Science 1998. **41**(2): p. 321-333.

11. Fabrizio Zucchi, Giordano Trabanell1 and Giancarlo Brunoro, *The Influence of the Chromium Content on the Inhibitive Efficiency of Some Organic Compounds.* Corrosion Science, 1992. **33**(7): p. 1135-1139.

12. B. G. Ateya, B. E. El-anadouli and F. M. El-nizamy, *The Effect of Thiourea on the Corrosion Kinetics of Mild Steel in H_2so_4.* Corrosion Science, 1984. **24**(6): p. 497-507.

13. M.A. Quraishi, F.A. Ansari, D. Jamal,, *Thiourea Derivatives as Corrosion Inhibitors for Mild Steel in Formic Acid.* Materials Chemistry and Physics, 2002. **77** (3): p. 687-690.

14. Xiaodong Zhao , Jie Yang and Xiqiu Fan, *Review on Research and Progress of Corrosion Inhibitors.* Applied Mechanics and Materials, 2011. **44-47**: p. 4063-4066.

15. Roberge, Pierre R., *Handbook of Corrosion Engineering, Chapter 10, P.833.* 2000: McGraw-Hill.

16. Jones, Loyd W, *Corrosion and Water Technology for Petroleum Producers.* 1988: Oil and Gas Consultants International.

17. J.L. Mora-Mendoza, J.G. Chacon-Nava, G. Zavala-Olivares, M.A. González-Núñez, and S. Turgoose, *Influence of Turbulent Flow on the Localized Corrosion Process of Mild Steel with Inhibited Aqueous Carbon Dioxide Systems.* Corrosion, 2002. **58**(7): p. 608-619.

18. Robert Lindsay , Stuar Lyon, *Introduction to Control of Corrosion by Environmental Modification*, in *Shreir's Corrosion*. 2010, Elsevier Ltd. p. 2891.

19. El–Maksoud, S. A. Abd, *The Effect of Organic Compounds on the Electrochemical Behaviour of Steel in Acidic Media. A Review.* International Journal of Electrochemcal Science 2008. **3**: p. 528 - 555.

20. schmitt, G., *Application of Inhibitors for Acid Media.* British corrosion journal, 1984. **19**(4).

21. A. Abdennabia, A. Abdulhadia, S. Abu-Orabia and H. Saricimenb, *The Inhibition Action of 1(Benzyl)1-H-4,5-Dibenzoyl-1,2,3-Triazole on Mild Steel in Hydrochloric Acid Media.* corrosion Science, 1996. **38**(10): p. 1791-1800.

22. Fouad Bentiss, Michel Traisnel, Herve´ Vezin, and Michel Lagrene, *Electrochemical Study of Substituted Triazoles Adsorption on Mild Steel.* Industrial and Engineering Chemistry Research, 2000. **39**(10): p. 3732-3736.

23. Haruyama, F. El-Taib Heakal and S., *Impedance Studies of the Inhibitive Effect of Benzotriazole on the Corrosion of Copper in Sodium Chloride Medium* corrosion Science, 1980. **20**(7): p. 887-898

24. Lewis, Gladius, *Adsorption Isotherm for the Copper-Benzotriazole System* British Corrosion Journal 1981. **16**(3): p. 169-71

25. Gomma, G.K., *Corrosion Inhibition of Steel by Benzotriazole in Sulphuric Acid.* Materials Chemistry and Physics, 1998. **55**(3): p. 235-240.

26. P.R.P. Rodrigues, A.H.P. Andrade and S.M.L. Agostinho, *Benzotriazole as Corrosion Inhibitor for Type 304 Stainless Steel in Water-Ethanol Media Containing 2 M H2so4.* British Corrosion Journal 1998. **33** (3): p. 211-213.

27. M. Desai, G. Thanki and M. Gandhi, *Thiourea and Its Derivatives as Corrosion Inhibitors.* Anti-Corrosion Methods and Materials, 1968. **15**(7): p. 12 - 16.

28. Namboodhiri, Reeta Agrawal and T., *Inhibition of Sulfuric Acid Corrosion of 410 Stainless Steel by Thioureas.* Corrosion Science, 1990. **30**(1): p. 37-52.

29. M. Özca, I. Dehri, and M. Erbil, *Organic Sulphur-Containing Compounds as Corrosion Inhibitors for Mild Steel in Acidic Media: Correlation between Inhibition Efficiency and Chemical Structure.* Applied Surface Science, 2004. **236**(1-4): p. 155-164.

30. Ashhari, M. Mahdavian and S., *Corrosion Inhibition Performance of 2-Mercaptobenzimidazole and 2-Mercaptobenzoxazole Compounds for Protection of Mild Steel in Hydrochloric Acid Solution.* Electrochimica Acta, 2010. **55**(5): p. 1720-1724.

31. Hui-Long Wang, Rui-Bin Liu and Jian Xin, *Inhibiting Effects of Some Mercapto-Triazole Derivatives on the Corrosion of Mild Steel in 1.0 M Hcl Medium.* Corrosion Science, 2004. **46**(10): p. 2455-2466

32. M. Rafiquee, Nidhi Saxena, Sadaf Khan and M. Quraishi, *Influence of Surfactants on the Corrosion Inhibition Behaviour of 2-Aminophenyl-5-Mercapto-1-Oxa-3,4-Diazole (Amod) on Mild Steel* Materials Chemistry and Physics, 2008. **107**(2-3): p. 528-533

33. Hamdy Hassan, Essam Abdelghani and Mohammed Amin, *Inhibition of Mild Steel Corrosion in Hydrochloric Acid Solution by Triazole Derivatives: Part I. Polarization and Eis Studies* Electrochimica Acta, 2007. **52**(22): p. 6359-6366

34. R. Álvarez-Bustamante, G. Negrón-Silva, M. Abreu-Quijano, H. Herrera-Hernández, M. Romero-Romo, A. Cuán and M. Palomar-Pardavé, *Electrochemical Study of 2-Mercaptoimidazole as a Novel Corrosion Inhibitor for Steels* Electrochimica Acta, 2009. **54**(23): p. 5393-5399

35. Landolt, D., *Fundamental Aspects of Electropolishing* Electrochimica Acta, 1987. **32**(1): p. 1-11

36. Gabe, D. R., *Electropolishing of Mild Steel in Phosphoric and Perchloric Acid Containing Electrolytes.* Corrosion Science, 1973. **13**(3): p. 175-185

37. Gabe, D. R., *Toward a Universal Electropolishing Solution.* Metallography, 1972. **5**: p. 415-421.

38. Lunder, Borge Holme and Otto, *Characterisation of Pitting Corrosion by White Light Interferometry.* Corrosion Science 2007. **49**(2): p. 391- 401.

39. A. El-Shafei, M. Moussa and A. El-Far, *The Corrosion Inhibition Character of Thiosemicarbazide and Its Derivatives for C-Steel in Hydrochloric Acid Solution* Materials Chemistry and Physics, 2001. **70**(2): p. 175-180

40. O. Benali, L. Larabi, M. Traisnel, L. Gengembra and Y. Harek, *Electrochemical, Theoretical and Xps Studies of 2-Mercapto-1-Methylimidazole Adsorption on Carbon Steel in 1m Hclo4.* Applied Surface Science, 2007. **253** (14): p. 6130-6139.

41. S. Raicheva, B. Aleksiev and E. Sokolova, *The Effect of the Chemical Structure of Some Nitrogen- and Sulphur-Containing Organic Compounds on Their Corrosion Inhibiting Action.* Corrosion Science, 1993. **34**(2): p. 343-350

42. X. L. Cheng , H. Y. Ma, S. H. Chen, R. Yu, X. Chen and Z. M. Yao, *Corrosion of Stainless Steels in Acid Solutions with Organic Sulfur Containing Compounds.* Corrosion Science 1999. **41**(2): p. 321-333.

CHAPTER SEVEN

GENERAL CONCLUSIONS

AND

FUTURE WORK

7 General Conclusions and future work

7.1 General Conclusions

In this research, corrosion performance of austenitic stainless steels, 316L and 245SMO, subsequent to immersion in 11.9M and 15.3M of acetic acid in presence of 18.7mM Br⁻ was studied by various means. The major conclusions drawn from the results and the discussions presented in chapters 4, 5 and 6 are as follows:

- Corrosion behaviour of austenitic 316L and 254SMO stainless steels at 90^0C changes significantly with increase in acetic acid concentration in the presence of bromide. In 11.9M-HAc-Br⁻, both steels show excellent corrosion resistance. In contrast, both steels corrode to some extent in 15.3M-HAc-Br⁻, with 316L displaying a much greater corrosion rate.

- The correlation between the up/down steps in OCP and corrosion rate by LPR observed for 254SMO is indicative of passivation after approximately 14 hours after immersion in 15.3M-HAc-Br⁻. This conclusion is also supported by the XPS results, as a stable passive film was observed on the surface of alloy over the immersion time.

- The 316L steel experiences uniform and pitting corrosion in 15.3M-HAc-Br⁻ and no passive surface film formed. The XPS results indicate a continual oxidation of Fe, Cr, Mo and Ni on the surface of the 316L stainless steel subsequent to the emersion in the 15.3M-HAc-Br⁻. Also, the contribution of the pits to the total weight loss was at least 60 % after 10 days of immersion.

- Intensive localised attack is evident on the surface of 316L, and is associated with presence of manganese sulphide inclusions whereas the localised attack of 254SMO steel is possibly associated with the presence of a small amount of sigma-phase.

- From the attempts which were made to improve the corrosion resistance of the 316L stainless steel in 15.3M-HAc-Br⁻ both electropolishing and nitric acid passivation treatments were not sufficient to give any noticeable protection from the aggressive solution. Also, no corrosion inhibition was achieved when the three organic inhibitors, BTA, TU and 2MBI were utilised.

7.2 Future work

Further experiments can be carried out to provide better understanding of the corrosion performance of the two stainless steels, 316L and 254SMO, in the acetic acid environments with the presence of Br ions. Below are some of the proposed future works:

- Results of the OCP and anodic polarization curves of 254SMO stainless steel concluded that the alloy was under active dissolution for the first 14 hours of the immersion in 15.3M-HAc-Br⁻ and then the surface became passive. Therefore, analysing the sample with SEM prior to passivation may give more insight into surface processes at this stage.

- The proposed reason(s) for the selective dissolution noticed for 254SMO samples tested in 15.3M HAc-Br⁻, could be further elucidated by investigating the presence of second phase (i.e. sigma) in a new polished sample employing standard method(s) for detecting second phase.

- In identical test conditions with only a difference in the flow rate of the electrolyte, there was no pitting corrosion observed for the 316L stainless steel, as concluded in the previous study by Turnbull et al [1]. Thus, studying any possible effect(s) of flow rate on the corrosion behaviour of these alloys would be interesting.

- In order to evaluate the extent of metallic dissolution from the surface of the steels, the content of dissolved elements, Fe, Cr, Mo or Ni, in the test solution could be evaluated by using Atomic Absorption Spectrometer (AAS).

- Study the behaviour of the constituent elements: iron, chromium, nickel and molybdenum in their pure state and compare that with the typical alloys (316L and 254SMO) with the aim of knowing which element(s) may possibly facilitate the passivity to corrosion in the test solutions.

References

1.   Alan Turnbull, Mary Ryan , Anthony Willetts and Shengqi Zhou, *Corrosion and Electrochemical Behaviour of 316l Stainless Steel in Acetic Acid Solutions.* Corrosion Science, 2003. **45**: p. 1051-1072.

APPENDIXES

Appendix I: Method of the solution resistance (Rs) calculations:

Given the low conductivity of the electrolyte (Acetic acid solutions), the possible impact of IR drop was considered for all of the PDP and LPR measurements. Solution resistance (R_s) value estimated for each system was achieved by re-plotting the potential (E) verses current density (*i*) on a linear scale for the uppermost 200-300mV/$_{SCE}$ of the anodic branch of the PDP curve.
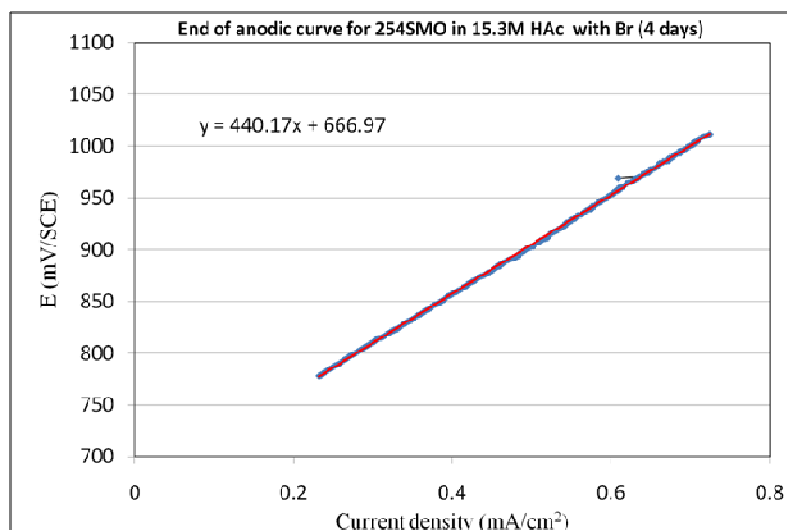
The gradient of the curve gives the solution resistance (R_s) multiplied by the area of the exposed sample. Thus, to have the solution resistance (R_s) in Ω, the values were divided by the area of the sample (3.93 cm²).

Table A-1 Solution resistance determined by the method described in the text for each system solution.

	R_s (Ω)				
	316L			**254SMO**	
	0.5 hour	**96 hour**		**0.5 hour**	**96 hour**
11.5M HAc	55	51		51	66
15.3M HAc	55	178		127	112

The actual potential (E_{actual}) is corrected based on the calculated IR drop for each test solution by:

$$E_{actual}= E_{recorded} -IR$$

Figure A-1 is an example shows the impact of the IR drop on PDP curves for alloys, 316L and 254SMO, immersed for 96hrs in 11.9M- HAc-Br⁻ at 90⁰C
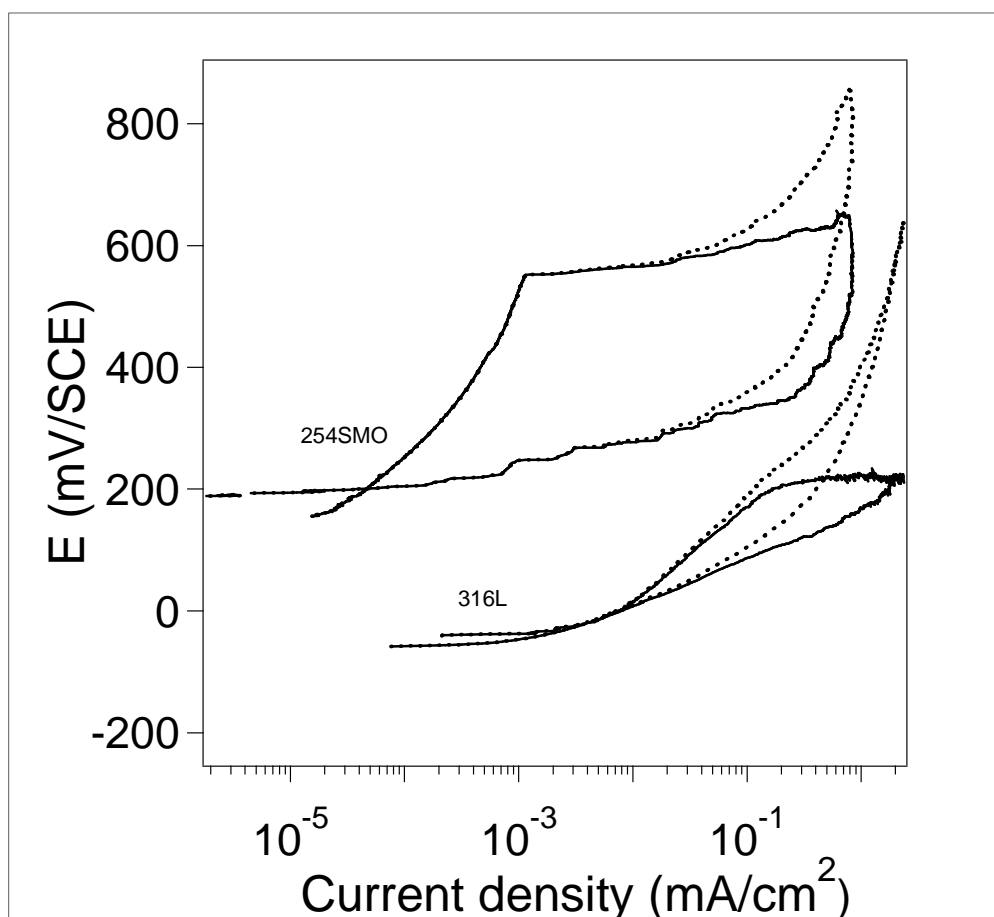

Figure A-1 Polarisation curves before (dotted lines) and after (solid lines) the IR drop correction for both alloys 316L and 254SMO immersed for 96hrs in 11.9M- HAc-Br⁻ at 90⁰C